Narrow bipolar events study based on broadband observations

Fernando Augusto Díaz Ortiz

Universidad Nacional de Colombia

Faculty of Engineering

Department Electric and Electronic Engineering

Bogotá, Colombia

2023

Narrow bipolar events study based on broadband observations

Fernando Augusto Díaz Ortiz

Submitted in partial fulfillment of the requirements for the degree of:
Doctor en Ingeniería Eléctrica

Principal Advisor:
Prof. Francisco José Roman Campos

Research field:
Atmospheric electricity
Research Group:
Electromagnetic Compatibility EMC-UN

Universidad Nacional de Colombia
Faculty of Engineering
Department Electric and Electronic Engineering
Bogotá, Colombia
2023

To my children,

María Fernanda *and* José Fernando.

Declaración de obra original

Yo declaro lo siguiente:

He leído el Acuerdo 035 de 2003 del Consejo Académico de la Universidad Nacional. «Reglamento sobre propiedad intelectual» y la Normatividad Nacional relacionada al respeto de los derechos de autor. Esta disertación representa mi trabajo original, excepto donde he reconocido las ideas, las palabras, o materiales de otros autores.

Cuando se han presentado ideas o palabras de otros autores en esta disertación, he realizado su respectivo reconocimiento aplicando correctamente los esquemas de citas y referencias bibliográficas en el estilo requerido.

He obtenido el permiso del autor o editor para incluir cualquier material con derechos de autor (por ejemplo, tablas, figuras, instrumentos de encuesta o grandes porciones de texto).

Por último, he sometido esta disertación a la herramienta de integridad académica, definida por la universidad.

Fernando Augusto Díaz Ortiz
Fecha 31/01/2023

I certify that I have read this dissertation and that, in my opinion, it is fully adequate in scope and quality as a dissertation for the degree of Doctor of Philosophy.

Prof. Francisco Jose Roman Campos, Ph.D. (Principal Advisor)
Universidad Nacional de Colombia
Bogotá, Colombia

I certify that I have read this dissertation and that, in my opinion, it is fully adequate in scope and quality as a dissertation for the degree of Doctor of Philosophy.

Prof. Herbert Enrique Rojas Cubides, Ph.D.
Universidad Distrital Francisco Jose de Caldas
Bogotá, Colombia

I certify that I have read this dissertation and that, in my opinion, it is fully adequate in scope and quality as a dissertation for the degree of Doctor of Philosophy.

Prof. Chandima Gomes, Ph.D.
University of Witwatersrand
Johannesburg, South Africa

I certify that I have read this dissertation and that, in my opinion, it is fully adequate in scope and quality as a dissertation for the degree of Doctor of Philosophy.

Prof. Joan Montanya, Ph.D.
Universitat Politecnica de Catalunya
Terrassa, Spain

I certify that I have read this dissertation and that, in my opinion, it is fully adequate in scope and quality as a dissertation for the degree of Doctor of Philosophy.

Prof. Shriram Sharma, Ph.D.
Tribhuvan University
Kathmandu, Nepal

Acknowledgements

I first express gratitude to my doctoral advisor, Professor Francisco Jose Roman Campos, for his trust and guidance. He allowed me to join a thriving research group where I had a tremendous learning experience. I am thankful for this valuable and enduring influence.

I express my appreciation to members of the Electromagnetic Compatibility Research Group (EMC-UN) for their collaboration, and more importantly, for the friendly conversations that made dealing with long working hours easier. I am grateful to all of them, with a special mention (in no particular order) to Carlos Rivera, Jorge Rodríguez, Carlos Gómez, Edwin Pineda, Ernesto Neira, Sergio Rivera, Alejandro Cristancho, Marlon Patiño, Fernando Albarracín, Andrés Gallego, Alexander Narváez, Alexander Alarcón, Herbert Rojas, and former professor John Jairo Pantoja.

I must say my deep sorrow for the untimely death of my colleague Elkin Muskus, with whom I shared fond memories for almost two decades. I pay tribute to his memory.

During my research internship in Sri Lanka, I must acknowledge the kindness of its people who showed me the beautiful country known as "The Pearl of the Indian Ocean.Ï am grateful to the Lightning and Atmospheric Electricity Research Group at the University of Colombo for making my work there possible. I want to give a special mention to Professor Mahendra Fernando for his technical expertise and valuable cultural insights. I also express my sincere appreciation to Manoj Rajakaruna, Sanka Nanayakkara, Ruwan Abeywardhana, and Ujitha Abeywickrema for their help and friendliness. You made my time away from home more enjoyable.

I thank my parents, José Manuel, and Rosa Inés, for their unwavering support and encouragement throughout my life, especially in recent years as they helped care for my children. Your help was essential in allowing me the time to dedicate to my work. This achievement would not have been possible without you. Gracias papá, gracias mamá.

To my brother Juan Manuel, my sister Paola Andrea, and my sister-in-law Liliana, there are not enough words to express my feelings, so I must say thank you for being there for each other and for making life a little bit brighter.

Some people were not involved directly in this work. Still, their presence and timeshare were essential to keep an unwinding mind ready to work. Thanks to the usual suspects, Francy, Carolina, Armando, and Felipe. Friends are the chosen family we create for ourselves.

From now on, I will proudly remember having been a part of one of the most prestigious universities in Colombia. Thank you, Universidad Nacional de Colombia.

María Fernanda and José Fernando, my loving children, I am well aware you do not know, but you were my strength when my will weakened.

Last but not least, to my wife Shirley, thanks for the time that belonged to you. I feel in profound debt for your patience. I am grateful for your encouragement that made this accomplishment possible. From now on, I want to enjoy the fruits of these busy years with you by my side.

Fernando Díaz
Fusagasugá, Colombia
January 2023

Resumen

Estudio de pulsos bipolares estrechos basado en observaciones de banda ancha

Este estudio determina las características de los pulsos bipolares estrechos (NBEs) en Bogotá, Colombia, proporcionando información sobre los NBEs en una región tropical observada desde un altiplano andino. La instrumentación y el software de rayos se crearon específicamente para este estudio y consisten en un módulo de medición de campo eléctrico, un módulo de medición de campo magnético y un interferómetro de rayos de banda ancha. Para la adquisición de datos, la instrumentación de rayos utiliza dos osciloscopios digitales que en conjunto proporcionan ocho canales.

Los instrumentos de rayos se desplegaron en el techo de un edificio en el centro de la ciudad de Bogotá. La campaña de medición recopiló datos desde el 14 de noviembre de 2019 hasta el 9 de abril de 2020 e incluye la segunda temporada de lluvias de 2019 y parte de la primera temporada de lluvias de 2020. El período de observación duró exactamente 148 días y registró 1.316 eventos relacionados con rayos.

La identificación de los NBEs involucró cuatro etapas: la primera etapa tuvo como objetivo eliminar el ruido de la señal adquirida, la segunda etapa involucró la identificación de los NBEs, la tercera etapa involucró la clasificación de los NBEs en función de sus formas de onda y, finalmente, la cuarta etapa involucró la medición de las características individuales de los NBEs. Este proceso se realizó en todos los eventos de rayos registrados.

Un resumen de los hallazgos obtenidos en este estudio es el siguiente: los NBEs están presentes en solo una sexta parte de toda la actividad de rayos detectada, y la mayoría de ellos son de polaridad positiva en una proporción de 3 a 1. La polaridad positiva tiene una duración más larga para el pulso principal y duración total que su contraparte. Con respecto a su tipo, el Tipo A (un pulso bipolar típico) es una ocurrencia rara, lo que significa que oscilaciones adicionales sobre la forma de onda básica es una característica común.

Combinando criterios de aislamiento temporal y espacial, el 13 % de los NBEs pueden considerarse NBEs aisladas, lo que sugiere que los NBEs restantes podrían estar relacionadas con el inicio de descargas intranubes, descargas nube-tierra (CG) o incluso NBEs con actividad posterior fallida. Aproximadamente el 80 % de los registros adquiridos durante este estudio presentan pulsos con duraciones menores a un microsegundo en distintos momentos.

Adicionalmente, hay 22 grupos de NBEs compuestos por dos o tres NBEs temporalmente cercanos.

La rara presencia de NBEs en la actividad regular de rayos sugiere que los NBEs no son la causa del inicio de los rayos. Esta afirmación está respaldada en este estudio por su presencia en solo una sexta parte de toda la actividad de rayos registrada. Los datos recopilados sugieren que los NBEs no son un evento aislado, sino que, se deduce que los NBEs son un fenómeno que tiene lugar como un efecto relacionado de algún CG o como parte del desarrollo de descargas eléctricas intranubes posteriores. El valor medio de la duración total del pulso sugiere que los NBE deben originarse a partir de alguna descarga eléctrica energética y de corta duración. Este resultado concuerda con la hipótesis de que las descargas eléctricas rápidas son el fenómeno responsable de la producción de NBEs. Al comparar las tasas de ocurrencia de NBEs, el resultado revela una relación aparente con la latitud, lo que significa que los NBE son más frecuentes en latitudes más bajas y también muestran una mayor proporción de NBEs de polaridad negativa. La tasa de ocurrencia del tipo A y el tipo C es similar a estudios previos, pero las proporciones para el tipo B y el tipo D ciertamente difieren, lo que exige un análisis más profundo para abordar este problema.

Palabras claves: rayos, eventos bipolares estrechos, pulso bipolar estrecho, descarga intranube compacta, interferometria.

Abstract

Narrow bipolar events study based on broadband observations

This study determines the features of NBEs in Bogotá, Colombia, providing insights into NBEs in a tropical region observed from an Andean high-plateau. The lightning instrumentation and software were created specifically for this study, consisting of an electric field measurement module, a magnetic field measurement module, and a broadband lightning interferometer. For data acquisition, the lightning instrumentation uses two digital oscilloscopes that together provide eight channels.

Lightning instruments were deployed on the roof of a building in the city center of Bogotá. The measuring campaign collected data spans from November 14, 2019 to April 9, 2020 and includes the second rainy season of 2019 and part of the first rainy season of 2020. The observation period lasted exactly 148 days and recorded 1,316 lightning-related events.

The identification of NBEs involved four stages: the first stage aimed at removing noise from the acquired signal, the second stage involved identifying NBEs, the third stage involved classifying NBEs based on their waveforms, and finally, the fourth stage involved measuring individual NBE features. This process was done on all recorded lightning events.

A summary of the findings of this study is as follows: NBEs are present in only one-sixth of all lightning activity detected, with most of them being of positive polarity in a ratio of 3 to 1. Positive polarity has a longer duration for the main pulse and total duration than its counterpart. Regarding their type, Type A (a typical bipolar pulse) is a rare occurrence, meaning that additional ringing over its basic waveform is a common feature.

By combining time and spatial isolation criteria, 13 % of NBEs can be considered to be truly isolated NBEs, suggesting that the remaining NBEs could be related to the initiation of IC, CG, or even NBEs with failed subsequent activity. Approximately 80 % of the records acquired during this study have sub-microsecond pulses at any moment of their process, and there are 22 groups of NBEs comprised of two or three temporally close NBEs.

The rare presence of NBEs in regular lightning activity suggests NBEs are not the cause of lightning inception. This statement is supported in this study by their presence in only one-sixth of all lightning activity recorded. Data collected suggests NBEs are not an isolated event, instead,

from data analysis, it is deduced that NBEs are a phenomenon that takes place as a related effect of some CG or as part of the development of subsequent intracloud electrical discharges. The mean value for total pulse duration suggests NBEs must originate from some energetic and short-duration electrical discharge. This result concurs with the hypothesis of fast electrical breakdowns are a responsible phenomenon for NBEs production. Comparing occurrence rates of NBEs, the effort reveals a relation to latitude meaning NBEs are more prevalent in lower latitudes also showing a higher proportion of negative polarity NBEs. The occurrence rate of type A and type C are similar to previous studies but proportions for type B and type D certainly differs demanding further analysis to address this issue.

Table of contents

List of Figures

List of Tables

List of symbols

Symbols with latin letters

Symbol	Term	SI Unit	Definition
A	Area of the circular plate	m^2	
A_z	Azimuth angle	rad	
Ca	Capacitance of the antenna	F	
c	Speed of light	m/s	
d	Separation between plates of the antenna	m	
E	Electric Field	V/m	
E_L	Elevation angle	rad	
G_{kl}	Autocorrelation function		
H	Virtual ionospheric height	m	Figure **A-2**
h	Height of NBE source	m	
h_{eff}	Effective height of the antenna	m	
h_{phy}	Physical height of the antenna	m	
R	Radius of the Earth	km	6,371 km
R_{kl}	Cross correlation function		
Q	Electric charge	C	
t	Time	s	

Symbols with greek letters

Symbol	Term	SI Unit	Definition
ϵ_0	Vacuum permittivity	F/m	$8,85 \times 10^{-12}$
ϵ_r	Relative permittivity	F/m	
θ_1	Angle of incidence over baseline 1	rad	
θ_2	Angle of incidence over baseline 2	rad	
ϕ_{kl}	Angle difference between signals s_k and s_l	rad	
ρ_b	Charge density	$\frac{\text{coulomb}}{\text{m}^3}$	
Φ	Electrostatic potential	$\frac{\text{joule}}{\text{coloumb}} = volts$	$\frac{W}{Q}$

List of Abbreviations

Abbreviature	Term
$BINTF$	Broadband Lightning Interferometer
CID	Compact Intracloud Discharge
CG	Cloud to Ground (lightning discharge)
FNB	Fast Negative Breakdown
FPB	Fast Positive Breakdown
$FWHM$	Full Width of Half Maximum
HF	High Frequency
IBP	Initial Breakdown Pulses
IC	Intra-Cloud Discharge (lightning discharge)
$INBE$	Initiator-type Narrow Bipolar Event
LF	Low Frequency
LMA	Lightning Mapping Array
NBE	Narrow Bipolar Event
NBP	Narrow Bipolar Pulse
TOA	Time of Arrival
VHF	Very High Frequency
VLF	Very Low Frequency
TGF	Terrestrial Gamma Ray Flashes

Abbreviature	Term
$TIPP$	Transionospheric Pulse Pair

1. Introduction

American Meteorological Association (AMS) defines lightning discharge as 'the series of electrical processes taking place continuously by which charge is transferred along discharge channels between electric charge centers of an opposite sign' [1]. This definition recognizes lightning as a natural compound phenomenon with charge transfer as the main focus. Despite decades of research, the conditions, intensities, dimensions, and context of these discharges are not well understood.

One of the ten open questions in lightning research remains the mechanism responsible for lightning inception [2]. The inception of lightning occurs deep inside the thundercloud, hidden from direct observation, and the first electrical processes are difficult to detect as they lack optical emissions or have weak emissions [3], [4], [5]. To date, lightning inception has not been captured on images. However, evidence suggests that initial discharges are related to bipolar leaders and their precursors, streamers, which can be both positive and negative polarity and present unusual propagation velocities [6], [7]. Some reports propose that the propagation and collision of streamers are responsible for strong electromagnetic radiation emissions in the HF and VHF bands [8]. Other studies suggest that fast propagating streamers are behind both Narrow Bipolar Events (NBEs) and lightning inception [7], [6].

Problem statement

NBEs are a type of intra-cloud process studied for more than four decades [9], [10]. Until now, some distinctive features of NBEs are well-known, namely their bipolar waveform [11], short temporal duration (i.e., typically less than 20 μs) [12], short spatial extension [6], high emission of electromagnetic radiation (especially in the VHF band) and scarce light emission [13], [14], [15].

NBEs are produced inside clouds, generally at an altitude higher than 6 km above ground level, although without any records of direct observations [16]. Previous studies suggest that the occurrence of NBEs can be affected by factors such as latitude [17], the size of the lower positive charge region in the base of the cloud [18], the type of storm [19], and even the stage of the storm or the geometry of leaders development [20]. Due to their ephemeral presence and still unknown role in lightning inception and development, comparative studies on NBEs have been performed over the years to find patterns [19], [21], [18].

However, despite all the available information about NBEs, one certainty remains: the features of narrow bipolar events in Colombia are unfamiliar to the lightning community. To date, there has been no study devoted to finding their characteristics, and thus, there is no certainty if claims about NBEs match those of NBEs in Colombia. The only known exception to this claim is a recent publication by Lopez et al. where four lightning initiation events (only one NBE was present) were observed over Colombia [22]. NBEs have been studied in China, Indonesia, Japan, Malaysia, Sri Lanka, Sweden, and the United States of America, but there is no information from Colombia. Thus, any work related to this topic must take information from other places and assume that it represents our context well.

Research question

Most studies about NBEs features have been performed in latitudes near or above subtropical regions. Most studies have been done in the USA where its lowest latitude corresponds to $29°N$ in Florida, meanwhile, Sweden is located above $59°N$. Japan lies between $20°N$, and $45°N$. As a result, tropical studies correspond to those performed in Sri Lanka (between $5°N$, and $9°N$), Malaysia (between $4°N$, and $2°N$), and Indonesia (between $6°N$, and $11°S$). One interesting fact about Indonesia is that corresponds to the antipode of Colombia located in the tropical region of the Western hemisphere been then so far the only study on NBE in this part of the world.

Addressing the lack of information on NBEs in Colombia the purpose of this work aims to answer the following research question:

What are the characteristic features of narrow bipolar events in Colombia?

Research hypothesis

The research question defined the gap that this dissertation addressed and that was tested using the following hypothesis:

The characteristics of NBEs in Bogotá, Colombia, are not significantly different from those found in other tropical regions.

Purpose of the study

The purpose of this study is to determine the features of narrow bipolar events waveforms in Bogotá, Colombia. As far as the author knows, NBEs studies have not been conducted in Colombia. Accordingly, there is no information about this type of electrical discharge or its eventual singularities in this part of the world. Therefore, this study aims to collect data to characterize NBEs determining their rate of occurrence, types, and waveform characteristics, among other elements of interest about NBEs in Colombia. The findings are intended to enrich knowledge about NBEs because they are useful in comparative studies with other near-equator places, where, similar studies have been developed (i.e., Sri Lanka, and Malaysia) [23], [24].

Significance of the Study

Lightning studies in Colombia are highly favorable due to its high flash density rate. In fact, ten Colombian sites are listed among the places with the highest flash rate density in the world [25, 26, 27]. Only a few countries in the Congo River basin have more sites on that list, making Colombia an ideal location for lightning research.

Located in a tropical region, Colombia offers a diverse range of scenarios for lightning studies due to its varied topography. The study was performed in Bogotá, the capital city of Colombia, located on a high Andean plateau at an altitude of 2,600 m.a.s.l. This unique location offers a natural observatory to observe lightning activity in a tropical region from a high-altitude site.

Delimitation of the Study

The lightning instrumentation was deployed on the roof of a building in the city center of Bogotá, a metropolis of eight million inhabitants located at 4° 42' 40"N, 74° 4' 20"W, and on the high plateau of Sabana de Bogotá. The city and the country's climate are strongly influenced by the Intertropical Confluence Zone (ITCZ) due to its geographical proximity, leading to alternating rainy and dry seasons twice per year.

The collected data ranges from November 14, 2019, to April 9, 2020, coinciding with the peak of Colombia's rainy seasons. The proper identification of lightning events was validated using lightning location data provided by Mr. Ronald Holle from Vaisala. Although the data is better suited for studying cloud-to-ground discharges, it was extremely useful for this study despite its lower accuracy in detecting intracloud activity.

One major limitation of this study was the poor timing of the commissioning of the broadband lightning interferometer at the beginning of 2020. Due to the pandemic restrictions, there was not

enough data collected to make significant contributions to the study of NBEs. The instrument was functioning, but its contributions were limited for the purpose of this study.

Original contributions

As a consequence of this work, the contributions of this dissertation are:

- Identification of the distinctive features of narrow bipolar events in the area of study.

- Identification of the relation between NBEs and other lightning activity in the area of study.

- Software for automatic identification of NBEs based on waveform shape.

- Software to determine optimal wavelet to denoise NBE signals.

- Software to apply analytic signal approach to estimate time delay between noisy signals.

- Development of instruments for measurement of electromagnetic fields related to lightning activity.

- Development of a broadband lightning interferometer.

- Software for source location based on interferometry.

Publications and other related work

Journal Papers

- Diaz, F., Ortiz, F., and Roman, F. Lightning climatology in Colombia. Theoretical and Applied Climatology (2022). https://doi.org/10.1007/s00704-022-04016-5.

- Diaz, F. and Roman, F. Electric Field Parameters of Narrow Bipolar Events in Colombia. Working paper expected to submit to IEEE Transactions on Electromagnetic Compatibility in 2023.

Conference proceedings

- Diaz, F., Gomez, C. and Roman, F. Time delay measurement based on the analytic signal for the lightning interferometer. International Conference on Lightning Protection (ICLP 2021), International Conference on Lightning Protection (SIPDA 2021). https://doi.org/10.1109/ICLPandSIPDA54065.2021.9627481.

- Diaz, F. and Roman, F. Wavelet denoising using an optimal selection of mother wavelet for compact intracloud discharges. International Conference on Lightning Protection (ICLP 2018). https://doi.org/10.1109/ICLP.2018.8503325.

- Diaz, F., Gomez, C., Lopez, J. and Roman, F. High-speed data acquisition system for radio atmospheric signals measurements based on software-defined radio. International Conference on Lightning Protection (ICLP 2017). https//doi.org/10.1109/ICLP.2016.7791426.

- Diaz, F. and Roman, F. Annual lightning events in Colombia: Why are they increasing?. International Symposium on Lightning Protection (SIPDA 2015). https://doi.org/10.1109/SIPDA.2015.7339324.

- Diaz, F. and Roman, F. Surface air temperature and lightning events in Colombia. Revista Facultad de Ingeniería Universidad de Antioquia (under review).

Patent application

- Díaz, Fernando and Gómez Carlos. Interferómetro de rayos de banda de ancha para la localización de fuentes de radiación con base en señales analíticas (Broadband interferometer for radiation sources location based on analytic signals). NC2022/0012472, filed September 7, 2022.

Software

- Diaz, Fernando. (2021). Programa para la selección de la wavelet óptima usando como criterios SNR, MSE y energía relacionadas con actividad eléctrica de nubes de tormenta.(Software for wavelet selection based on SNR, MSE and energy criteria related to electrical activity of thunderstorms).13-88-60, filed December 30, 2021.

- Díaz, Fernando. (2022). Programa para interferómetro de rayos. (Software for lightning interferometer). 13-92-52, filed October 03, 2022.

Additional work

- Suarez, A. and Díaz, F. Análisis de mediciones de rayos con Python (Lightning measurements analysis with Python). Master's degree thesis. Actual.

Outline of the thesis

This document is organized into five chapters, a bibliography, and appendixes. **Chapter 2** presents a literature review on narrow bipolar events. **Chapter 3** describes the research design; methodology of this study. Additionally, the descriptions of built instrumentation and algorithms developed for data collection and processing. **Chapter 4** presents collected data analysis and discussion of findings. **Chapter 5** contains a summary, conclusions, implications, and recommendations for future works. The document concludes with the **Bibliography** and **Appendixes** sections.

2. Literature Review

2.1. Introduction

This chapter presents a literature review related to the nature of narrow bipolar events. This compendium is pertinent because establishes a theoretical framework for this research. Most findings are results of studies in subtropical regions, with a couple of exceptions in Sri Lanka, Malaysia, and Southeast China. For comparative purposes of studies, it is worth mentioning, that there are small but significant differences in instrumentation specifications and environmental conditions affecting signal propagation.

NBEs have been known for more than 40 years, and during this time, they have been named based on researchers' preferences. Indeed, some names distinguish between the physical event and the observable effect. Therefore, besides NBEs, they are also referred to as Narrow Bipolar Pulses (NBPs) or Compact Intracloud Discharges (CIDs) [28], [29], [9].

On the other hand, in the lightning physics context, lightning inception prevails as an unanswered question. Currently, two plausible theories intend to explain the nature of this process. One states the creation of enough runaway electrons to initiate an electrical discharge inside the cloud fostered by showers of high energy particles (i.e., Extensive Area Shower (EAS) mainly cosmic rays) [30]. The other one, states lightning discharges initiate as a consequence of a sudden intensification of the local electric field, strong enough to initiate streamers from the surface of hydrometeors [31].

In both cases, the existence of NBEs is considered a related event taking place before, simultaneously, or after lightning inception. Although both theories fail to explain why NBEs are rare events. To address this situation, two possible explanations are the absolute absence of the process that generates them or, most of the time, they are too weak to be detected. In any case, it is an open question of how the NBEs are related to lightning inception.

2.2. Narrow Bipolar Events

2.2.1. Polarity and height of occurrence

According to the initial pulse's polarity, NBEs are classified as positive or negative polarity. To illustrate their basic waveform, Figure **2-1** shows two NBEs, one of positive and one of negative polarity. Positive polarity NBEs are more frequent in a proportion of ten to one, developing between the main negative charged region and the upper positive charged region of the cloud [32]. Interestingly, this region concurs with the area known to originate intracloud discharges [33]. Meanwhile, negative NBEs are mainly located between the upper positive charged region and the upper negative screening layer of the cloud [34].
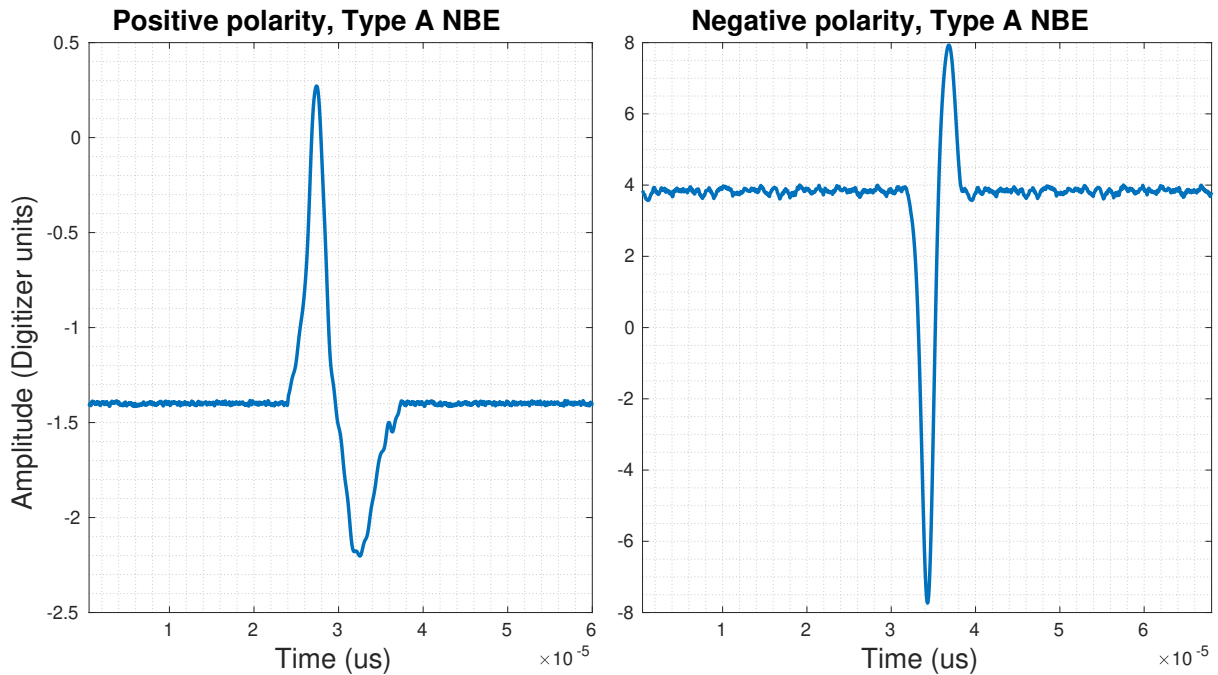
Figure 2-1.: Waveforms of two NBEs. According to the atmospheric electricity sign convention, the left-side image corresponds to a positive polarity NBE. Meanwhile, the right-side image corresponds to a negative polarity NBE. (Source: signals recorded by the author)

Those locations imply positive NBEs tend to originate between 8 km and 16 km, while, negative NBEs between 13 km and 19 km [16], [24], [35]. Depending on the instrumentation employed, height estimation varies in complexity and accuracy. A commonly used approach to determine the height of an NBE using a single station is available in Appendix A. To clarify this matter, Table **2-1** presents a compendium of studies.

Table 2-1.: A compilation of findings about the estimation of NBEs height source.

Author	Country	Year	Height positive NBE (km)	Height negative NBE (km)
Smith et al.[14]	USA	1996	8-11	-
Smith et al.[36]	USA	1998-2001	7-15	15-20
Nag et al. [37]	USA	2008	16	-
Wu et al. [16]	China	2010	8-16	16-19
Lu et al. [38]	China	2010	9.6	-
Karunarathna et al. [28]	USA	2011	8-19	-
Wu et al. [34]	Japan	2011	5-16	13-16
Liu et al. [33]	China	2012	7-20	10-19
Wu et al. [39]	Japan	2013	8-16	13-19
Zhang et al. [35]	China	2013	7-15	14-19
Ahmad et al. [24]	Malaysia	2015	8-16	-

2.2.2. NBE Waveform

Finally, about this matter, Table **2-2** and Table **2-3** show a compendium of results about time features of positives and negatives NBEs in different latitudes.

2.2.3. Relation with other lightning activity

Most of the initial studies on NBE presumed they were isolated events because they have no other electrical activity during hundreds of milliseconds before or after their occurrence [49]. Later, based on satellite observations, Jacobson et al. [50] suggested NBEs were isolated processes only possibly related to intracloud discharges. However, recent works using improved instrumentation suggest the opposite, leading to consider them as an integral part of the initial process of regular cloud discharges [6].

Actually, isolation is not an easy or straightforward definition because of the spatial extension of lightning. Recent works suggest better instrumentation would facilitate the detection of weaker emissions of NBEs. Other works, extend the isolation definition to include both temporal and spatial dimensions. Consequently, to declare an NBE as an isolated event, no other electrical activity must occur before or after the NBE occurrence, and no other electrical activity must be present in an area around the NBE [51].

Table 2-2.: Compendium of results obtained in previous studies of time-related features for positive NBE pulses.

Reference	Rise time (μs)	FWHM (μs)	Zero crossing (μs)	Pulse duration (μs)
LeVine et al. [9]	-	-	<10	10-20
Cooray et al. [40]	4 ± 1.3	-	13 ± 4.9	75 ± 25.9
Willett et al. [41]	-	2.40 ± 1.4	10-15	20-30
Medelius et al. [42]	1.82 ± 0.87	1.60 ± 0.87	7.7	22
Smith et al. [14]	2.30 ± 0.8	4.70 ± 1.3	-	25.8 ± 4.9
Sharma et al. [23]	2.60 ± 1.1	1.84 ± 0.89	2.40 ± 1.6	5.78 ± 2.1
Nag et al. [21]	-	-	-	24
Zhang et al. [43]	2.6 ± 0.5	2.2 ± 0.3		16 ± 1.4
Lu et al. [29]	-	4.60 ± 1.0	-	27.2 ± 6.6
Hazmi et al. [44]	1.64 ± 0.51	3.24 ± 1.20	5.23 ± 1.14	15.06 ± 6.38
Gunasekara et al. [45]	1.38 ± 0.47	1.93 ± 0.33	4.66 ± 1.29	16.42 ± 8.43

Table 2-3.: Compendium of results obtained in previous studies of time-related features for the negative NBE pulses.

Reference	Rise time (μs)	FWHM (μs)	Zero crossing (μs)	Pulse duration (μs)
Willet et al. [41]	-	2.4 ± 1.4	-	20-30
Medelius et al. [42]	1.82 ± 0.87	1.83 ± 0.63	-	-
Smith et al. [14]	-	-	4.7 ± 1.3	25.8 ± 16.7
Dong et al. [46]	2.06 ± 1.14	2.89 ± 1.02	-	-
Ahmad et al. [47]	1.6 ± 1.0	2.2 ± 0.7	9.0 ± 45	24.6 ± 17.1
Zhang et al. [43]	2.2 ± 0.2	1.9 ± 0.1	-	12.1 ± 1.3
Wang et al. [48]	1.5	-	-	23
Gunasekara et al. [45]	0.58 ± 0.17	1.38 ± 0.25	3.01 ± 0.54	19.21 ± 3.06

Regarding their role, Bandara et al. [52] suggests the existence of low altitude negative NBE (less than 8 km) that seems to initiate negative CG. Therefore, NBEs would be part of lightning inception but they do not necessarily occur at the beginning of all electrical activity in the cloud. Then, some researchers differentiate between NBE with related activity from those that have none (i.e., Initiator-type NBE INBE and the rest of NBE) [39], [53]. Another interesting suggestion from those studies is that the altitude of NBEs might strongly influence subsequent discharges, thus, higher altitudes NBEs relate to weaker subsequent activity. Therefore, that activity turns more challenging to detect giving the impression of isolated NBEs.

There are additional relations between NBEs and lightning activity. Transient Luminous Events (TLEs) are electrical discharges originating from or above the top of thunderclouds. So far, several types of TLEs have been identified differing in physical production mechanism: Examples of TLE are elves, halos, sprites, blue jets, and gigantic jets. Findings show the previous or simultaneous presence of NBEs during the occurrence of TLEs. For example, Liu et al. [54] establish a relation between negative NBE and blue discharges. Meanwhile, Marshall et al. [55] suggest elves doublets are the ionospheric signature of high altitude NBE (probably negative polarity NBEs).

Finally, other findings demonstrate that thunderstorms are sources of both continuous, and intermittent gamma-ray emissions, named Terrestrial Gamma-Ray Flashes (TGFs) [56]. Once again, some evidence link TGFs with NBEs [57], [58], [59].

2.2.4.   Optical emission

NBEs seem to generate no optical emission and, if there is any, had not been recorded to date [48]. Satellite-based observations have detected strong VHF emissions from the top of thunderstorms in which VHF emissions are detected as a pair of pulses called Transionospheric Pulse Pairs (TIPPs). Apparently, the particular signature is due to satellite antenna receiving both direct and reflection paths of NBEs [60], [61], [62], [63]. Also, those studies found a low degree of correlation between VHF emissions and optical records, confirming scarce light emission from NBEs [15], [64]. Consequently, most knowledge about NBEs come from indirect observations. Some remarkable exceptions are the observations reported by Lopez et al. [22] and Soler et al.[65] about blue emissions coming from the top of the clouds related to NBEs. Other works reporting blue emissions related to NBEs can be found in Liu et al.[66], and Husbjerg et al.[67].

2.2.5.   HF and VHF emissions

NBEs' strong electromagnetic radiation has always caught the attention of researchers since their discovery. NBEs emit intense radiation comparable to that generated by ordinary

cloud-to-ground (CG) with a particular radiation signature in both HF (High Frequency) and VHF (Very High Frequency) bands [9], [68]. Indeed, NBEs are known as the most powerful natural source of electromagnetic radiation in those bands. Therefore, they are detectable up to hundreds of kilometers from the emission source [6], [50], [17].

Several studies have estimated that NBEs emission power ranges from 1 KW to 100 KW [15], [6], [7]. According to the given values, peak current is estimated around 20 KA, and charge moment change between 100 $C - m$ and $1,000$ $C - m$ [49], [7], [6].

2.2.6. Meteorological aspects

NBEs are frequent in certain types of storms and tend to occur more regularly in a specific evolution stage of thunderstorms [34], [19], [64]. Even more, NBEs seems heavily related to the strength of deep convection inside storms, therefore, their rate of occurrence could serve as a proxy to warn about the presence of severe storms [69].

The latter condition is convenient in regions without access to radar or satellite meteorological data because NBEs could be used as a complement to early warning systems (EWS) for severe weather. In the same context, their presence is used as an index to determine the behavior of extended or dispersed convective systems responsible for severe weather. Therefore, NBEs detection complements information about convective systems, such as configuration, life cycle, and duration, among other elements.

2.2.7. Latitude dependence

Some studies indicate a probable relationship between the rate of occurrence and latitude. According to Ahmad et al., [18] as latitude decreases, NBEs appear more frequently. The physical explanation behind this condition could be the vertical extent of clouds, because their extension also varies with latitude, being larger near the equator. This reason suggests NBEs should be more frequent in tropical regions.

Other studies found that the ratio between positive and negative NBEs also changes with latitude. Positive NBEs look more frequent in subtropical thunderstorms, meanwhile, the proportion looks more uniform in tropical regions. Estimated NBEs ratio of occurrence exist for Sri Lanka [45]; Malaysia [47]; Japan [34]; China [70], [71], [16], [72]; USA [14], [73], [69], [64], [19]; Sweden [23], [18]. Table **2-4** summarizes findings about this matter.

Table 2-4.: Compendium of findings regarding the dependence of NBEs from latitude. Adapted from [29].

Reference	Pct. of NBEs	Pct. of positive NBEs	Pct. of negative NBEs
Smith et al. [74]	1.4 %	71 %	29 %
Suszcynsky et al. [69]	less than 1.7 %	63 %	37 %
Smith et al. [36]	3.4 %	58 %	42 %
Jacobson et al. [64]	less than 0.4 %	77 %	23 %
Wiens et al. [19]	-	77 %	23 %
Nag et al. [21]	-	97.5 %	2.5 %
Ahmad et al. [47]	-	59 %	41 %
Zhu et al. [75]	10 %	87 %	13 %
Sharma et al. [23]	-	100 %	0 %
Wu et al. [71]	-	66 %	34 %
Wu et al. [16]	-	82 %	18 %
Wang et al. [48]	-	100 %	0 %
Wu et al. [34]		91 %	9 %
Lu et al. [29]	0.034 %	100 %	0 %

2.2.8.   Mechanism of production

Based on interferometric observations, a pair of processes named Fast Positive Breakdown (FPB) and Fast Negative Breakdown (FNB) looks like the physical mechanism behind NBEs production [**?**], [68], [6]. Apparently, FPB is composed of millions of positive streamers developing from hydrometeors in virgin air [76]. Meanwhile, FNB would be some corona or streamer wave [77], [7]. The term fast is given to both discharges as a consequence of their remarkable speed, reaching one-third of the speed of light [78]. In both cases, streamers propagation looks responsible for the strong VHF emissions characterizing this phenomenon [8]. The same observations establish a length for discharge channel ranging from 100 m to $2,400$ m, confirming the short spatial extension of NBEs, relatively small compared to other lightning discharges.

2.3.   Instrumentation

2.3.1.   Flat plate antennas

Flat plate antennas are well-known sensors used to convert the electric field associated with lightning into a current at its terminals. The first detailed studies of this antenna for the measurement of both large amplitude and transient pulses were made by Baum for the purpose of measuring Electromagnetic Pulses (EMP) associated with nuclear detonations [79]. However, promptly they were used to study pulses related to lightning [80].

Their physical structure comprises one or two conductive plates, generally oriented parallel to the ground. One-plate configuration uses the ground as a reference meanwhile, the two-plate configuration attached one plate to the ground as the reference allowing to stands the plates on a vertical pole. In both cases the upper plate, the ambient electric field induces an electrical charge on its surface producing an electrical current that flows proportional to the electric field's derivative on the antenna's terminals. As the antenna is basically a capacitor, the sensed current is related to the voltage through a derivative as is defined in Equation (2-1).

$$i_a(t) = C_a \frac{dV_a}{dt} \tag{2-1}$$

where V_a is a voltage directly proportional to the ambient electric field, i_a is the current flowing from the antenna, and C_a is the capacitance of the antenna.

The capacitance of a flat plate antenna can be estimated using Equation (2-2).

$$C_{antenna} = \epsilon_0 \epsilon_r \frac{A}{d} \tag{2-2}$$

where A is the area of the plate and d is the gap between plates.

Therefore, to have a signal directly proportional to the electric field is required to determine the integral of the signal coming from the antenna. The common practice uses electronic circuits to perform this integration, although some studies have used numerical integration with satisfying results. The integration process is expressed as shown in Equation 2-3

$$v_a(t) = \frac{1}{C_a} \int i_a dt \tag{2-3}$$

Regarding the integration stage, this is a simple circuit comprising an RC network (R resistor, C capacitor) and an operational amplifier (op-amp) [81]. The circuit's layout connects the RC network in parallel to the antenna. In this way, current from the antenna charges the capacitor; meanwhile, the resistor serves as a path to discharge the capacitor. Components' values define a time-constant affecting rate change of voltage across the capacitor's terminals. Consequently, the time constant is the width of an observation window over which the integral is performed [82]. The op-amp's role is to serve as a line driver that boosts the incoming signal's power to drive the cable's impedance.

Figure **2-3** shows the integration circuit schematic used for both FA and SA. The only difference among them is the time constant estimated as $R \times C$. This value must be "short"for a FA, and "long"for a SA, whose, definition is entirely subjective. Then, FA and SA are defined based on the type of signals expected to detect. Figure **2-2** shows the merger of flat plate antenna with the integration stage (for the case of FA and SA), plus equipment to perform data acquisition.
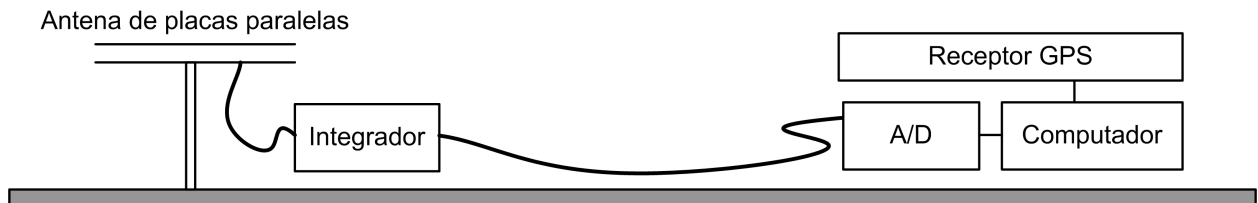
Figure 2-2.: Block diagram of the measuring system using flat plate antennas. For both FA and SA the only difference is a change in time-constant values.

If the signal coming from the antenna is not integrated, it corresponds to the derivative of the

ambient electric field dE/dt. Some relevant findings on NBEs phenomenology have been obtained using dE/dt antennas [9]; [83]; [28].
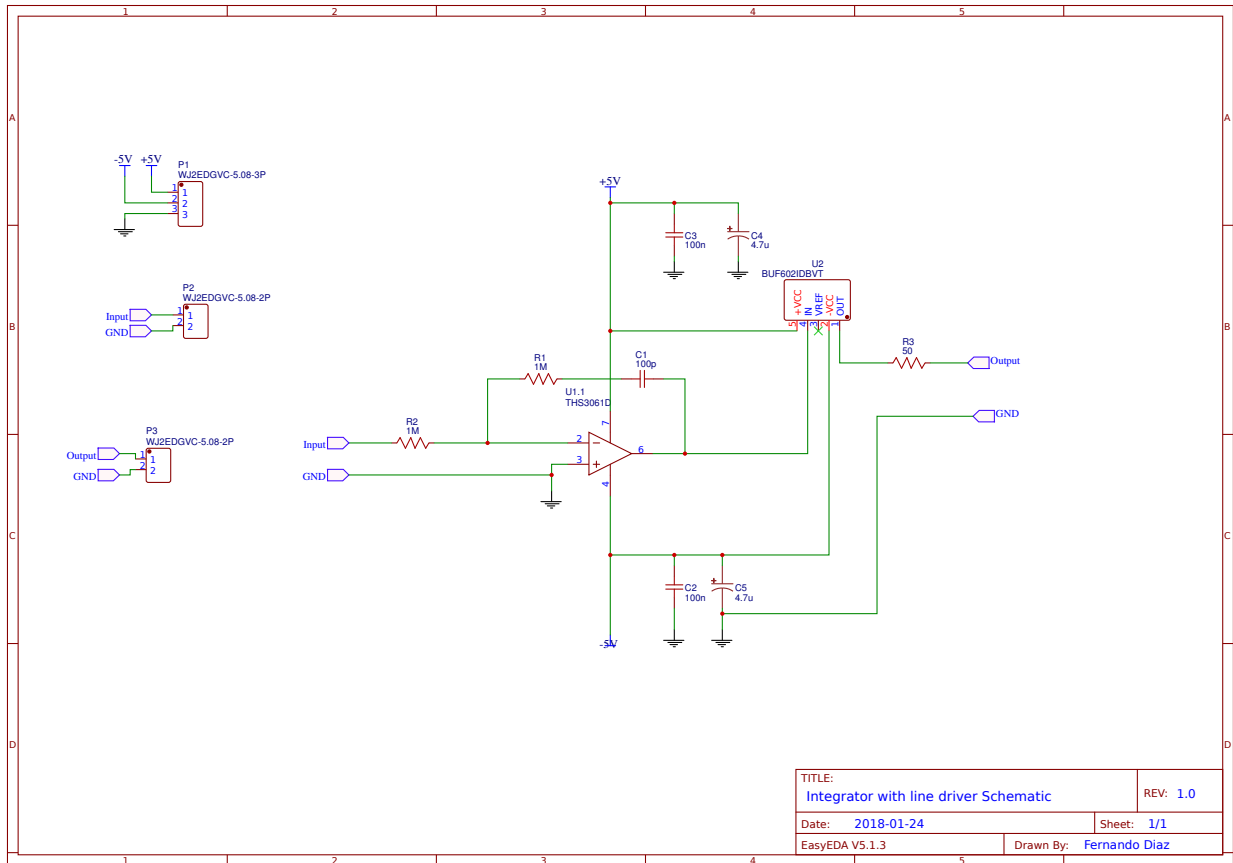
Figure 2-3.: Electronic schematic of integration stage for both FA and SA. The only difference between them is a change in time-constant values.

2.3.2. Broadband lightning interferometer

The first proof of concept of a lightning interferometer was developed by Warwick [84]. His work demonstrated the feasibility of tracking the motion of lightning inside the cloud. At the same time, Proctor [85] developed a Time-Of-Arrival (TOA) mapping technique to map discharge channels in the cloud. Later, Hayenga extended Warwick's work implementing perpendicular crossed baselines so the azimuth-elevation location could be determined with improved accuracy [86].

In 1989, Rhodes [87] increased central frequency from 34 MHz to 274 MHz to have a more compact baseline and more cycles per integration period. Shao [88] proposed baselines lengths that were not integer multiples of each other to solve fringes ambiguities. Kawasaki [89] developed techniques based on the principle that a single fixed pair of antennas is equivalent to having many

baselines. Finally, the latest developments in lightning interferometers are oriented to improve accuracy and reduce uncertainties [90].

Nowadays, a broadband lightning interferometer (INTF) can be defined as an array of closely spaced antennas, typically 10 to 100 m apart, devoted to detecting electric field emissions from lightning activity, centered around HF and VHF bands [91]. INTF aims to establish the spatial coordinates of the emission source by processing arriving signals. A single baseline provides enough information to calculate a single angle of arrival. Hence, it is required to have an additional baseline to establish two arrival angles, typically azimuth and elevation angles [92], [93]. Adding more baselines only improves estimation accuracy.

The azimuth angle tells the bearing of the emission source referenced to the North magnetic pole, and the elevation angle gives the bearing referenced to ground level. For a single INTF, these two angles can be plotted separately against time to show temporal evolution in each dimension. But a common representation is to combine both angles in a single plot. In this scenario, due to a lack of knowledge about the distance to the emission source, it is assumed the discharge occurs over an imaginary semi-hemisphere of normalized radius.

Regularly, INTF uses an array of flat plate antennas, but some implementations have used discone antennas, V dipoles, and loop antennas [94], [95], [35]. These alternatives aim to provide better antenna performance or to be more resilient to harsh weather, such as snow and heavy rain. For example, discone antennas offer better bandwidth; dipole antennas provide a better radiation pattern. Both antennas are better at dealing with snow and other types of precipitation.

The INTF operates as a standalone instrument, but complementary lightning instrumentation is required to have validated findings. Most of the time, this means working along with antennas intended to measure the same emissions, but in lower frequency bands or concurrently with other systems such as Lightning Mapping Arrays (LMA) or Lightning Location Systems (LLS) [96], [97].

A single INTF provides a source location in two dimensions. If three-dimensional coordinates are required, exist three alternatives: the first option is to use other INTF located some kilometers apart, and the second option is to use complementary instrumentation such as LMA or LLS. The third option is to make an educated guess based on assumptions of propagation speed [35], [98], [94], [99].

Nowadays, the procedure of estimating a single source location can be done thousands of times every second; thus, it is possible to follow the temporal development of an electrical discharge inside the cloud. That explains the main output of an INTF: a lightning map. With some additional work, it is possible to assemble individual pictures to produce a video, showing the temporal development of a discharge [100].
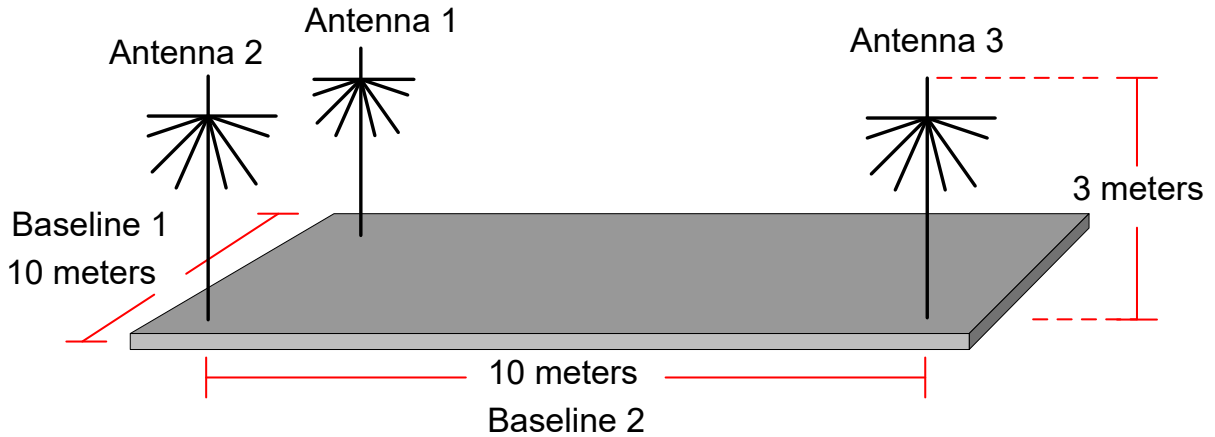
Figure 2-4.: The physical configuration of a typical lightning interferometer. The baseline is the separation between a pair of antennas. The optimum orientation is to align the baselines in North-South, East-West fashion.

Technically speaking, baselines' orientation can be arbitrary, but mathematical formulas demonstrate orthogonal orientation is the optimal setup. This configuration has the advantage of configuring three baselines with three antennas. Even more, orthogonal baselines should align in a North-South, East-West fashion. Any misalignment from this orientation can be compensated via factors in equations if this situation is intentional; otherwise, it adds an error in location accuracy. A detailed explanation of a set of generalized equations to calculate the source's location when there are an arbitrary orientation and non-orthogonal based lines are reported in Stock's dissertation [90].

INTF's main disadvantage is a high demand for the hardware involved in analog-to-digital conversion. For example, an INTF with 60 MHz bandwidth (e.g., 20 MHz to 80 MHz) demands a sampling rate of at least 160 $MSamples/s$. If three channels are considered with 8 bits resolution, the result is a continuous data stream of 480 MBytes every second. That amount of data imposes significant challenges for data acquisition, storage, and signal processing algorithms [100].

Due to the relatively short length of baselines, time difference estimation between signals is a challenging issue. The time difference is regularly assessed using the cross-correlation function. Therefore, the actual time difference comes after processing two-time series looking for a time difference or a phase difference between them [93].

For time difference, cross-correlation finds a lag related to the time delay between the signals. For phase difference, the phase spectrum of the cross-correlation function gives a linear function whose slope is the phase difference between signals [92].

3. Methodology

3.1. Introduction

This study aims to determine features of NBEs in Bogotá, Colombia providing insights into NBEs in a tropical region observed from an Andean high-plateau. The main contributions of this study are NBEs feature identification, built instrumentation, and collected data. This chapter is organized as follows: the first section presents the study design, and the second section describes data collection procedures. The third section details the instrumentation built for this study. The fourth section describes the methods of data processing employed and the fifth section introduces this study's limitations.

3.2. Study design

Previous studies have reported that thunderclouds in tropical regions have greater vertical development compared to those in subtropical latitudes [101]. This results in a more slender cloud structure, with a less intense mixed-phase region, and a higher ratio of IC to CG, making tropical regions a more favorable environment for studying intracloud activity.

The author's motivation is around lightning inception, thus the first step is to study NBEs because of their apparent relation to this process. In this context, the hypothesis driving the study was that NBEs features in Bogotá, Colombia, are not significantly different from those found in other tropical regions despite the city's altitude.

To fulfill its goal, the author designed and built a set of instruments to measure changes in electric and magnetic fields associated with lightning. The instruments form a lightning measurement station that includes electric field and magnetic field measurement subsystems and a broadband lightning interferometer. The author used Matlab (a numeric computing environment created by Mathworks) to develop software for filtering, pattern identification, location estimation, and data visualization. Matlab was chosen due to the author's familiarity with the software and its signal-processing toolboxes. The author used Matlab 2020a in the study.

3.3.   Data collection procedures

Lightning data was collected using the following principles:

- Principle 1: Data must be collected using random sampling, without prior selection of months, days, times, or storm types for the lightning measurement station operation.

- Principle 2: Data size was defined as "sampling to redundancy," without a prior size defined at the start of the study.

The result of these principles was to gather a vast data set for confident generalization of findings related to NBEs.

The available data ranges from November 14, 2019, to April 9, 2020, covering almost five months and 148 days, including the second rainy season of 2019 and most of the first rainy season of 2020.

This study collected 1,316 lightning events, recorded by the measurement station as single records of 500 ms from eight antennas (i.e., FA, SA, dE/dt, two loop antennas), and three interferometer antennas. Table **4-1** and Appendix B provide a brief and extended description of the data, respectively. The study had 148 days of continuous observations, 48 days of lightning activity, and 1,316 recorded events. Figure **3-1** is a bar diagram of daily observations over 148 days, showing two groups coinciding with the region's rainy seasons.

The 500 ms record length was chosen as a compromise between a wide observation window and the maximum record size set by data processing limitations. A 1 ms increase in observation time would result in 1 million additional samples per channel due to the BINTF's sampling rate.
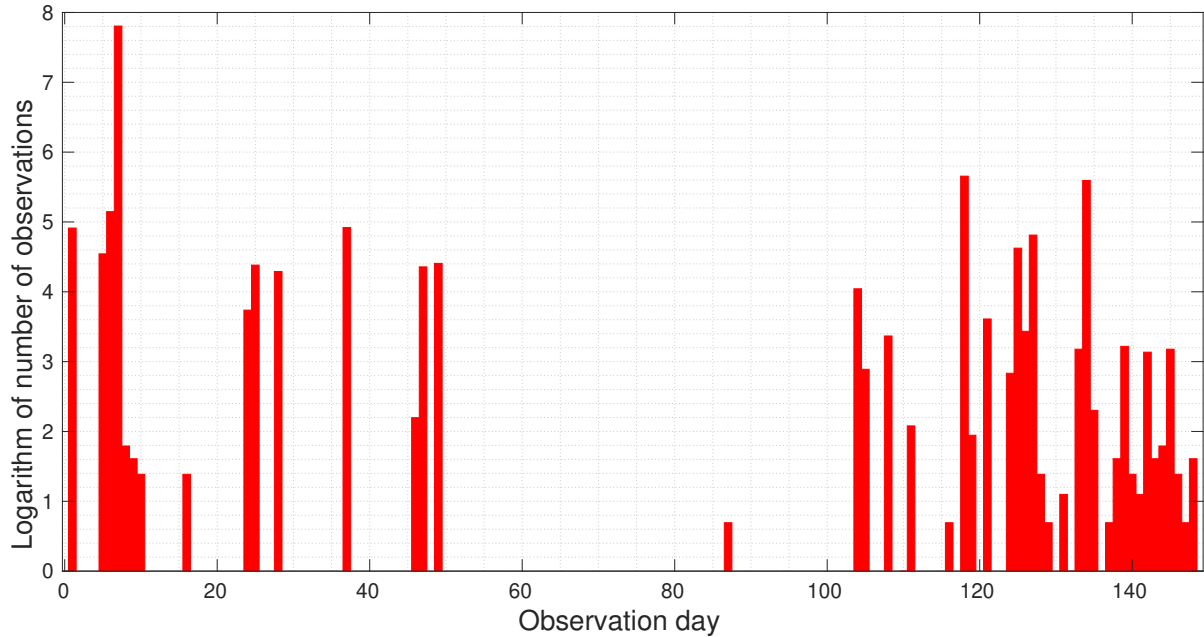
Figure 3-1.: A bar diagram shows 148 days of continuous observation, where the height of each bar represents the logarithm base 10 of the number of lightning events detected on that day. The grouping of bars matches the two rainy seasons at the observation site.

To verify that the records obtained by the measurement station were indeed related to lightning activity, the author used data from a lightning location system and compared the records with those from third-party instrumentation. The lightning location system (LLS) data was kindly provided by Mr. Ronald Holle, a senior scientist at Vaisala [1]. This data contains observations around Bogotá, Colombia, and covers an area of approximately 700,000 km^2. The data available ranges from January 1, 2016, to December 31, 2020, and includes around 79 million flashes, a sample of which is shown in Table **3-1**. By comparing the observation period of this study with the Vaisala data set, it was found that there were 1,313,830 flashes during the 148 days of observation.

LLS data is a relevant validation tool but has some drawbacks. First, LLS data does not differentiate between IC and CG as shown in the snippet presented in Table **3-1**. Second, LLS has a detection efficiency below 100 %, thus, some events are not recorded at all, and others are wrongfully identified [102]. Third, the detection efficiency is better for electrical discharges with predominant vertical channels, such as CG.

---

[1]https://www.vaisala.com/en/lightning-digital

Table 3-1.: Excerpt of LLS data provided by Vaisala for the area of study for the period from January 1, 2016, to December 31, 2020.

Event number	Date	Time	Latitude	Longitude	Peak current
60643408	2019-09-23	00:50:20.740	3.3616	-76.8464	-12.5 KA
60643409	2019-09-23	00:50:20.753	3.3963	-76.8125	-23.4 KA
60643410	2019-09-23	00:50:21.906	3.0627	-76.5683	-14.8 KA
606434118	2019-09-23	00:50:22.523	5.7304	-76.9572	-9.9 KA

3.3.1. Instrumentation development

The author designed and built lightning instrumentation to capture signals from thunderstorms for this study. The lightning measurement station comprises three modules: an electric field subsystem, a magnetic field subsystem, and a broadband lightning interferometer.

Magnetic field subsystem

The magnetic field subsystem, a VLF receiver, detects magnetic field variations generated by thunderstorms. The module comprises two loop antennas, orthogonally mounted, to offer an omnidirectional radiation pattern well suited for a direction-finding (DF) system. The loops were oriented in north-south and east-west directions.

Loop antennas are two equilateral triangles, 2 m side and 13 turns per loop using wire gauge 16 AWG. A single mast at the apex of both triangles is meant to support antennas. The final height of the array is 1,7 m. This configuration results in an antenna with an effective area of 1,7 m^2, antenna resistance of 1 Ω, and antenna inductance of 1 mH. Figure **3-2** shows a photograph of the antennas described.
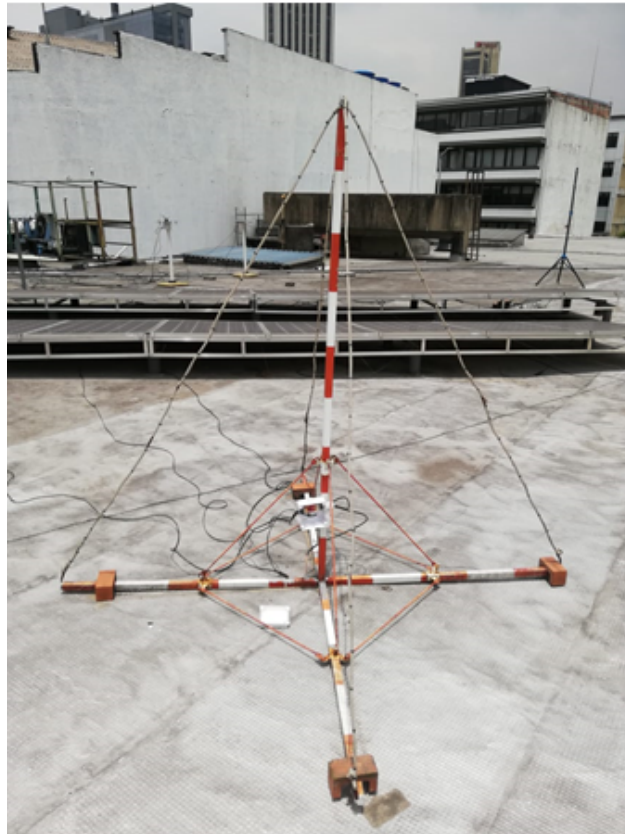
Figure 3-2.: Photograph of pair of loop antennas, orthogonally mounted, built for this study, deployed on a building's roof in the city center of Bogotá, Colombia.

One drawback of this type of antenna lies in its small value of radiation resistance, which limits the sensitivity of loop antennas. A summary of specifications for the constructed loop antennas is presented in Table **3-2**.

Table 3-2.: Compendium of loop antenna parameters.

Parameter	Value
Shape	Triangular
Length of side	$2,01\ m$
Area	$A = 1{,}752\ m^2$
Number of turns	$N = 13$
Wire diameter	$d = 1{,}2903 \times 10^{-3}\ m$
Inductance	$L = 1mH$
Resistance	$R_a = 1\ \Omega$
Sensitivity	$S_0 = 2{,}70 \times 10^{-4}\ VHz^{1/2}m^{-1}$

Each antenna is connected to a differential amplifier to filter and amplify the impinging signals. Figure **3-3** illustrates the electronic schematic and final implementation of these circuits.
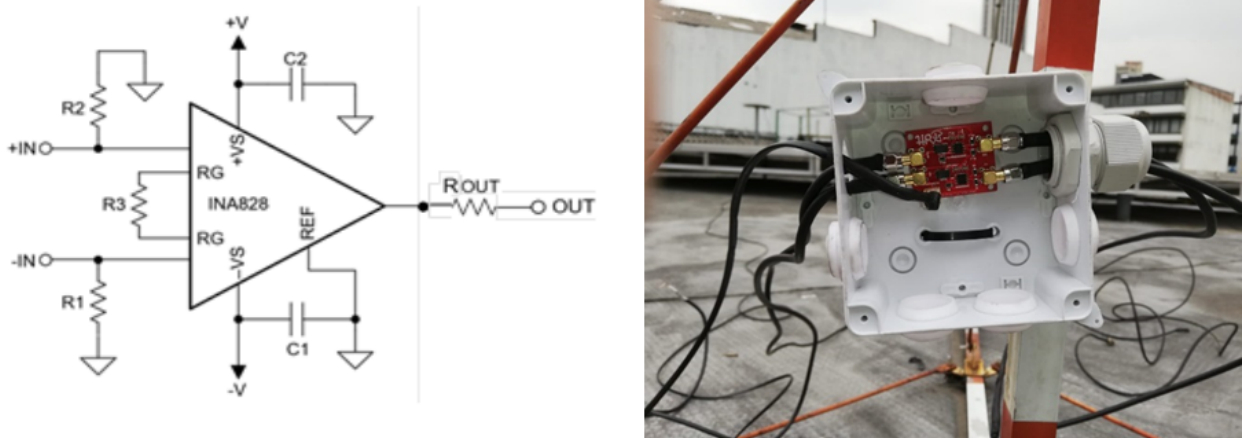
Figure 3-3.: Electronic schematic and picture of amplification and impedance circuits to conditioning signals coming from loop antennas.

Electric field subsystem

The electric field subsystem comprises three RF chains described as follows, and depicted in Figure **3-4**:

- One RF chain with a short time constant for an integration stage. This is the fast antenna (FA).

- One RF chain with a larger time constant for an integration stage. This is the slow antenna (SA).

- One RF chain without integration stage. This aims to measure the derivative of the ambient electric field. This is a dE/dt antenna.

- One GPS receiver to generate timestamps to mark acquired records.
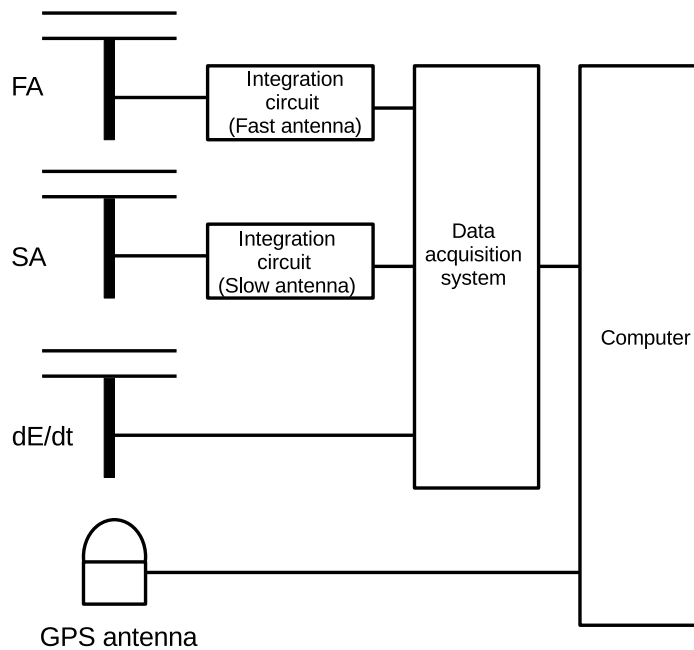
Figure 3-4.: Block diagram of measurement system for the ambient electric field, depicting three RF chains comprising the system. The GPS antenna aims to generate timestamps to mark records.

These three RF chains used flat plate antennas, which were made of circular plates cut from a 2 mm gauge aluminum sheet. The diameter of these circular plates was 0,45 m, and they were arranged in pairs to form a capacitor-like configuration [103]. The separation between plates was created using four 10 mm tall cylinders of high-density polyethylene. Electrical connections between plates, wires, and connectors were made using a mix of hand soldering and rivets. The resulting bandwidth of this configuration is about 30 Mhz.

After assembly, each antenna was oriented parallel to the ground to minimize the effect of the horizontal component of the ambient electric field. They were installed 1 m above the floor by a self-supporting tubular aluminum pole. Figure **3-5** shows photographs that depict the details of the described antenna.

Figure 3-5.: Photograph of a pair of flat plate antennas built for this study.

Fig. **3-6** shows the COMSOL model used to estimate the theoretical capacitance of flat plate antenna (156 pF). Then, experimental verification was done using an RCL meter (Phillips, PM6304 model) to determine the antenna's capacitance in a range from 100 Hz to 1 MHz. Figure **3-7** shows obtained results, where, the dotted line marks the theoretical (simulated) value of capacitance.

Surface: Electric potential (V)
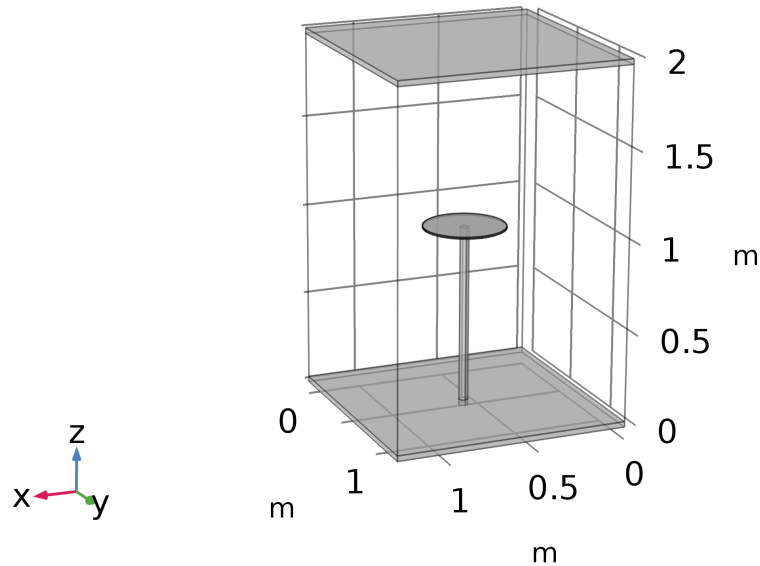
Figure 3-6.: Model used to simulate the behavior of flat plate antennas built for this study.

If the lower plate of the flat plate antenna is grounded, then, the non-grounded plate senses the vertical component of the ambient electric field.
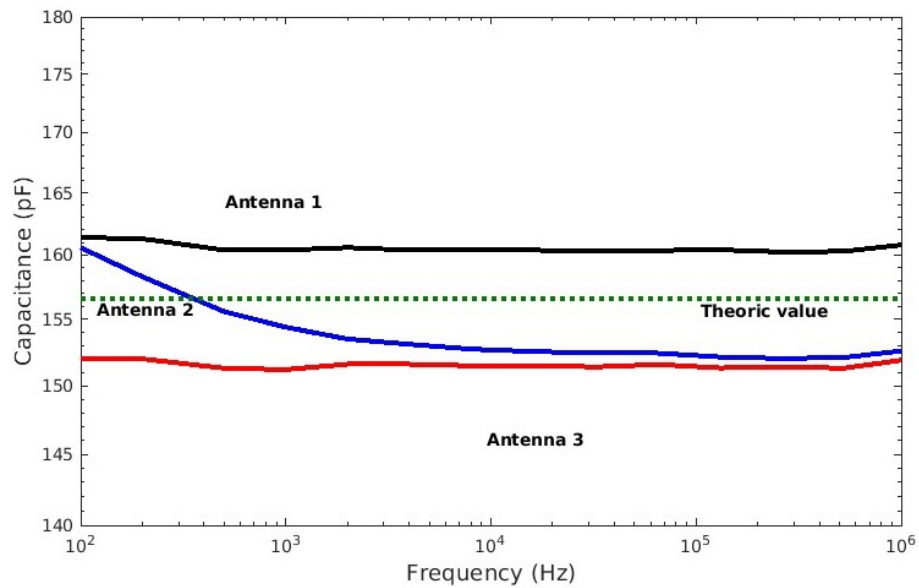
Figure 3-7.: Capacitance values were measured for three parallel flat-plate antennas ranging from 100 Hz to 1 MHz. The dotted green line is the reference showing the theoretical value of capacitance.

The bandwidth of the SA, FA, and dE/dt antennas were also calculated from laboratory-developed experimental measurements. The cut-off frequency was determined at -3 dB, and the frequency sweep step was set at 1 kHz. The measurements of both the SA and FA antennas included their respective integration circuits. Fig. **3-8** shows an experimental setup to measure the characteristics of flat plate antennas. The FA has an electronic decay time of 1 ms, while the SA has an electronic decay time of 10 s. The dE/dt antenna has a bandwidth ranging from about 0 Hz to 3.2 MHz. Additional calibration procedures and testing of the instruments mostly follow the described work by Rojas in his dissertation [104] .

Figure 3-8.: Physical setup used in laboratory facilities to determine physical characteristics of flat plate antennas built for this study.

Broadband lightning interferometer

The broadband lightning interferometer consists of an array of three antennas, a low-noise amplifier, a band-pass filter, a sampling system, a GPS receiver, and a storage unit. The antennas used in this implementation were vertical dipoles with a bandwidth of 20 MHz to 230 MHz. The antennas were located at the vertices of a right triangle with a baseline of 10 meters.
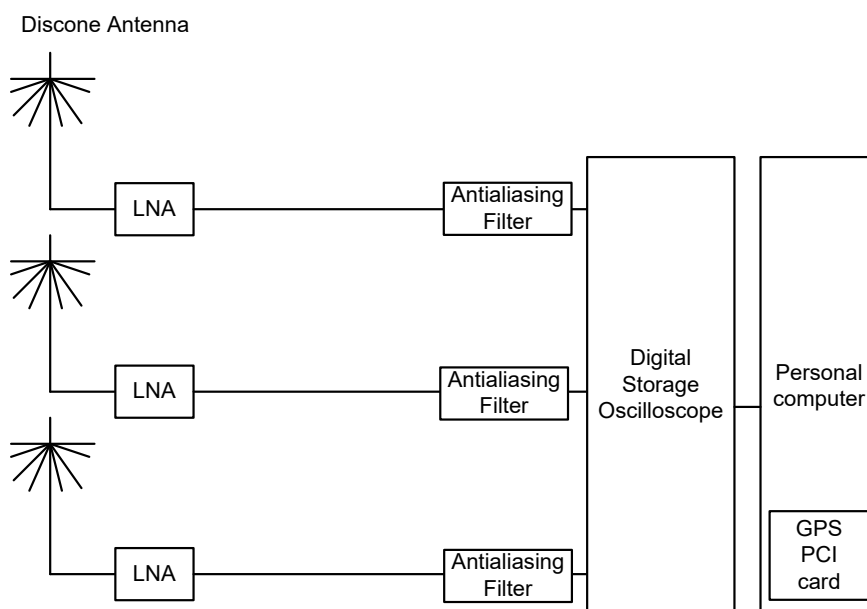
Figure 3-9.: Block diagram of a broadband lightning interferometer. Three RF chains configure two baselines, each with a low noise amplifier and an antialiasing filter before the data acquisition stage.

One baseline has a North-South orientation; meanwhile, the other has an East-West orientation. A low noise amplifier with a bandwidth from 10 MHz to 500 MHz and an anti-aliasing filter (DC to 81 MHz) cascaded together are connected to each antenna limiting the channel's bandwidth to 60 MHz (from 20 MHz to 80 MHz). The signals from the antennas were conducted to a four-channel oscilloscope (Picoscope 6404C) through segments of 20 meters of RG58 coaxial cable. Figure **3-9** shows a graphical depiction of the described instrument.

The sample time for analog to digital conversion was 3.2 ns, which means a sampling frequency of 312.5 MHz. This frequency imposes a practical upper limit to impinging signals of 156.25 MHz; additionally, every acquired sample is converted to a word of 8 bits. The record length was established to 350 ms with a pre-trigger time varying between 100 ms and 150 ms because the focus is on the initial activity. This setup produces 62.5 million samples per event. The entire system was triggered whenever a threshold was exceeded. Figure **3-10** shows a screen capture of one capture performed by INTF.
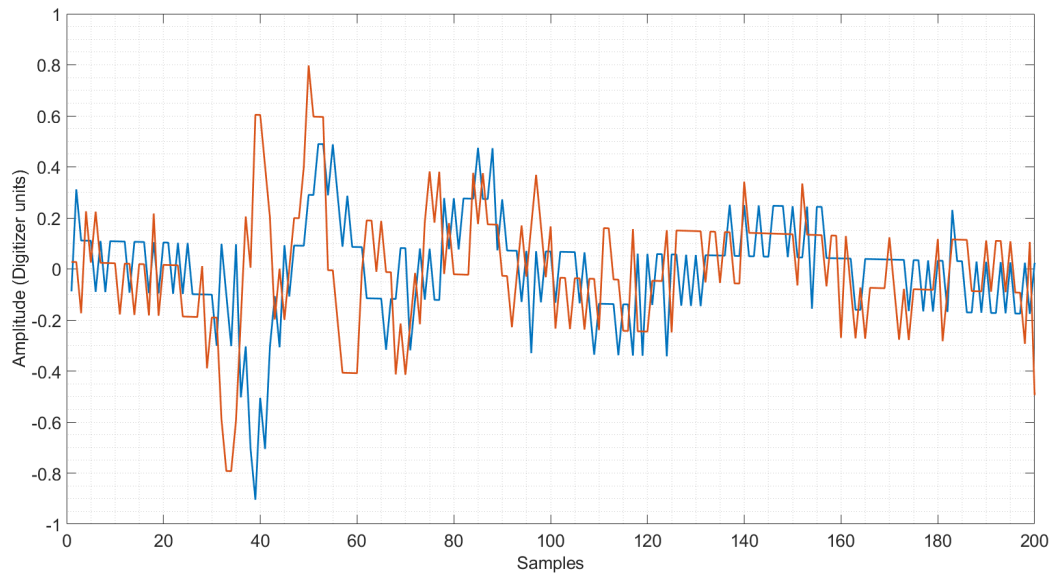
Figure 3-10.: A small segment of signals captured by the interferometer. The image shows a small time difference between signals that need to be estimated.

The deployment precise location of the lightning measurement station was on a building's roof located at the city center of Bogotá, Colombia (4° 36′ 46" N latitude, 74° 04′ 14" O longitude). Figure **3-11** shows the physical deployment of INTF's antennas.

Figure 3-11.: Depiction of the broadband lightning interferometer. The separation between antennas is 10 meters and the orientation of the array is North-South, East-West.

3.4. Data processing

As mentioned, signals from antennas were digitized by two oscilloscopes. The output of each oscilloscope is a single file with format *psdata* (*psdata* is the file format of Pico Technology) for every triggering event. Then, every record produces two *psdata* files, one from the $6404C$ model oscilloscope and one from the $5444D$ model oscilloscope. The first one has the signals from the INTF and FA. The second file has the signals from SA, dE/dt, and loop antennas. The files were stored continuously in a computer's hard drive every time a threshold trigger was exceeded. The threshold trigger was adjusted for one antenna of the INTF. Figure **3-12** shows a screen capture of the Picoscope program.
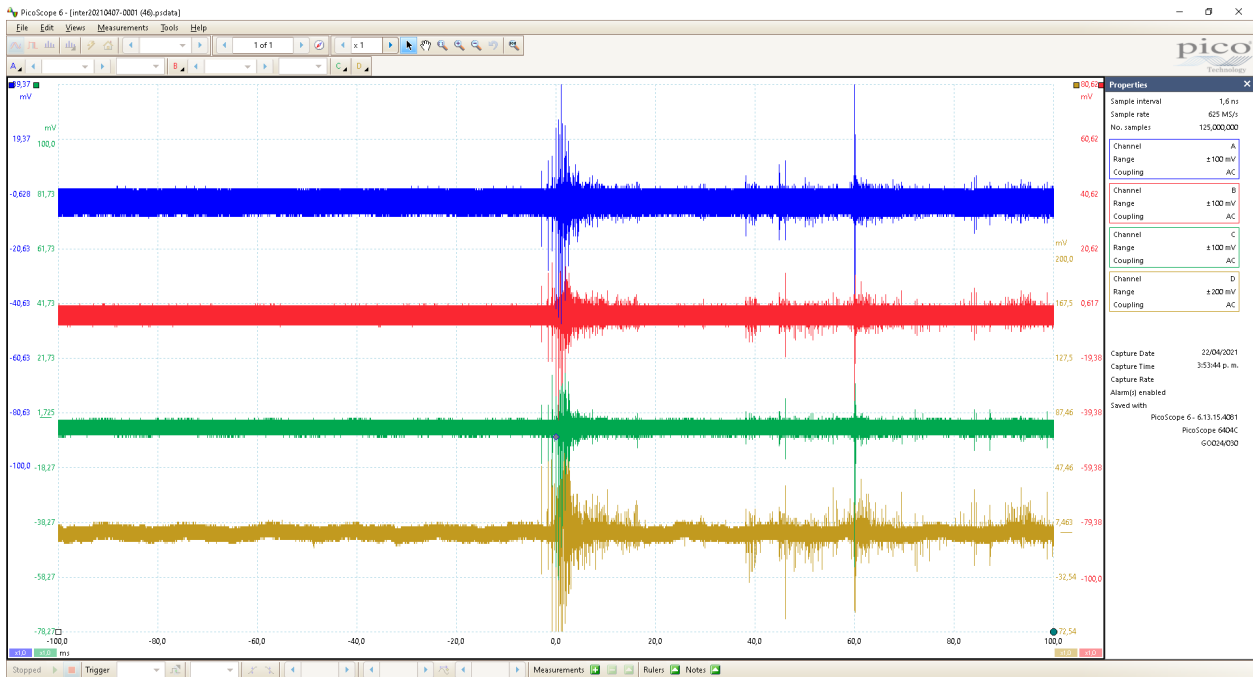
Figure 3-12.: Screenshot of Pico Technology software (PicoScope) that manages the digital oscilloscopes used by the lightning measurement station.

The *psdata* file format is not directly compatible with *Matlab*. Although oscilloscope's software can save data in real-time in *mat* format, this option only works with limitations, especially related to the size of files. Therefore, the best solution to this complication was recording samples in *psdata* format and then converting them to *mat* files. This process was time-consuming, but it was the way to extract the acquired data.

The software selected by the author to develop all programs required for processing lightning data in this study was *Matlab*, the numeric computing environment created by Mathworks. The selection was motivated by the author's familiarity with the software but especially by the vast set of toolboxes available to ease tasks required for signal processing. Several versions of *Matlab* were used but release 2020a was the last one used in this study.

Theoretical framework

Regarding its waveform, NBEs have two distinctive features: a unique bipolar waveform and short duration, usually less than 20 μs. The typical waveform has a main initial pulse followed by an opposite polarity overshoot. As mentioned, the polarity of the initial pulse defines the polarity of the NBE.

However, NBEs waveforms are not always equal due to additional ringing on the basic waveform. Identification of those additional structures is achieved by employing instruments with better accuracy, and higher sampling rates [47]. Consequently, it is possible to classify NBEs based on their waveforms. For this purpose, various approaches are defined, some recognizing four types, meanwhile, others identify eleven types of NBEs [51], [105].

At this point, it is relevant to mention the influence of propagation conditions on the waveforms detected. For example, measurements near the beach can assume lightning taking place above the ocean propagate over an infinite conductive path. Meanwhile, propagation over land means propagation occurs over a finite conductive path. The latter conditions mean a pulse detected will suffer from widening and distortion [106].

Regarding pulse duration, previous studies coincide in establishing a mean value around 20 μs with a fast rise time around 2 or 3 μs [44], [45], [38]. The rise time is one of the shortest known for intracloud discharges. A short duration suggests NBEs are linked to a spatially limited electrical discharge. This is the reason behind the name: compact intracloud discharge [12].

For this study, metrics to evaluate time-related features of NBEs are rise time, full width at half maximum (FWHM), zero-crossing time, and pulse duration. This set of metrics has been defined for a long time to assess waveform features therefore studies performed by Smith et al. [14], Sharma et al. [23], Nag et al. [21], Lu et al. [38], Karunarathne et al. [51] are examples of studies using the same metrics. The selection of the same metrics was intended to ease comparison purposes. Figure **3-13** presents the graphical description of the metrics and their respective definitions are as follows:

- Rise time: Time difference between the 10 % and 90 % of the maximum amplitude of the initial half cycle of the pulse.

- Full width at half maximum (FWHM): Time difference between the points of 50 % of the maximum amplitude of the initial half cycle of the pulse.

- Zero-crossing time: Time difference between the first and second zero-crossing point of the initial half cycle of the pulse.

- Pulse duration: Time difference between the 10 % of the maximum amplitude of the initial half-cycle and the 10 % of the maximum amplitude of the overshoot.
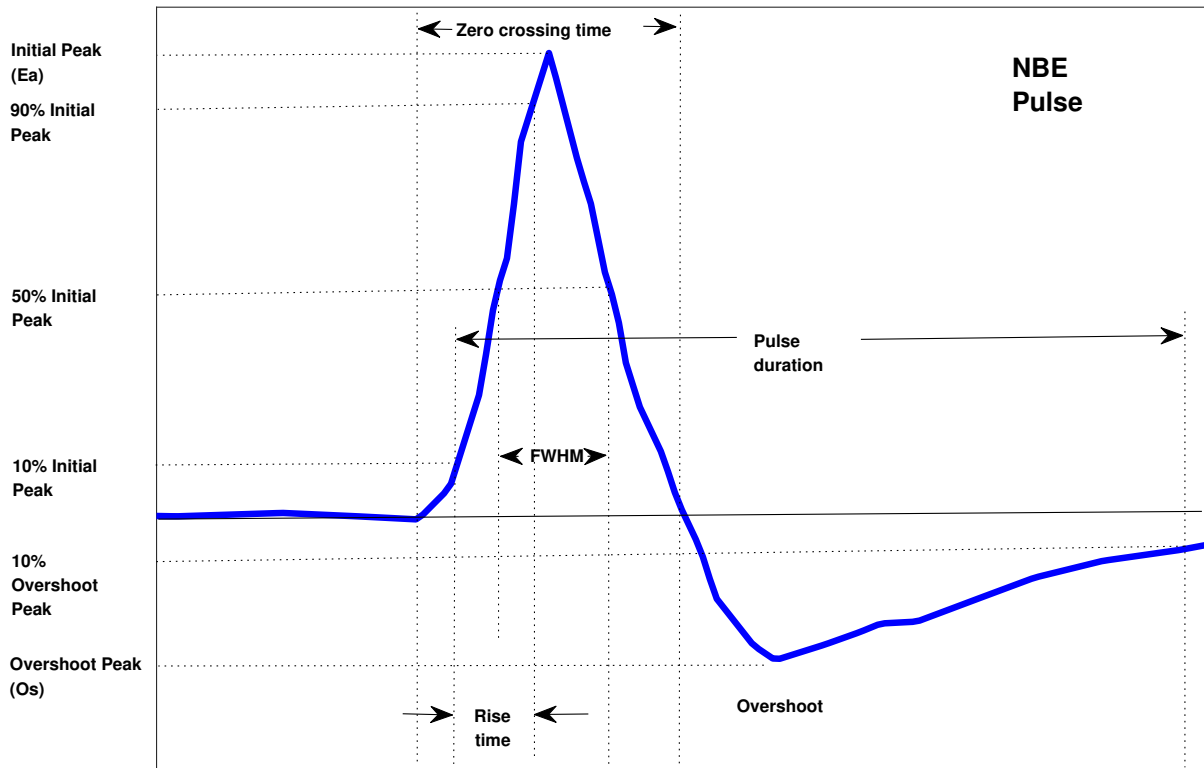
Figure 3-13.: Graphical description of metrics system used to assess time-related features of NBE pulses.

3.4.1.   Narrow bipolar events denoising

Karunarathne et al. [28] identified four NBE classes and Leal et al.[107] reported 11 classes. The two studies' findings overlap, with 4 of Leal's classes matching those of Karunarathne and 5 being variations of previous classes. The remaining class, NBE type 11, is a novel waveform. For this study, the 11 NBEs reported by Leal were selected.

A collection of 58 mother wavelets was chosen for this research, as each wavelet has unique characteristics that make it suitable for describing different types of waveforms. The properties such as orthogonality, compact support, symmetry, and vanishing moments affect the denoising results based on wavelet decomposition. The full list of wavelets is in Table **3-3**.

Table 3-3.: Complete list of wavelets used in this study to determine the best one to denoise NBEs.

Wavelet	Wavelet	Wavelet	Wavelet	Wavelet	Wavelet
Db1	Db11	Sym11	Bior2.2	Bior5.5	Rbio3.3
Db2	Sym2	Sym12	Bior2.4	Bior6.8	Rbio3.5
Db3	Sym3	Coif1	Bior2.6	Rbio1.1	Rbio3.7
Db4	Sym4	Coif2	Bior2.8	Rbio1.3	Rbio3.9
Db5	Sym5	Coif3	Bior3.1	Rbio1.5	Rbio4.4
Db6	Sym6	Coif4	Bior3.3	Rbio2.2	Rbio5.5
Db7	Sym7	Coif5	Bior3.5	Rbio2.4	Rbio6.8
Db8	Sym8	Bior1.1	Bior3.7	Rbio2.6	dmey
Db9	Sym9	Bior1.3	Bior3.9	Rbio2.8	
Db10	Sym10	Bior1.5	Bior4.4	Rbio3.1	

Denoising procedure

The denoising procedure simulates three scenarios: SNR equals 10dB, 0dB, and -10dB. Additive white Gaussian noise interferes with the signals and each pulse's simulation is repeated 100 times. Additionally, each simulation is performed 8 times, for each decomposition level, and repeated for every wavelet in the collection. This results in over 500,000 denoising calculations.

Entropy can be used as a measure of disorder in a dataset. This is relevant because entropy can manifest some hidden traits of datasets that are not obvious by other means as the mean or the median. However, entropy estimation is not a simple task, because of the bias that noise and size of data can introduce in calculations. Nowadays exist, two popular algorithms to estimate the entropy of a dataset, namely approximate entropy (appEn) and sample entropy (SampEn). The latter is a mathematical algorithm well-suited for the quantification of regularity in short and noisy data sets. A low value in this metric indicates that the time series is deterministic, while a high value indicates randomness. Due to the random nature of noise, a low value of SampEn is a valid metric to assess the presence of noise in a signal.

In two out of three different SNR scenarios, rigrsure gives the best results using statistical parameters as metric for selection. Soft thresholding gives the best result in all three scenarios. Finally, Fig. **3-14** shows the outcomes for mother wavelet selection, in this case, rbio 3.1 is the best option. In this way, for denoising purposes, wavelet rbio3.1 with four-level decomposition, soft

thresholding, and rigrsure threshold is the optimal selection to denoise NBEs pulses up to -10 dB SNR.
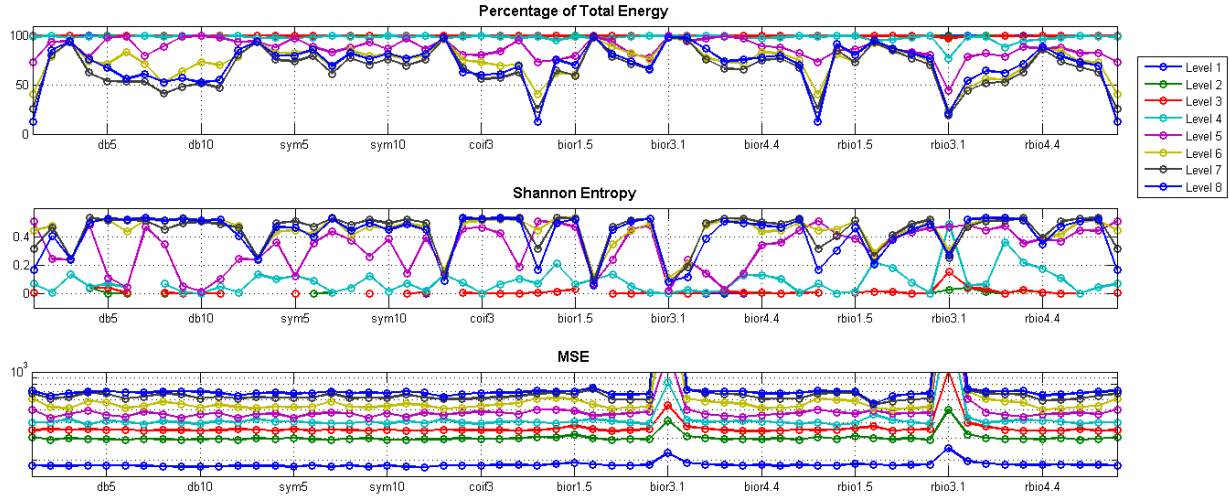
Figure 3-14.: Graphical description of metrics system used to determine best wavelet to denoise NBEs pulses.

3.4.2.   Narrow bipolar events identification

Identification of NBEs was made in four stages: the first stage aimed at noise removal from the acquired signal, the second stage intended to identify NBEs positively, the third stage was a classification process based on NBE waveforms, and finally, the fourth stage comprised measurement of individual NBE features.

The mentioned process was done on all recorded lightning events (i.e., 1,316 records). The whole process was computing-intense because each event contains more than seven million samples per record that were checked in small batches of 512 samples to find an NBE.

In the first stage, signals from FA were digitally filtered with a lowpass filter. The employed filter was an IIR (infinite impulse response filter) with a cut-off frequency of 630 kHz aimed to remove unwanted high-frequency signals. Figure **3-15** and Figure **3-16** show both frequency response and zero-pole map of the referred lowpass filter. Also, a digital bandstop filter was used to remove the unwanted presence of hum interference (i.e., 60 Hz interference).
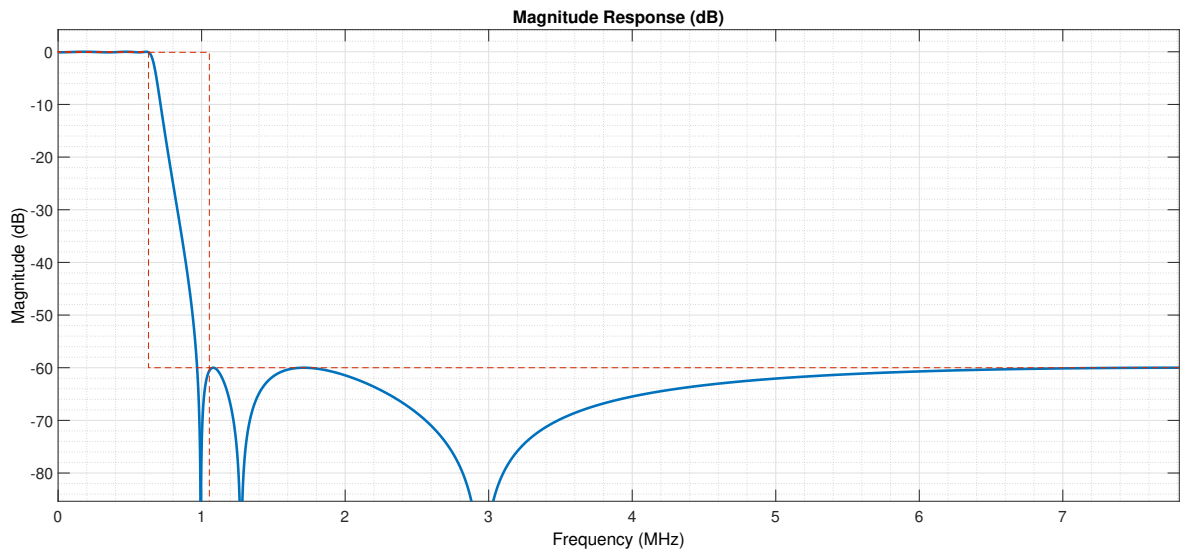
Figure 3-15.: Frequency response of lowpass filter used to filter signals acquired before NBE detection.
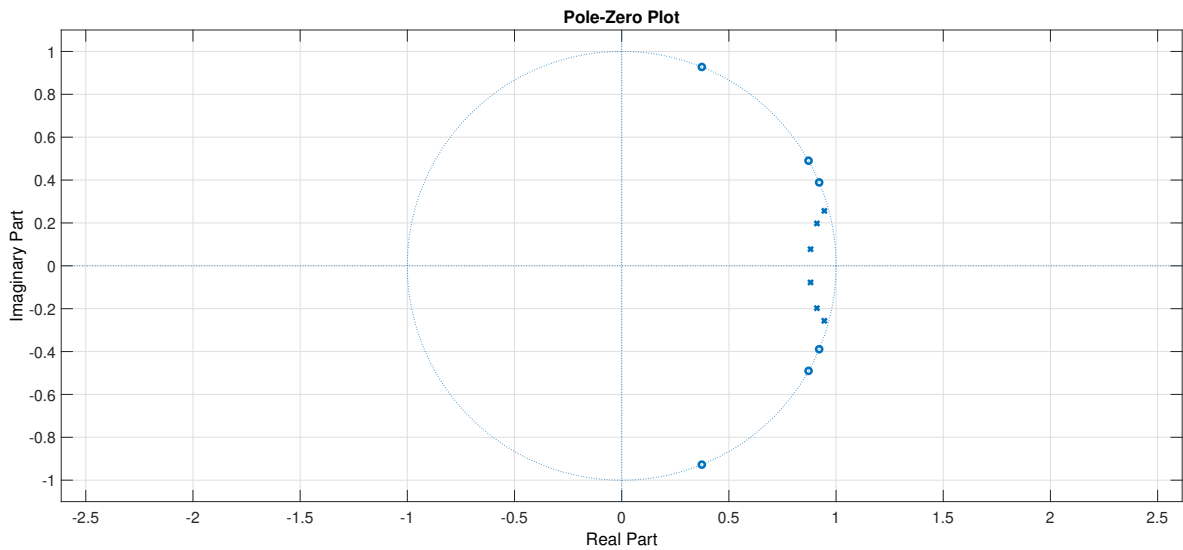
Figure 3-16.: Zero pole map of lowpass filter used to filter signals acquired before NBE detection.

After filtering, signals were normalized using a z-score approach. The advantage of this normalization is signal retains its waveform properties; meanwhile, the mean value of the signal becomes 0. Equation 3-1 shows the mentioned approach. Here x is the sample data, μ is the mean value, and σ is the standard deviation of x. Figure **3-17** shows a comparison between a sample window and its normalized version.

$$z = \frac{x - \mu}{\sigma} \tag{3-1}$$
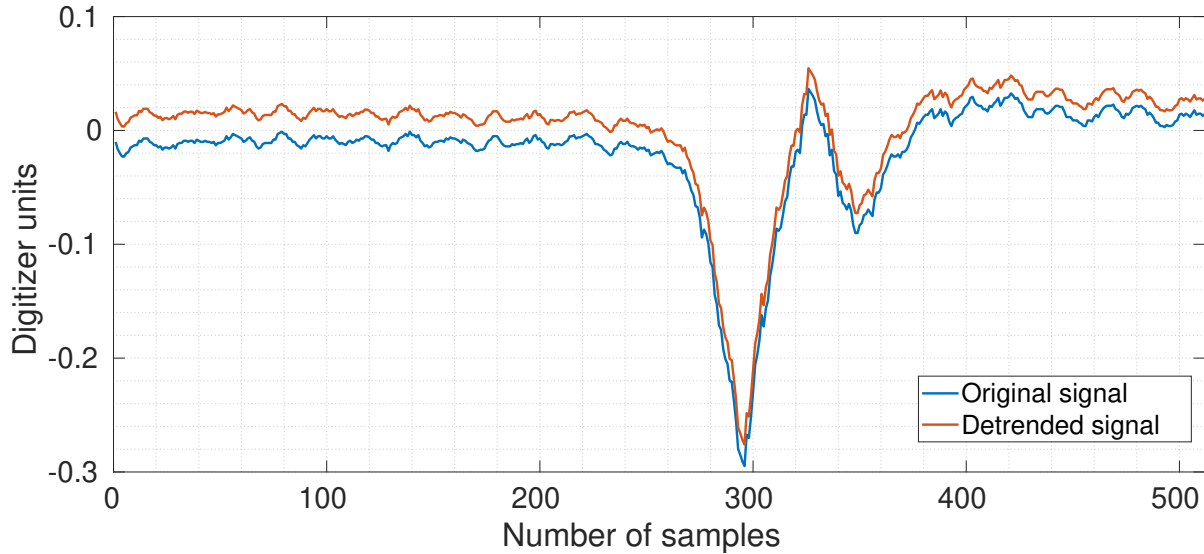
Figure 3-17.: Example of a normalized signal compared with its original version.

The second stage aims for the NBEs identification. Filtered signals were divided into segments of (65,5 μs) to compare against an NBE template through a correlation function. The referred template pondered typical NBE waveforms reported in a previous study. A single template suits better to tolerate slight differences between pulses because of additional ringing structures after or before main pulses.

The reference template was a calculation extracted from a scheme classification proposed by Leal et al. in a paper of 2017 [105]. In that paper, eleven types of NBEs were proposed; thus, the author calculated the mean value of all of them. The left side of Figure **3-18** shows the eleven kinds of NBEs proposed by Leal et al., meanwhile, the right side shows the average signal computed in this study as a reference pattern for NBE identification.

These four features were chosen in agreement with legacy studies such as Ahmad et al. [47] that discussed the presence of additional ringing or fines pulses on the basic waveform of an NBE.
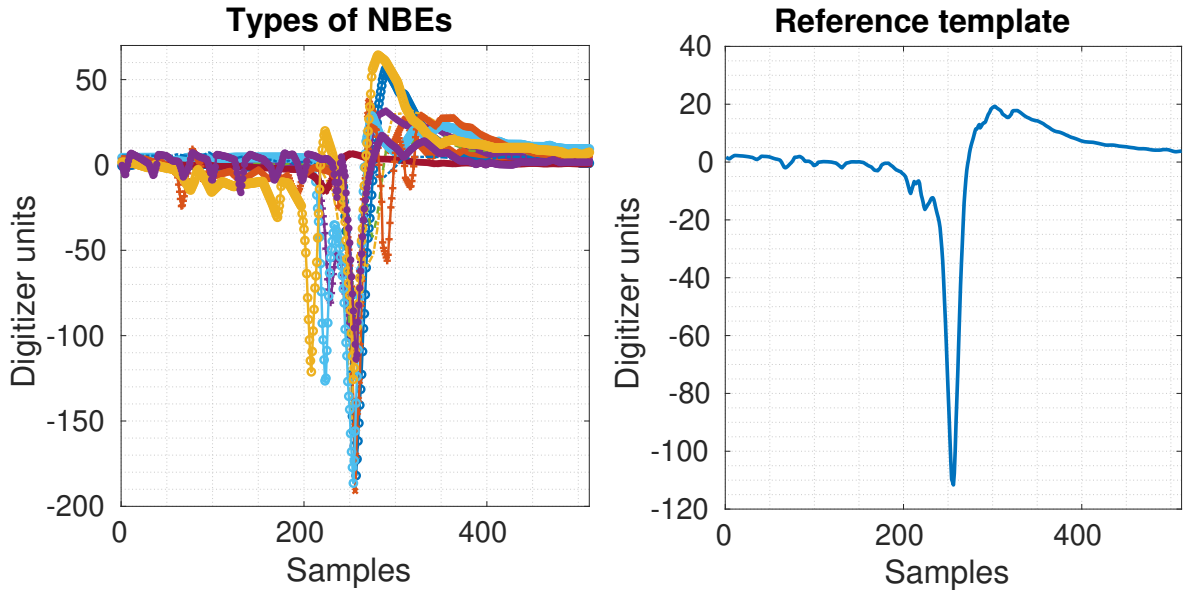
Figure 3-18.: The left side corresponds to 11 types of NBEs reported by Leal et al. [105]. The right side shows the reference pattern obtained as an average value of 11 types of NBEs.

An observation window and the reference pattern were processed using a sliding window approach to identify potential NBEs. The approach had a step of 128 samples over the record, resulting in over 65,000 windows per lightning event. Four consecutive windows were weighted equally to form one candidate and if their final value was above the decision threshold, the window was marked as a potential NBE.

The frequency spectrum of each potential NBE was analyzed using a non-parametric approach, specifically Thomson's multitaper power spectral method, to obtain a more reliable signal representation. An example of this estimation is shown in Figure **3-19**.

Equation 3-2 and Equation 3-3 show the mathematical description of the method used for spectral estimation. Equation 3-2 explains how the method uses K different Slepian sequences to obtain K different periodograms.

$$S_k(f) = \Delta t \left| \sum_{n=0}^{N-1} g_k(n)x(n)e^{-j2\pi f n\Delta t} \right|^2 \tag{3-2}$$

Meanwhile, Equation 3-3 shows that outcome is just the average of the K modified periodograms.

$$S^{(MT)}(f) = \frac{1}{K} \sum_{k=0}^{K-1} S_k(f) \tag{3-3}$$
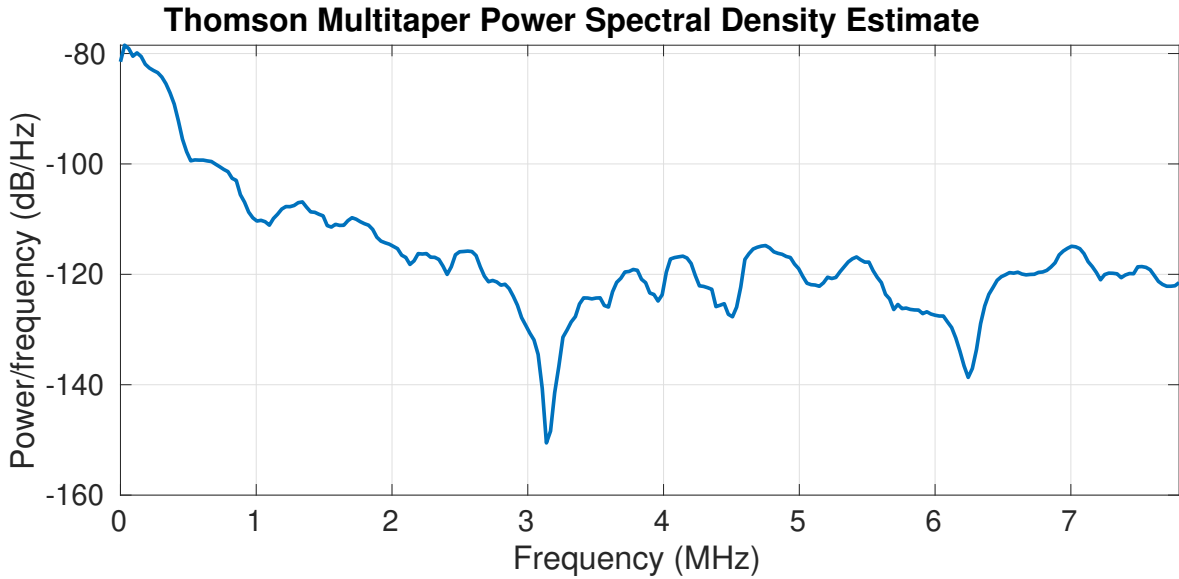
Figure 3-19.: Non-parametric estimation of the power density of NBE pulse detected over Bogotá on November 14, 2019.

Frequency analysis of candidate NBE is necessary because NBE's spectrum has a typical pattern showing a steady magnitude decrease from tens of kHz to about 3 MHz [108]. This behaviour can be corroborated in Figure **3-19**.

The methods described ensure reliable identification of NBE because they combine both time and frequency domain analysis.

3.4.3.   Data processing from broadband lightning interferometer

The location of a VHF source is a process heavily dependent on precise estimation of time delay between a pair of signals [109]. Time delay estimation must be a piece of reliable information because it is a fundamental value to compute bearing angles for the location of a source. An accurate assessment is challenging because the range of values is diminutive (i.e., tens of nanoseconds). Therefore, even the slightest error in mathematical calculation produces a bias on angle estimation [110].

To solve the challenge, precision on hardware features related to INTF is necessary. Baselines orientation, antenna height, baseline length, or cable longitude are crucial aspects for the successful operation of the instrument. Furthermore, connectors and circuits were double-checked to assess additional delay values, bandwidth limitations, and other losses due to these components or external interference [111].

Once counting on reliable information from the antennas, the standard approach to assess time delay is to obtain cross-correlation functions from pairs of signals. The location of the peak value is related to a time value where the two signals align. Thus, a zero lag means a pair of signals arrived simultaneously at INTF. Equation 3-4 shows the definition of the cross-correlation function used in this work.

$$R(\tau) = X(f)Y^*(f) \tag{3-4}$$

Generally, a pre-filtering stage improves estimation and reduces windowing effects. The addition of referred stage is known as the generalized cross-correlation function (GCC). The "generalized"term refers to a weighting function [112]. There are plenty of variations around these weighting functions that are out of the scope of this study; thus, the author, for the interested reader, suggests some excellent articles about this subject [113],[114]. Equation 3-5 shows a definition of the generalized cross-correlation function. From Equation 3-4 and Equation 3-5, it is an apparent difference between them lies in a presence of a weighting function $W(f)$.

$$R_{gcc}(\tau) = W(f)X(f)Y^*(f) \tag{3-5}$$

where $W(f)$ corresponds to the Fourier Transform of the weighting function; $X(f)$ and $Y(f)$ correspond to the Fourier Transform of received signals.

The disadvantage of using GCC or any other method related to the cross-correlation function is that the estimated time delay is always a multiple of the sample time. This negative aspect forces additional processing such as interpolation around the peak value to get a better result closer to the actual value of time delay [90].

An additional disadvantage is identifying an exact maximum value in the cross-correlation function because this task is challenging with noisy signals. As a result, the function tends to have a broader peak, adding uncertainty to the calculated maximum value. This broadening effect is undesirable because uncertainty rises in this scenario worsening time-delay estimation.

Figure **3-20** explains this scenario. The first plot depicts the resulting cross-correlation function in an ideal context. The plot corresponds to the cross-correlation function of the reference pattern with its delayed version. The second plot corresponds to the cross-correlation function of a pair of noisy signals. A comparison between these two results makes clear the effect of noise. The third plot shows a close-up of the peak value, making clear the uncertainty about the actual value of the maximum. The ordinary solution to this problem is to interpolate around the peak of the curve.
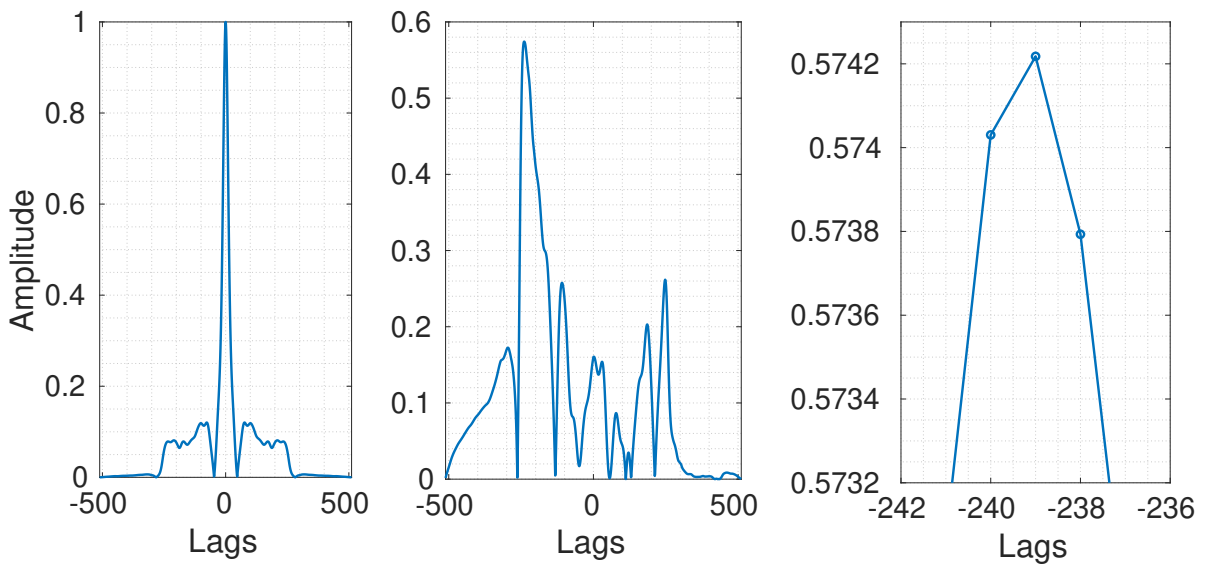
Figure 3-20.: The left side figure depicts the cross-correlation function of an NBE with high SNR. The center plot shows the crosscorrelation function of an NBE with low SNR. The right side shows a close-up of the center plot. It is apparent the uncertainty about the actual value of the maximum in the noisy scenario.

Consequently, uncertainty around the peak location of the cross-correlation function is a reason to find some alternatives to improve the accuracy of the current method. The idea to solve this problem came from a well-known technique applied to seismic signals. The approach is used in seismology to identify patterns from instant values, both amplitude and frequency of seismic signals [115], [116]. To achieve its aim procedure involves converting real-valued signals to analytic signals and using them to perform required cross-correlation.

The analytic signal approach

In 1948, Ville presented the notion and potential applications of analytic signals in signal processing [117]. Since then, this signal representation has proved to be quite convenient in fields like seismology and telecommunications. The main feature of analytic signals is a magnitude value

of zero for all the negative parts of its frequency spectrum. This concept is illustrated in Figure **3-21**.
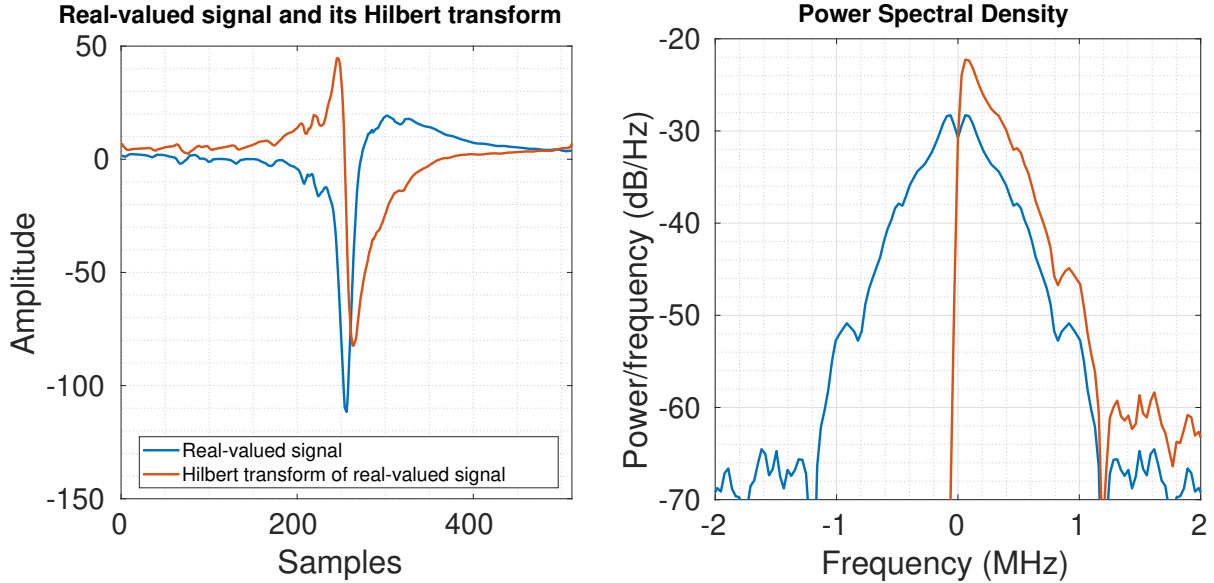
Figure 3-21.: The left side image compares a real-valued NBE and its corresponding Hilbert transform. The right side image shows the power spectral density of a real-valued NBE and its corresponding analytic-valued version.

An analytic signal results from adding a real-valued signal plus its Hilbert-transformed version. In this context, the input signal is the in-phase signal, and the output signal is the quadrature signal (i.e., the analytic signal). The principal component of this procedure is the Hilbert transform, whose Fourier transform is defined as shown in Equation 3-6.

$$H(f) = \begin{cases} -j & \text{if } f \geq 0 \\ j & \text{if } f < 0 \end{cases} \tag{3-6}$$

The previous definition means Hilbert transform works as an all-pass filter, non affecting the magnitude component of the frequency spectrum but the phase component. The transform only changes the phase of the real-valued signal by $-90°$. An expression for the Hilbert transform in the time domain is obtained using the inverse Fourier transform, as expressed in Equation 3-7.

$$y(t) = HT\{x(t)\} = \widehat{x}(t) = \frac{1}{\pi t} * x(t) \tag{3-7}$$

Figure **3-22** illustrates the frequency spectrum of Hilbert transform described in previous equations.
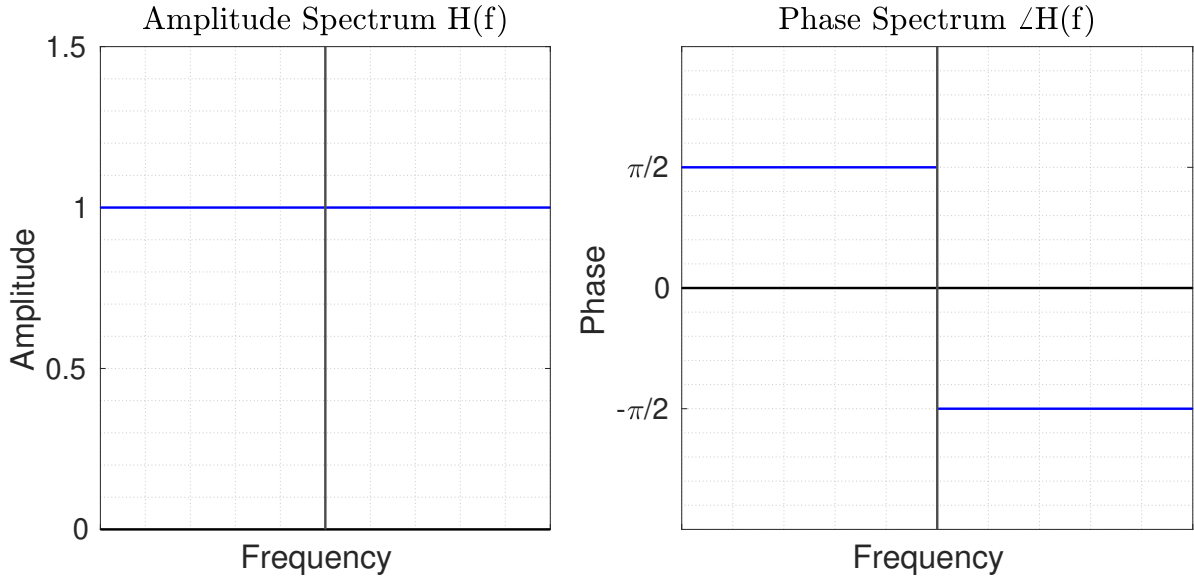
Figure 3-22.: Amplitude and phase-frequency spectrum of Hilbert transform. This shows transformation behaves as an all-pass filter non affecting amplitude spectrum. On the contrary, the phase is affected, including an additional 90° phase.

Fourier transform of an analytic signal $(\widehat{X}(f))$, can be seen as the multiplication of the Fourier transform of the real-valued signal times a signum function. This representation is presented in Equation 3-8.

$$Y(f) = \widehat{X}(f) = -j sgn(f) \times X(f) \tag{3-8}$$

The mentioned expressions apply to continuous-time signals. For discrete-time signals, the expressions are modified considering the periodicity of their Fourier transform. This condition can be seen in the adjusted definition presented in Equation 3-9.

$$H(\Omega) = \begin{cases} -j & \text{if} \quad 0 \leq \Omega \leq \pi \\ j & \text{if} \ -\pi < \Omega < 0 \end{cases} \tag{3-9}$$

Again, taking the inverse Fourier transform, we have an expression in the discrete-time domain

calculated over one period of Ω.

$$h[n] = \frac{1}{2\pi} \int_{-\pi}^{\pi} H(\Omega)e^{jn\Omega} \tag{3-10}$$

The discrete-time domain expression is not constant but a *sinc* function due to the bounded nature of the in-phase signal (i.e., a finite number of samples of the input signal).

$$h[n] = \begin{cases} \frac{2}{\pi} \frac{sin^2(n\pi/2)}{n} & \text{if} \quad n \neq 0 \\ 0 & \text{if} \quad n = 0 \end{cases} \tag{3-11}$$

Therefore, summing the real-valued signal and its Hilbert transformed version, it is established a definition for an analytic signal as shown in Equation 3-12.

$$z(t) = x(t) + HT\{x(t)\} = x(t) + j\widehat{x}(t) \tag{3-12}$$

The corresponding discrete-time Fourier transform of Equation 3-12 is shown in Equation 3-13

$$Z(f) = X(f) + jsgn(f)X(f) \tag{3-13}$$

or alternatively as in Equation 3-14.

$$Z(f) = \begin{cases} 2X(f) & \text{if} \quad f \geq 0 \\ 0 & \text{if} \quad f < 0 \end{cases} \tag{3-14}$$

Analityc signals and cross-correlation function

Analytic signals bring novelty in time delay estimation because the cross-correlation of real-valued signals is always related to a lag where the function's maximum occurs. This approach works appropriately with noise-free signals or high SNR signals. However, frequently acquired signals by INTF have low SNR. In the presence of noise, the peak of the cross-correlation function has an un-sharpened peak. This condition adds uncertainty to precise time delay estimation and

forces additional processing to estimate a more accurate value.

On the other hand, the cross-correlation function between pairs of analytic signals is always an odd function, which means time delay is invariably related to a zero-crossing point instead of a maximum point of a curve. This change reduces uncertainty because consistently, there is only a single point where the function crosses zero. Consequently, further calculations are no longer required saving processing time dedicated to this task.

To exemplify the advantage of calculating a time delay using analytic signals, Figure **3-23** shows cross-correlation functions of noisy signals. One used real-valued signals and the other an analytical version of them. For the real-valued signals, there is uncertainty about the peak value location. Meanwhile, in the second approach, it is quite simple to establish the zero-crossing point of the cross-correlation function. The latter is a single point without uncertainty about its actual location. Thus, no more calculations are required to establish the time delay.

Due to the cyclic nature of the discrete-time cross-correlation function, in this study, an unbiased cross-correlation operator was used to get a more accurate result. That approach implies adding zeros (i.e., zero padding) to incumbent signals to simulate an acyclic operation.
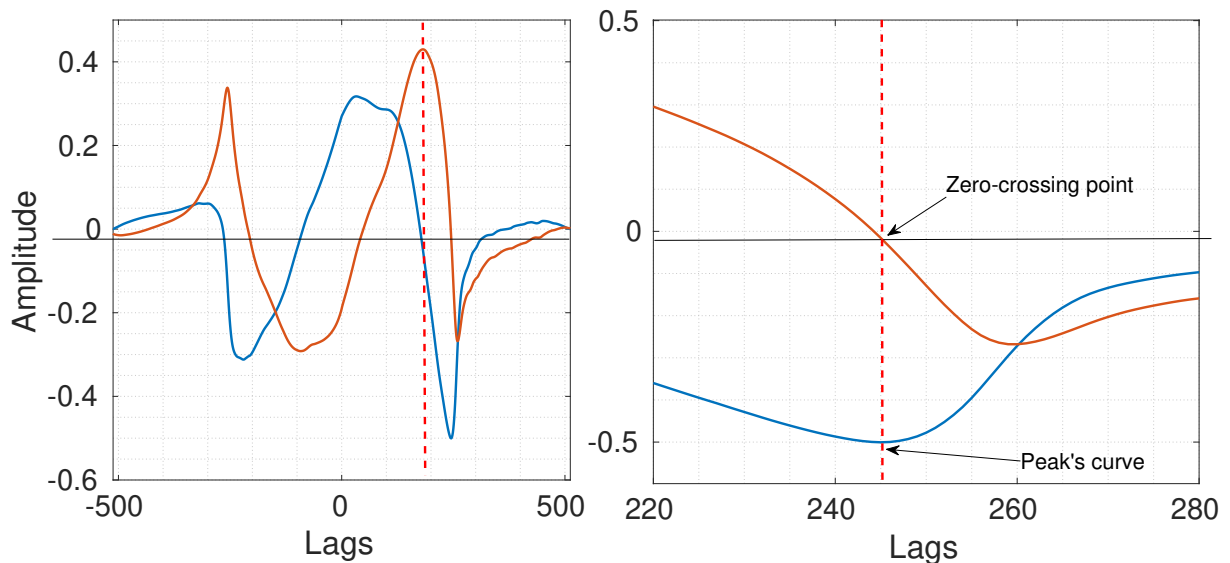
Figure 3-23.: Cross-correlation function of a candidate NBE using both its real-valued and its analytic version. The left side image shows two cross-correlation functions. The right side image shows a close-up of the zero-crossing point versus the maximum value of the curve.

Source location using broadband lightning interferometer

Signals impinging on a baseline pair of antennas differ in time of arrival. In other words, there is a time delay between them (τ_d). If the time delay is known, then the relation between this value and the angle of arrival (α) can be expressed as shown in Equation 3-15. In this equation, d is the baseline (i.e., the separation between antennas in meters), and v is the propagation speed of waves through the atmosphere, generally assumed equal to the speed of light. The value of the angle of arrival, β, comes from the other baseline.

$$\alpha = acos\left(\frac{c \times \tau_{d1}}{d}\right) \tag{3-15}$$

Then azimuth (AZ) and elevation (EL) angles are estimated combining the arrival angles (α and β) as shown in Equation 3-16.

$$\cos\left(\alpha\right) = \sin\left(AZ\right)\cos\left(EL\right)$$
$$\cos\left(\beta\right) = \cos\left(AZ\right)\cos\left(EL\right) \tag{3-16}$$

Indeed, expressing α and β as functions of their respective time delays, τ_{d1} and τ_{d2}, AZ and EL, can be calculated as shown in Equation3-17.

$$AZ = atan\left(\frac{\tau_{d1}}{\tau_{d2}}\right)$$
$$EL = acos\left(\frac{v}{d}\sqrt{\tau_{d1}^2 + \tau_{d2}^2}\right)$$
$$or \tag{3-17}$$
$$AZ = atan\left(\frac{\beta}{\alpha}\right)$$
$$EL = acos\left(\sqrt{\beta^2 + \alpha^2}\right)$$
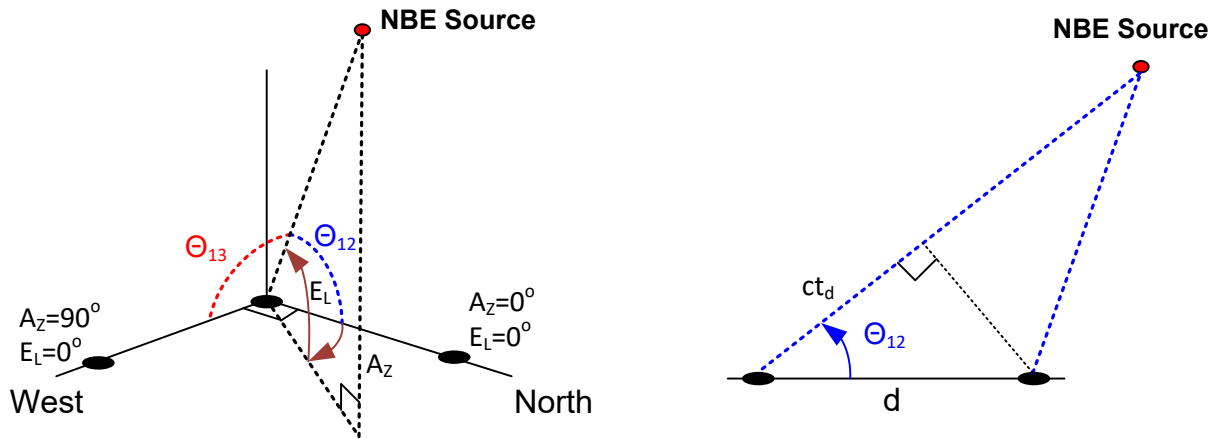
Figure 3-24.: The lightning interferometer's geometry to estimate the emission source's location. The right-hand image shows the definition of the angle of arrival for a single baseline. The left-side image shows the combination of two baselines resulting in the location of a source defined by its azimuth and elevation angles.

INTF estimates delay thousands of times for a single lightning event. Indeed, there are millions of samples in an observation window of 200 ms. In this way, it is possible to find thousands of emission sources during that lapse. The number of sources found depends on the algorithm used to process data. Generally, more processing allows the detection of more sources, but processing time also increases rampantly. A higher number of sources is due to the algorithm's ability to detect weaker emissions. The success of this operation is defined by the amount of overlapping in a sliding window approach. In this work, overlapping uses two or more continuous windows to detect one source.

3.5. Limitations

3.5.1. Limitations related to the electric field subsystem

Both installation and placement of antennas impact the measured value of the ambient electric field. This value turns out to be affected by mismatches of impedance in the RF chain, insertion losses, the noise figure of hardware, external interference, antenna coupling, and the effective height of the antenna, among others. All these factors are summarized under the measuring factor concept, which adjusts the measured value to compensate for all mentioned effects. For SA and FA antennae, the measuring factor has a value of 0.85; meanwhile, dE/dt antenna's measuring factor is 0.8. The difference between values is due to the absence of the antenna's integration circuit.

3.5.2.   Limitations related to the broadband lightning interferometer

Angular resolution

The angular resolution refers to the ability of INTF to distinguish between two RF sources. If separation is by an angle smaller than angular resolution and coincides, then sources are indistinguishable. From diffraction theory, specifically the Rayleigh criterion, it is established that angular resolution is related to baseline length (d) and wavelength of highest frequency detected by INTF ($\lambda_{shortest}$). This relation is shown in Equation 3-18.

$$\Delta\beta \approx \lambda_{shortest}/d \tag{3-18}$$

In this work, the angular resolution is around 12 °. That value means two emissions co-occurring and separated less than 12 ° over the horizon are indistinguishable. Using higher frequencies or lengthening baselines are two possible solutions to improve angular resolution. Still, this value is only relevant when two or more emissions arrive at the antennas simultaneously. However, that situation is less probable because of the short integration time to identify individual sources.

Angular uncertainty

The angular uncertainty refers to vagueness around calculated values for both azimuth and elevation angles by BINTF. As mentioned, those values are calculated from the estimated time difference between arriving signals, as it is shown in Equation 3-16. But, due to noise, these time values always have some uncertainty. Thus, the expected lowest value of angular uncertainty according to Crao-Rower Lower Bound is found using Equation 3-19. The mentioned limit alludes to the strong relation between angular uncertainty and the signal-to-noise ratio of impinging signals. It also establishes the best-case scenario of uncertainty associated with the estimated value.

$$\sigma_\tau^2 \geq \left(\frac{3}{8\pi^2}\right)\left(\frac{1+2\text{SNR}}{\text{SNR}^2}\right)\left(\frac{1}{\text{BW}(3f_c^2 + \text{BW}^2/4)}\right) \tag{3-19}$$

With time uncertainty estimated is possible to determine an uncertainty value for the elevation and azimuth angles. The expressions are shown in Equation 3-20. Again v is the assumed propagation speed, and d is the baseline length.

$$\sigma_{Az} = \left(\frac{v}{d}\right) \left(\frac{1}{cos(EL)}\right) \sigma_{un} \qquad (3\text{-}20)$$

$$\sigma_{EL} = \left(\frac{v}{d}\right) \left(\frac{1}{sin(EL)}\right) \sigma_{un} \qquad (3\text{-}21)$$

4. Findings and analysis

4.1. Introduction

This chapter encompasses data collected during a measuring campaign extending for 148 days, accounting for 1,316 recorded events. The observation period started on November 14, 2019, and was finalized on April 9, 2020. The campaign took place in Bogotá, Colombia, located at an altitude of approximately 2,600 meters above sea level on an Andean plateau.

Every single record was processed to identify the presence of NBE through a cross-correlation function between observations and a reference template. Later, identification validation was done using an energy spectral density analysis. Finally, the identified pulse was evaluated to determine its waveform characteristics: FWHM, rise time, zero-crossing time, and total duration time. Finally, wider comparisons were performed to determine the relationship between the NBE and other recorded lightning activity.

Obtained results were used to find similarities, and differences with previous studies, prioritizing studies developed in tropical latitudes. In spite of slight differences in instrumentation and especially location conditions of lightning instrumentation, it was possible to obtain some relevant insights about NBEs in Colombia.

In this way, this study provides insights into NBEs in a tropical region observed from an Andean high-plateau. Features identification in this region, together with built instrumentation and collected data, are the main contributions of this study.

This chapter continues as follows: the first section presents the background settings for this research, especially, detailing data collection. The next section introduces waveform features used for NBEs characterization. The chapter finalizes with two sections: one section devoted to data analysis and one section to findings discussion.

4.2.   Background and settings

Lightning instruments were deployed on a building's roof in the city center of Bogotá. Available data ranges from November 14, 2019, to April 9, 2020. This period comprises 148 days or roughly five months of data. The period includes the second rainy season of 2019 and part of the first rain of 2020. In Colombia, regularly the first rainy season corresponds to the quarter of March, April, and May, and the second rainy season corresponds to the quarter of September, October, and November.

During the 148 days of continuous observations, 1,316 lightning-related events were recorded by lightning instrumentation. In this context, a lightning event comprises a single record of 500 ms, where a single recording contains the signals from eight antennas (three from the BINTF, plus FA, SA, DF, and dE/dt). Due to its extension, the collection of the events serving as the data source for NBEs analysis is summarized in Table **4-1**, but there is an alternate detailed version in Appendix B.

Table 4-1.: Summary of thunderstorms recorded during measuring campaign.

Number	Storm date	Lightning events	NBE detected
1	Nov-14 2019	136	26
2	Nov-18 2019	94	40
3	Nov-19 2019	173	63
4	Nov-20 2019	185	52
5	Nov-21 2019	6	5
6	Nov-22 2019	90	21
7	Nov-23 2019	2	1
8	Nov-29 2019	81	23
9	Dec-11 2019	74	4
10	Feb-25 2020	20	2
11	Feb-26 2020	11	1
12	Mar-03 2020	8	1
13	Mar-10 2020	286	49

Table 4-1 – continued from previous page

Number	Storm date	Number of records	NBE detected
14	Mar-11 2020	3	3
15	Mar-13 2020	10	1
16	Mar-16 2020	13	2
17	Mar-26 2020	215	47
18	Mar-27 2020	10	1
19	Mar-29 2020	2	1

4.3. Findings

4.3.1. Occurrence rate of NBEs

The procedure to identify NBEs was introduced in Section 3.4.2. Results show 193 NBEs were detected out of 1,316 events. Thus, NBEs are a rare event, although it is not possible to determine if this is due to a lack of generating events or because they are too weak to be detected. In this study, NBEs were detected in 15 % of all records obtained. This result is similar to previous studies performed in lower latitudes (Sri Lanka (10 %) [23], East China (10 %) [75]).

Figure **4-1** visually presents these results and compares them to previous studies, showing similar levels in studies conducted in lower latitudes. This comparison appears to support a relationship between NBEs and latitude. The reason for this might be the height of the tropopause, which allows for greater vertical development of thunderclouds and offers favorable conditions for NBE production.
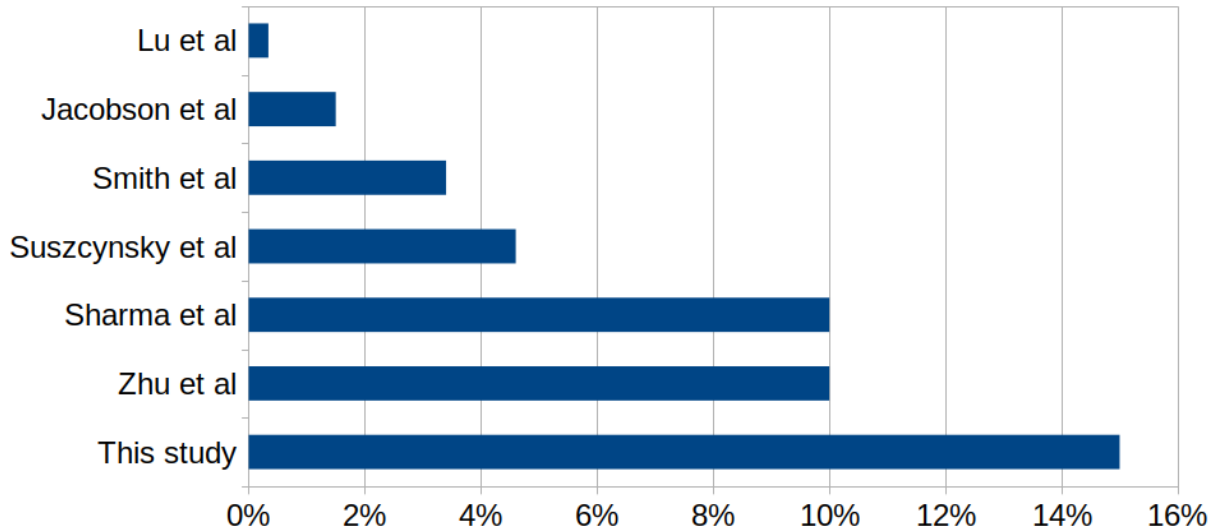
Figure 4-1.: The figure shows the proportion of NBEs occurrence.

4.3.2. Polarity of NBEs

Classifying NBEs according to the 'atmospheric sign convention', 133 out of 193 were identified as having positive polarity (68.9 %) and 60 out of 193 were identified as having negative polarity (31.1 %). The results confirm the prevalence of positive polarity NBEs over negative (about 3 to 1 ratio), similar to values reported by previous studies (Smith et al. (71 % vs 29 %) [14], Wu et al. (66 % vs 34 %) and Suszcynsky et al. (63 % vs 37 %) [69]). This result is a probable consequence of the high altitude origin of negative NBE that produces weaker emissions on the ground. Table **4-2** summarizes NBEs polarity ratio in previous studies. The geometric mean values of this compendium are 78 % positive NBEs, and 22 % negative NBEs.

Table 4-2.: Comparison of findings according to NBEs polarity.

Reference	Percentage of positive NBEs	Percentage of negative NBEs
Smith et al. [74]	71 %	29 %
Suszcynsky et al. [69]	63 %	37 %
Smith et al. [36]	58 %	42 %
Jacobson et al. [64]	77 %	23 %
Wiens et al. [19]	77 %	23 %
Nag et al. [21]	97.5 %	2.5 %
Ahmad et al. [47]	59 %	41 %
Zhu et al. [75]	87 %	13 %
Sharma et al. [23]	100 %	0 %
Wu et al. [71]	66 %	34 %
Wu et al. [16]	82 %	18 %
Wang et al. [48]	100 %	0 %
Wu et al. [34]	91 %	9 %
Lu et al. [29]	100 %	0 %
This study	**68.9 %**	**31.1 %**

4.3.3.   NBE waveform types

Four waveform types (Type A, Type B, Type C, and Type D) were used in this study. The same as previous studies for ease of comparison (Karunarathne et al. [51], Ahmad et al. [118], Medelius et al. [42], Nag et al. [21]). According to this categorization, a Type A pulse is a typical bipolar pulse with the main pulse followed by an overshoot. In contrast, Type B is a pulse including extra peaks or ringing in the overshoot portion of the signal. Type C and Type D are waveforms with additional ringing after or before the main pulse, respectively.

Type A
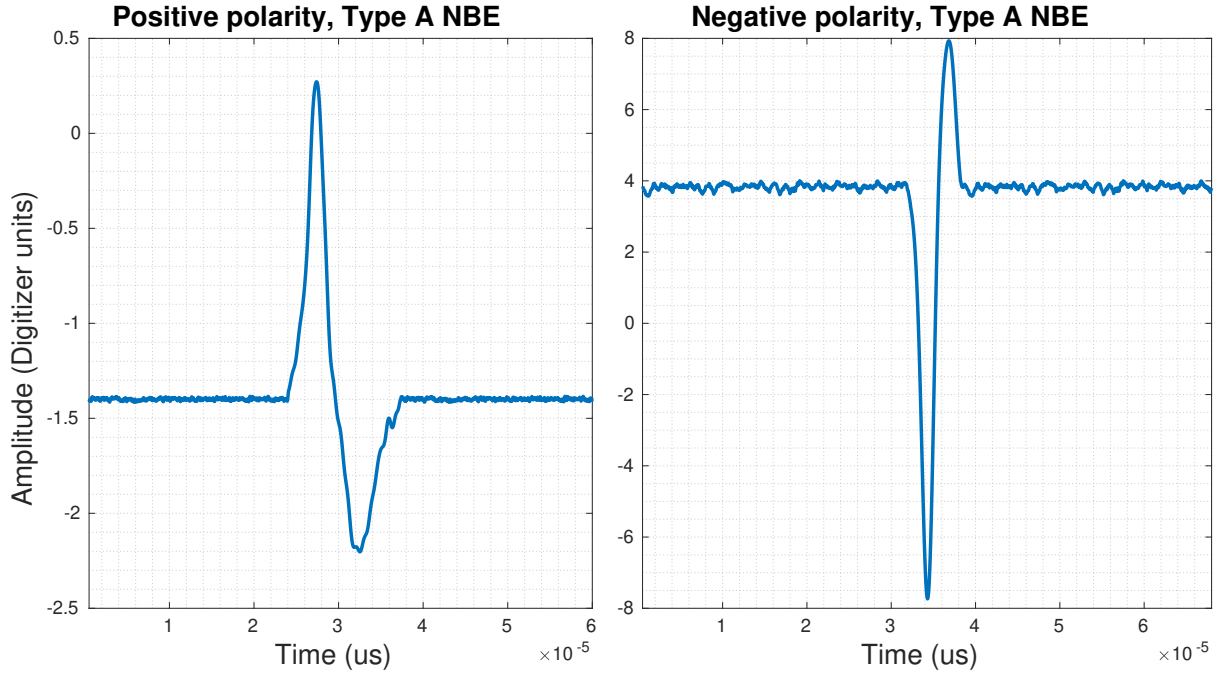
Figure 4-2.: Left image shows a type A positive polarity NBE pulse. The right image shows a type A negative polarity NBE pulse.

In this study, Type A waveforms were 8.8 % of the pulses detected. Previous studies varied around this category; meanwhile, Ahmad et al. [118] found 61 %, Medeelius et al. [42] found 42 %, Leal et al. [105] found 24.4 %, and Karunarathne et al. [28] only found a 2 %. Comparison of these results are presented in Table **4-3**. Fig.**4-2** depicts two examples of type A NBE pulses, one positive polarity, and one negative polarity.

Table 4-3.: Comparison of findings of Type A pulses.

Study	Type A
Bandara et al. [119]	2 %
Karunarathne et al. [28]	1 %
Leal et al. [11]	27 %
This study	**8.8 %**

Among the reasons behind these uneven results could be the accuracy of the instrumentation, sampling rate, and distance between the measurement station and the NBE source. Better

instrumentation is able to detect minor changes so the rarity of Type A pulses. Distance is also relevant because of the effects of propagation over finite conductive terrain [120]. Discriminated by polarity, Type A positive polarity was 6.7 %, and Type A negative polarity was 2.0 % of the total.

Type B
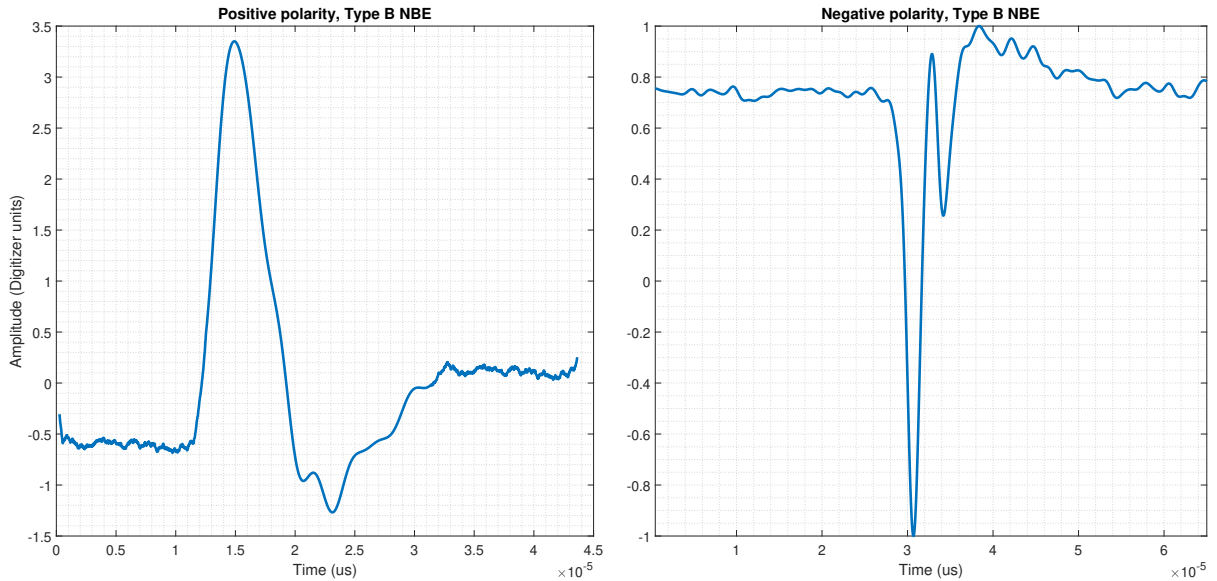
Figure 4-3.: Left image shows a Type B positive polarity NBE pulse. The right image shows a Type B negative polarity NBE pulse.

In this work, Type B pulses accounted a 41.4 % of the total. This result makes type B the second most common type of waveform found in this study. Some previous studies defined sub-types of Type B because they distinguish between ringing occurring after and before the peak value of the overshoot. That is the case in Medelius et al. [42], and Ahmad et al. [118]. Considering both variations, Type B is the first or the second most common type of pulse. A comparison of this result with previous studies is presented in Table **4-4**. Fig.**4-3** depicts two examples of Type B NBE pulses, one positive polarity, and one negative polarity. Discriminated by polarity, Type B of positive polarity was 61 %, and the negative polarity was 39 %.

Table **4-4**.: Comparison of findings of Type B pulses.

Study	Type B
Bandara et al. [119]	34 %
Karunarathne et al. [28]	63 %
Leal et al. [11]	46 %
This study	**41.4 %**

Type C
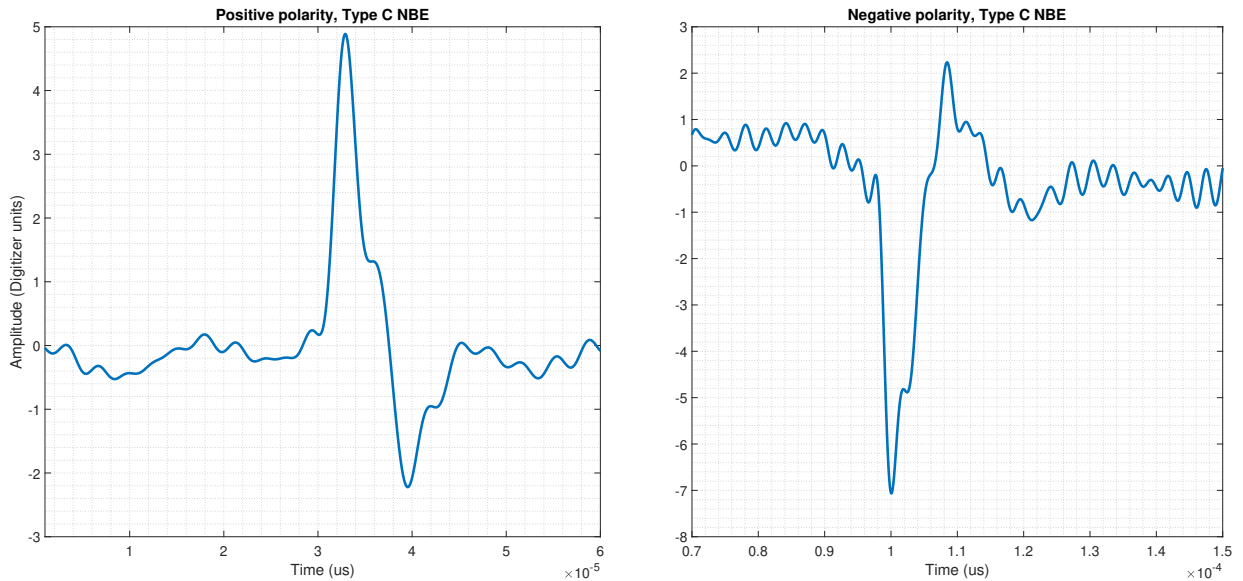
Figure 4-4.: Left image shows a Type C positive polarity NBE pulse. The right image shows a Type C negative polarity NBE pulse.

Type C pulses amounted to 6.2 % of the total NBEs. Karunarathne et al. [28] found 13 % of Type C, meanwhile, Medelius et al. [42], and Ahmad et al. [42] identified just one pulse of this type. Leal et al. [121] reported 17 %. A comparison of results is presented in Table **4-5**. Fig.**4-4** depicts two examples of Type C NBEs pulses, one positive polarity, and one negative polarity. According to their polarity, Type C of positive polarity counts 83 % and negative polarity 17 %.

Table 4-5.: Comparison of findings of Type C pulses.

Study	Type C
Bandara et al. [119]	52 %
Karunarathne et al. [28]	13 %
Leal et al. [11]	17 %
This study	**6.2 %**

Type D
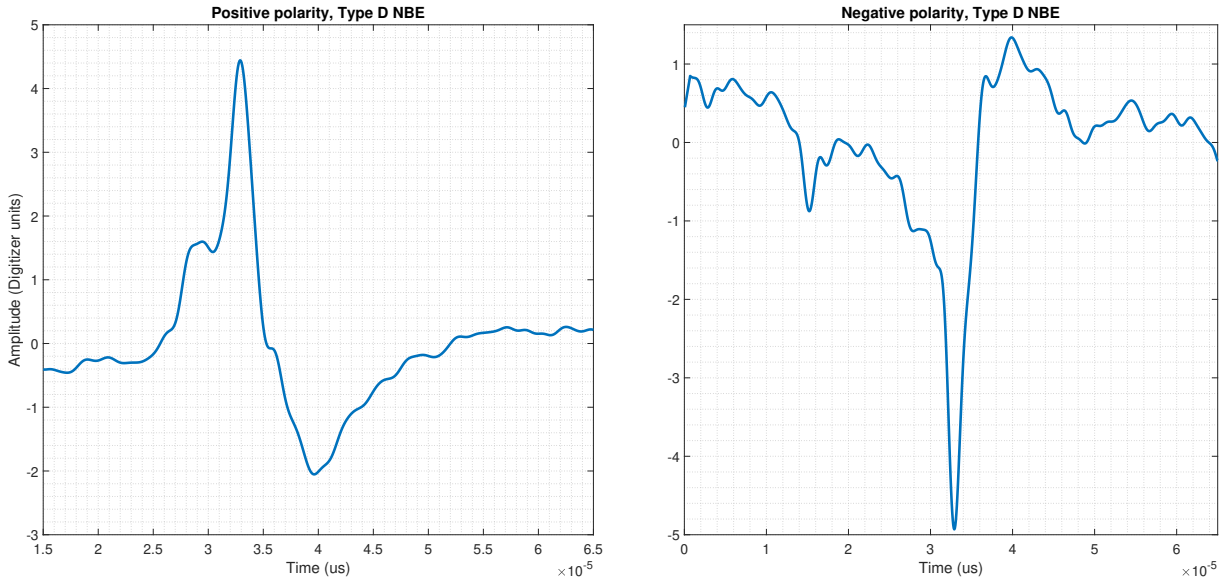
Figure 4-5.: Left image shows a Type D positive polarity NBE pulse. The right image shows a Type D negative polarity NBE pulse.

In this study, Type D pulses were 43.5 % of total NBEs recorded. This value significantly differs from similar studies (Karunarathne et al. [28] 19 %, Leal et al. [121] 10 %). The methodology is probably responsible because many NBEs have additional ringing, both on the main pulse and the overshoot. In that case, referred studies prioritized additional pulses on the overshoot; thus, pulses are classified as Type B. For this author, the relevant feature is the initial half-cycle, so for the same situation, in this study, classification derives to a Type D. Comparison of results are presented in Table **4-6**. Type D pulses were positive polarity at 74 % whereas 26 % were negative polarity. Fig.**4-5** depicts two examples of type D NBE pulses, one positive polarity, and one negative polarity.

Table 4-6.: Comparison of findings of Type D pulses.

Study	Type D
Bandara et al. [119]	13 %
Karunarathne et al. [28]	19 %
Leal et al. [11]	10 %
This study	**43.5 %**

A compendium of results obtained after classifying NBE pulses by their waveforms is shown in Table **4-7**, meanwhile, Fig. **4-6** shows a comparison of findings against previous studies.

Table 4-7.: Types of waveforms detected from the measuring campaign.

Type of waveform	Positive polarity	Percentage	Negative polarity	Percentage	Total number of pulses	Percentage
A	13	6.7 %	4	2.0 %	17	8.8 %
B	49	25.3 %	31	16.0 %	80	41.4 %
C	9	4.6 %	3	1.5 %	12	6.2 %
D	62	32.1 %	22	11.3 %	84	43.5 %
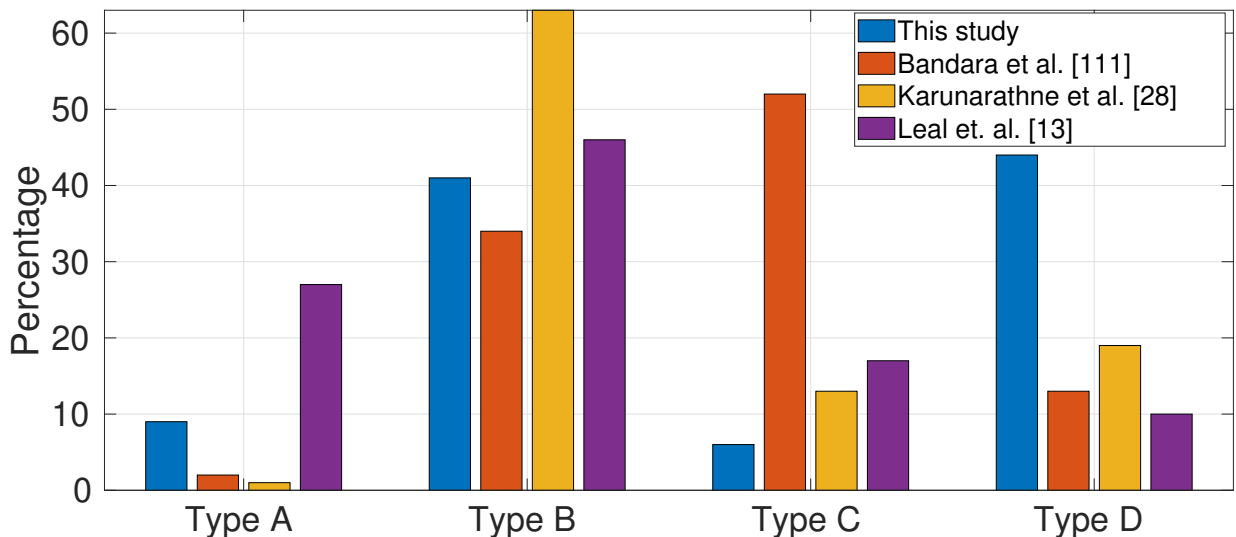
Figure 4-6.: The figure shows a comparison of types of NBEs in different studies.

4.3.4.   NBE temporal characteristics

The criteria used to characterize NBE waveforms were identical to previous studies: rise time, FWHM, zero-crossing time, pulse duration, and the initial half-cycle to overshoot peak value ratio. Definitions are as follows:

- Rise time: The time difference between the 10 % and 90 % of the maximum amplitude of the initial half cycle of the pulse.

- Full width at half maximum (FWHM): It is the time difference between the points of 50 % of the maximum amplitude of the initial half cycle of the pulse.

- Zero-crossing time: The time difference between the first and second zero-crossing point of the initial half cycle of the pulse.

- Pulse duration: The time difference between the 10 % of the maximum amplitude of the initial half-cycle and the 10 % of the maximum amplitude of the overshoot.

- The ratio between peak values of the initial half-cycle and the overshoot (O_s/P_a).

From this point on, the following subsections introduce results using previously defined metrics. The results are organized by type and polarity.

Positive NBEs characteristics

Rise time

This study found that rise time of positive polarity NBEs had a mean value of 2.6 µs and a standard deviation of 2.1 µs. These values correlate well with previous studies, particularly those in similar latitudes (Sri Lanka [23], East China [75]). Figure **4-7** displays a comparison of various studies in a bar diagram.
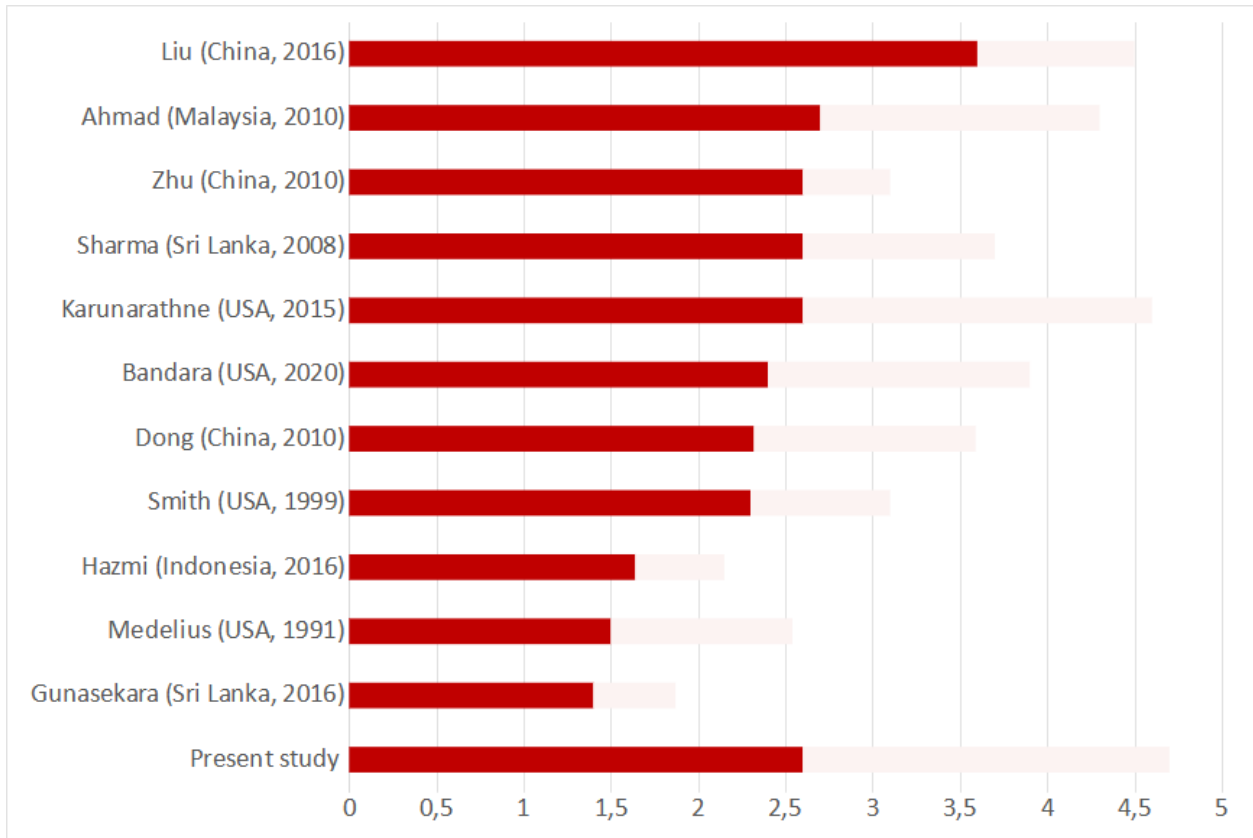
Figure 4-7.: The figure shows a comparison of proportions of positive NBEs according to their rise time.

Full Width Half Maximum

This study found that FWHM of positive polarity NBEs had a mean value of 2.6 µ*s* and a standard deviation of 1.3 µ*s*. These values correlate well with previous studies, particularly those in similar latitudes (Sri Lanka [23], Malaysia [47]). Figure **4-8** displays a comparison of various studies in a bar diagram.
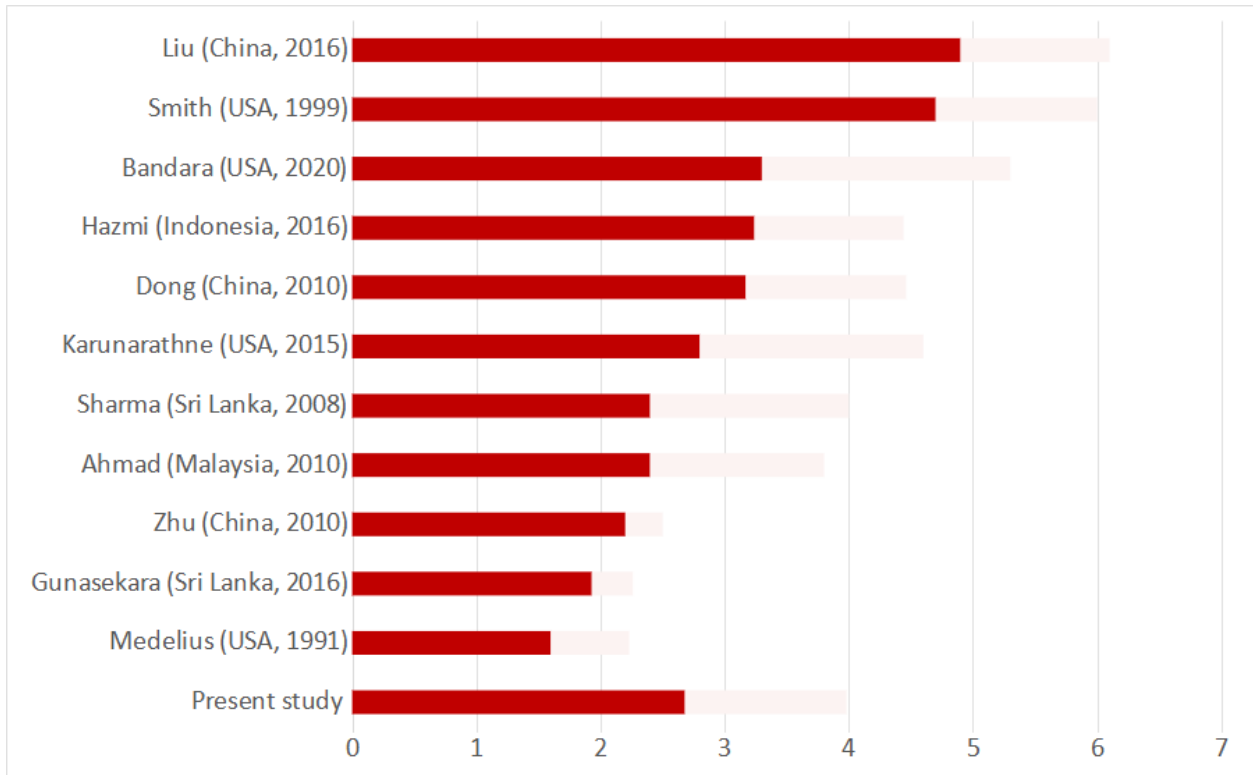
Figure 4-8.: The figure shows a comparison of proportions of positive NBEs according to their FWHM.

Zero crossing time

This study found that zero crossing time of positive polarity NBEs had a mean value of 7.8 µs and a standard deviation of 2.8 µs. These values correlate well with previous studies, particularly with East China [33]. Figure **4-9** displays a comparison of various studies in a bar diagram.
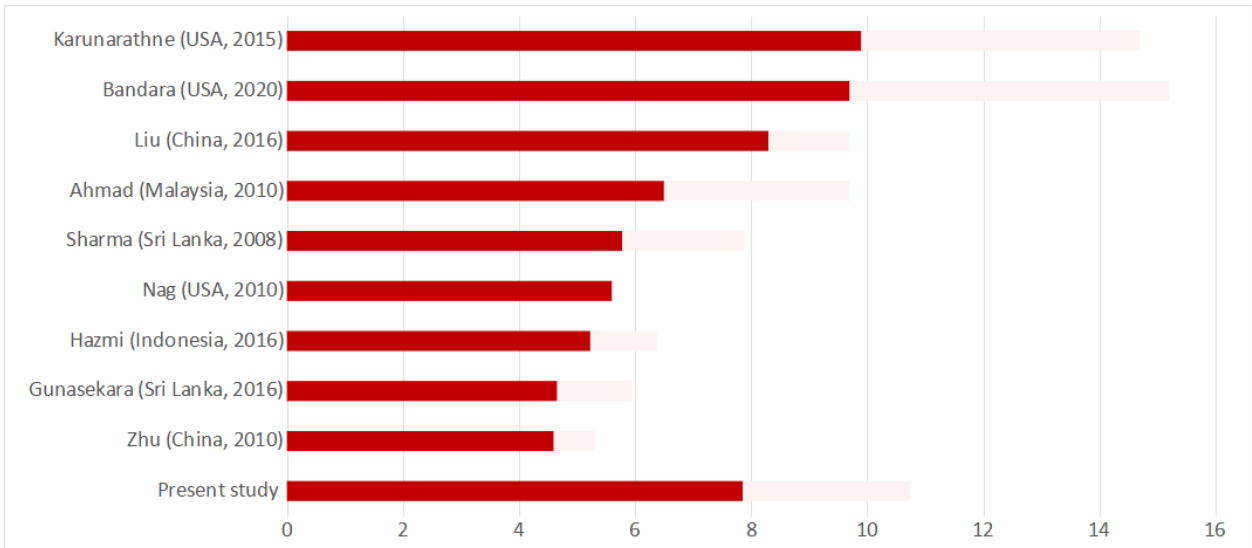
Figure 4-9.: The figure shows a comparison of proportions of positive NBEs according to their Zero-crossing.

Total pulse duration

This study found that the total pulse duration of positive polarity NBEs had a mean value of 10.5 µs and a standard deviation of 4.9 µs. These values correlate well with previous studies (Indonesia [33], Sri Lanka [23]). Figure **4-10** displays a comparison of various studies in a bar diagram.
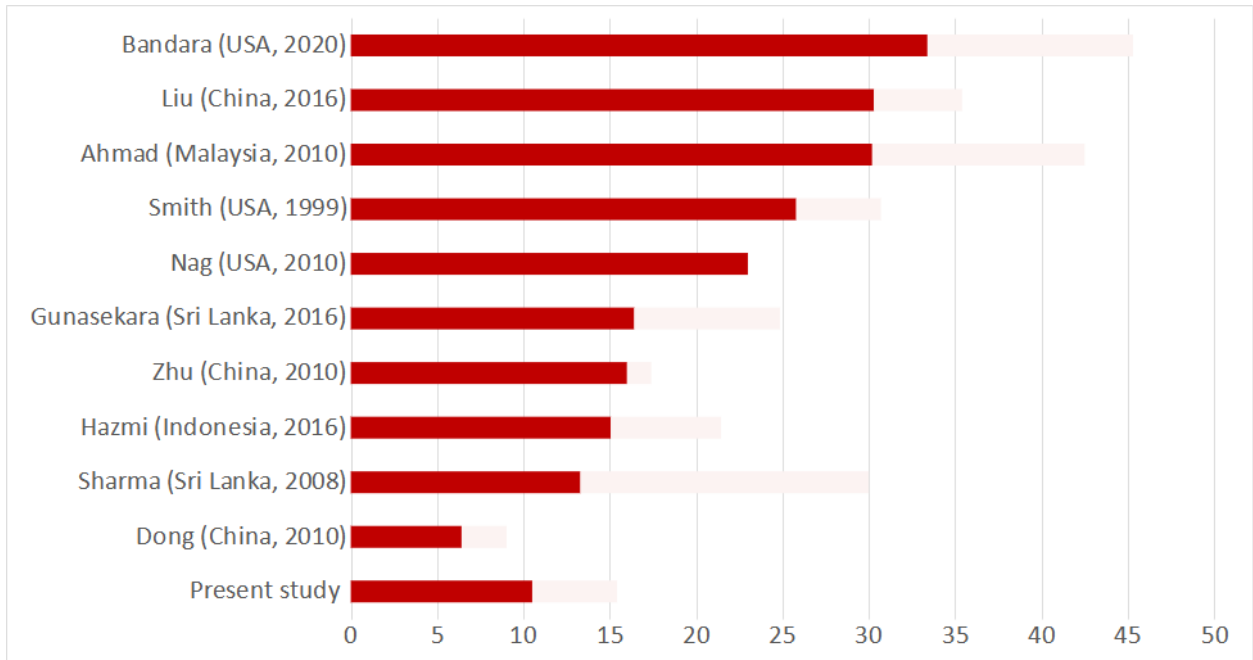
Figure 4-10.: The figure shows a comparison of proportions of positive NBEs according to their pulse total duration.

Negative NBEs characteristics

Rise time

This study found that the rise time of negative polarity NBEs had a mean value of 1.8 µs and a standard deviation of 1.1 µs. These values correlate well with previous studies, particularly those in similar latitudes (Sri Lanka [23], East China [75]). Figure **4-11** displays a comparison of various studies in a bar diagram.
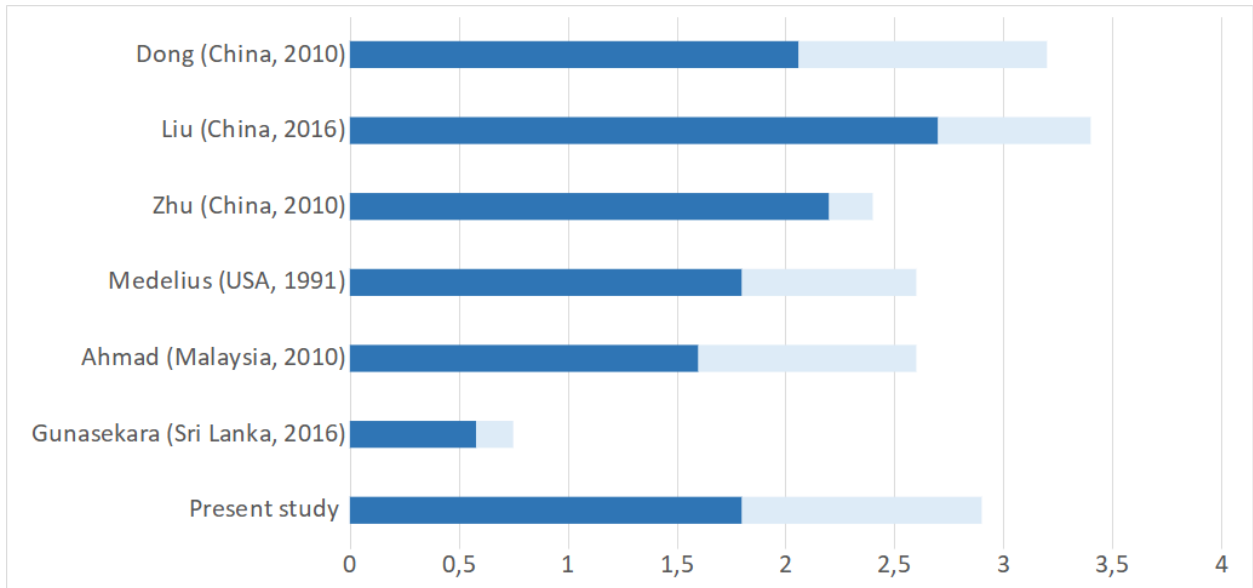
Figure 4-11.: The figure shows a comparison of proportions of negative NBEs according to their rise time.

Full Width Half Maximum

This study found that FWHM of negative polarity NBEs had a mean value of 2.1 µs and a standard deviation of 0.7 µs. These values correlate well with previous studies, particularly those in similar latitudes (Sri Lanka [23], Malaysia [47]). Figure **??** displays a comparison of various studies in a bar diagram.
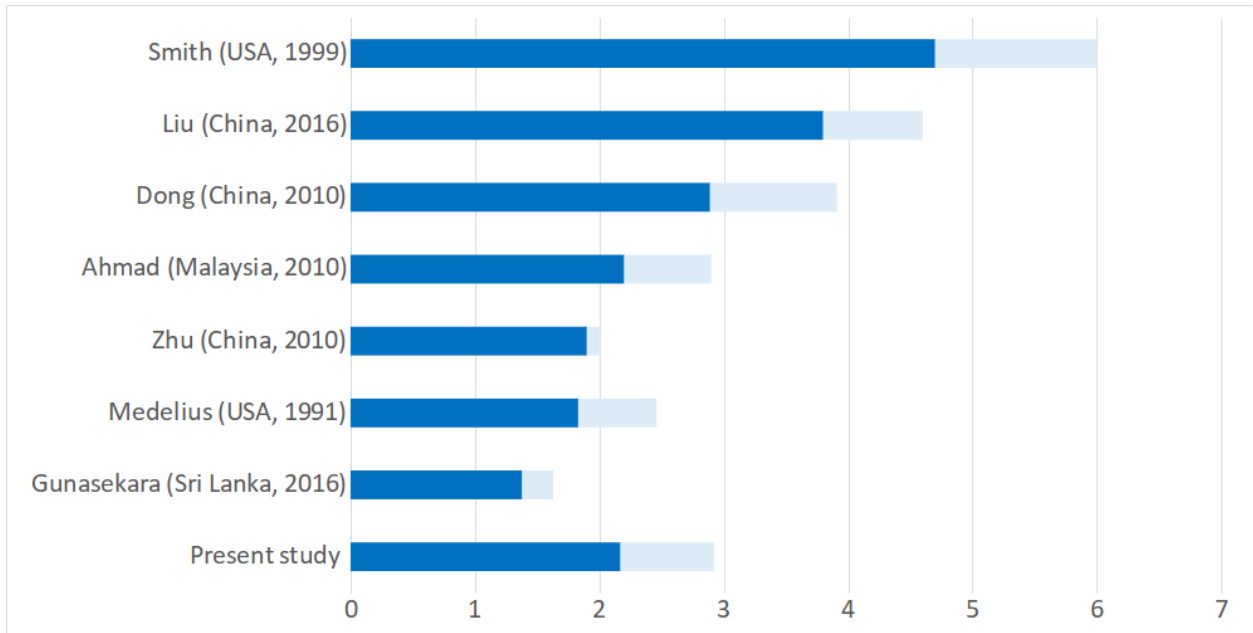
Figure 4-12.: The figure shows a comparison of proportions of negative NBEs according to their FHWM.

Zero crossing time

This study found that zero crossing time of negative polarity NBEs had a mean value of 9.6 µs and a standard deviation of 2.9 µs. These values correlate well with previous studies, particularly with East China [33]. Figure **4-13** displays a comparison of various studies in a bar diagram.
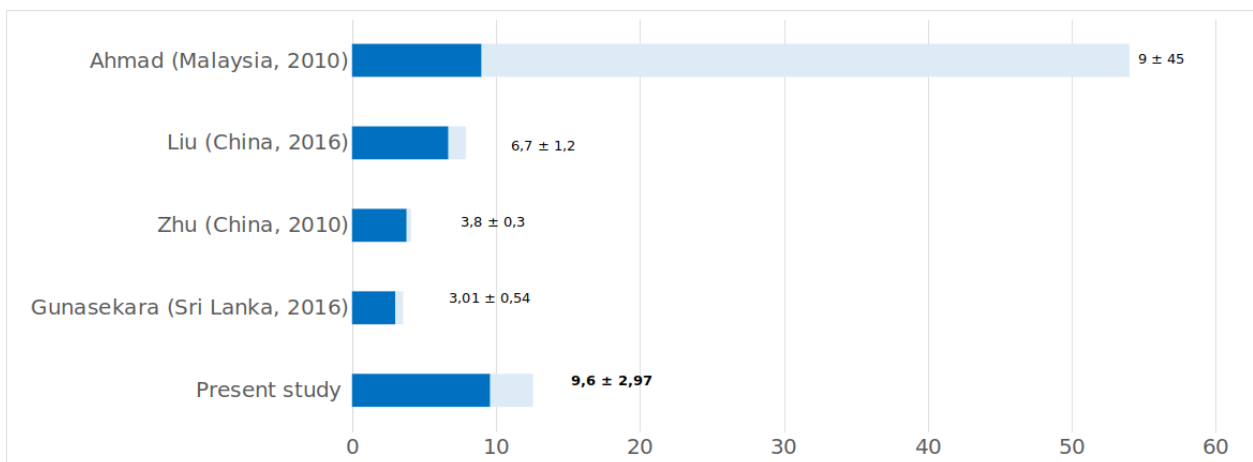
Figure 4-13.: The figure shows a comparison of proportions of negative NBEs according to their Zero-crossing.

Total pulse duration

This study found that the total pulse duration of negative polarity NBEs had a mean value of 11.6 µ*s* and a standard deviation of 3.7 µ*s*. These values correlate well with previous studies (Indonesia [33], Sri Lanka [23]). Figure **4-14** displays a comparison of various studies in a bar diagram.
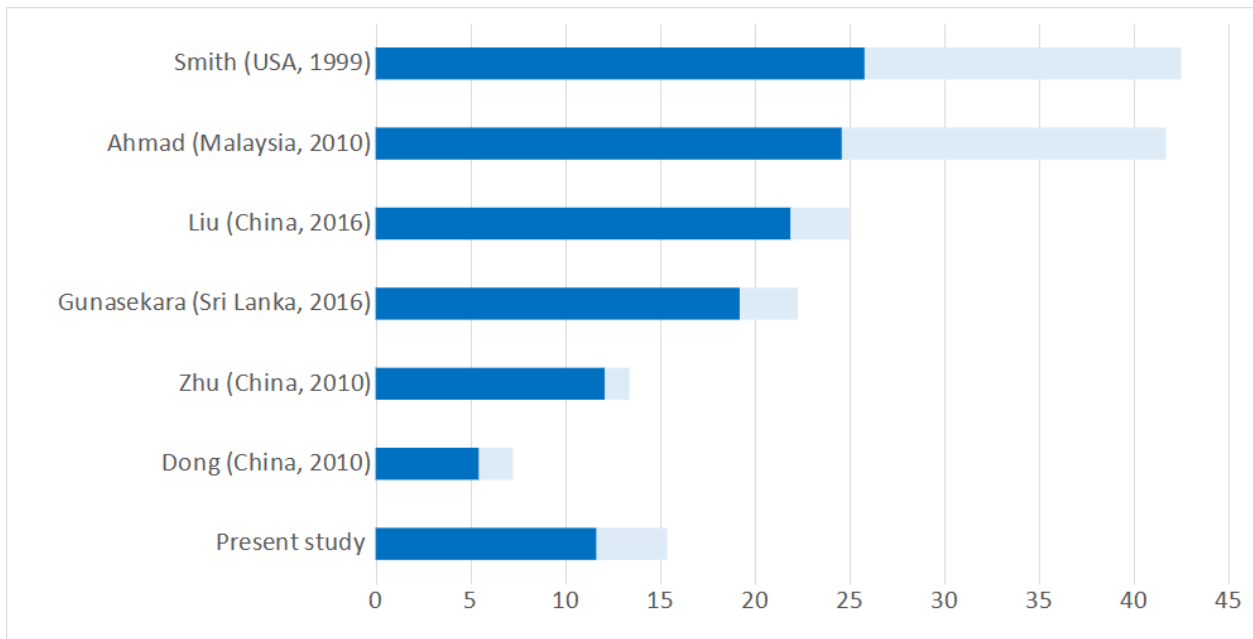
Figure 4-14.: The figure shows a comparison of proportions of negative NBEs according to their pulse total duration.

Positive polarity Type A characteristics

Based on the metrics defined, arithmetic mean values plus its corresponding standard deviation for positive polarity Type A are shown in Table **4-8**.

Table 4-8.: Waveform properties of positive polarity Type A.

Variable	Mean value	Standard deviation
Rise time (10 %-90 %)	1.7 μs	0.9 μs
FWHM	2.4 μs	0.8 μs
Zero crossing time	6.0 μs	1.7 μs
Total pulse duration	11.4 μs	7.4 μs

Negative polarity Type A characteristics

The arithmetic mean values plus its corresponding standard deviation for negative polarity Type A are shown in Table **4-9**.

Table **4-9**.: Waveform properties of negative polarity Type A.

Variable	Mean value	Standard deviation
Rise time (10 %-90 %)	1.6 μs	0.3 μs
FWHM	1.6 μs	0.2 μs
Zero crossing time	4.1 μs	0.5 μs
Total pulse duration	6.5 μs	0.8 μs

Positive polarity Type B characteristics

The arithmetic mean values plus its corresponding standard deviation for positive polarity Type B are shown in Table **4-10**.

Table **4-10**.: Waveform properties of positive polarity Type B.

Variable	Mean value	Standard deviation
Rise time (10 %-90 %)	2.5 μs	1.5 μs
FWHM	2.6 μs	1.1 μs
Zero crossing time	7.0 μs	2.6 μs
Total pulse duration	18.2 μs	6.1 μs

Negative polarity Type B characteristics

The arithmetic mean values plus its corresponding standard deviation for negative polarity Type B are shown in Table **4-11**.

Table 4-11.: Waveform properties of negative polarity Type B.

Variable	Mean value	Standard deviation
Rise time (10 %-90 %)	1.9 μs	0.9 μs
FWHM	2.1 μs	0.6 μs
Zero crossing time	5.8 μs	2.2 μs
Total pulse duration	14.7 μs	5.9 μs

Positive polarity Type C characteristics

The arithmetic mean values plus its corresponding standard deviation for positive polarity Type C are shown in Table **4-12**.

Table 4-12.: Waveform properties of positive polarity Type C.

Variable	Mean value	Standard deviation
Rise time (10 %-90 %)	1.9 μs	0.8 μs
FWHM	2.7 μs	1.6 μs
Zero crossing time	8.5 μs	3.2 μs
Total pulse duration	18.1 μs	8.3 μs

Negative polarity Type C characteristics

The arithmetic mean values plus its corresponding standard deviation for negative polarity Type C are shown in Table **4-13**.

Table 4-13.: Waveform properties of negative polarity Type C.

Variable	Mean value	Standard deviation
Rise time (10 %-90 %)	0.9 μs	0.5 μs
FWHM	2.4 μs	1.8 μs
Zero crossing time	6.2 μs	3.5 μs
Total pulse duration	11.8 μs	5.6 μs

Positive polarity Type D characteristics

The arithmetic mean values plus its corresponding standard deviation for positive polarity Type D are shown in Table **4-14**.

Table **4-14**.: Waveform properties of positive polarity Type D.

Variable	Mean value	Standard deviation
Rise time (10 %-90 %)	6.2 μs	3.6 μs
FWHM	3.1 μs	2.3 μs
Zero crossing time	10.7 μs	4.9 μs
Total pulse duration	19.9 μs	8.6 μs

Negative polarity Type D characteristics

The arithmetic mean values plus its corresponding standard deviation for negative polarity Type D are shown in Table **4-15**.

Table **4-15**.: Waveform properties of negative polarity Type D.

Variable	Mean value	Standard deviation
Rise time (10 %-90 %)	4.7 μs	2.2 μs
FWHM	2.8 μs	1.5 μs
Zero crossing time	9.5 μs	3.7 μs
Total pulse duration	16.4 μs	7.3 μs

Fig. **4-15** summarizes results obtained related to the rise time of NBEs, focusing on comparison with previous studies. Positive NBEs are similar to the mean value, while negative NBEs are above the mean value.
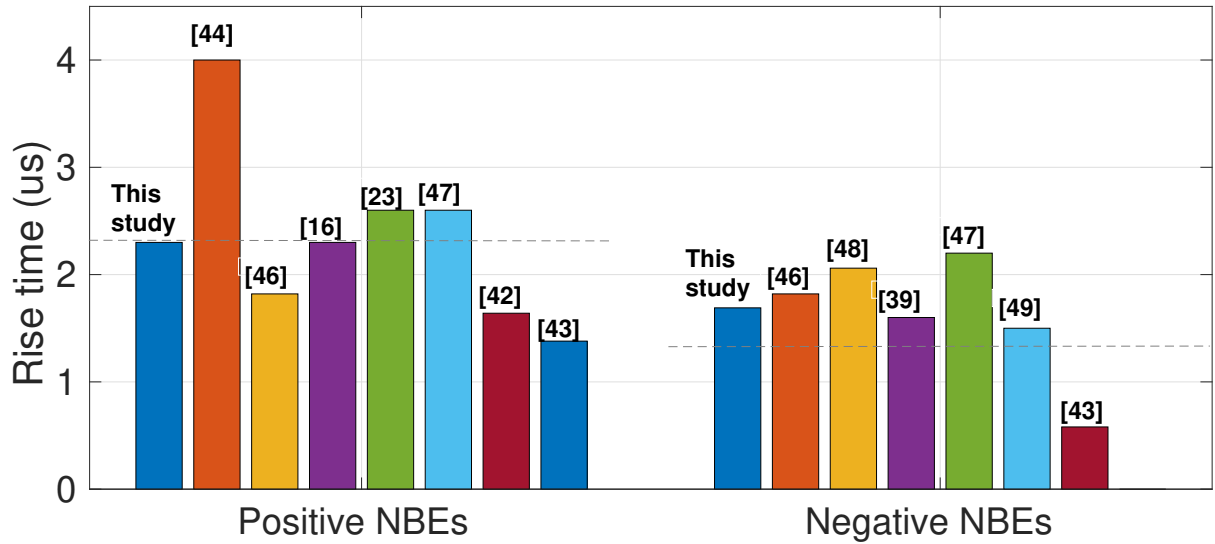
Figure 4-15.: The figure shows a comparison of proportions of NBEs according to their polarity in different studies.

Fig. **4-16** summarizes results obtained related to zero-crossing time of NBEs, focusing on comparison with previous studies. Positive NBEs are similar to the mean value, while negative NBEs are above the mean valuel.
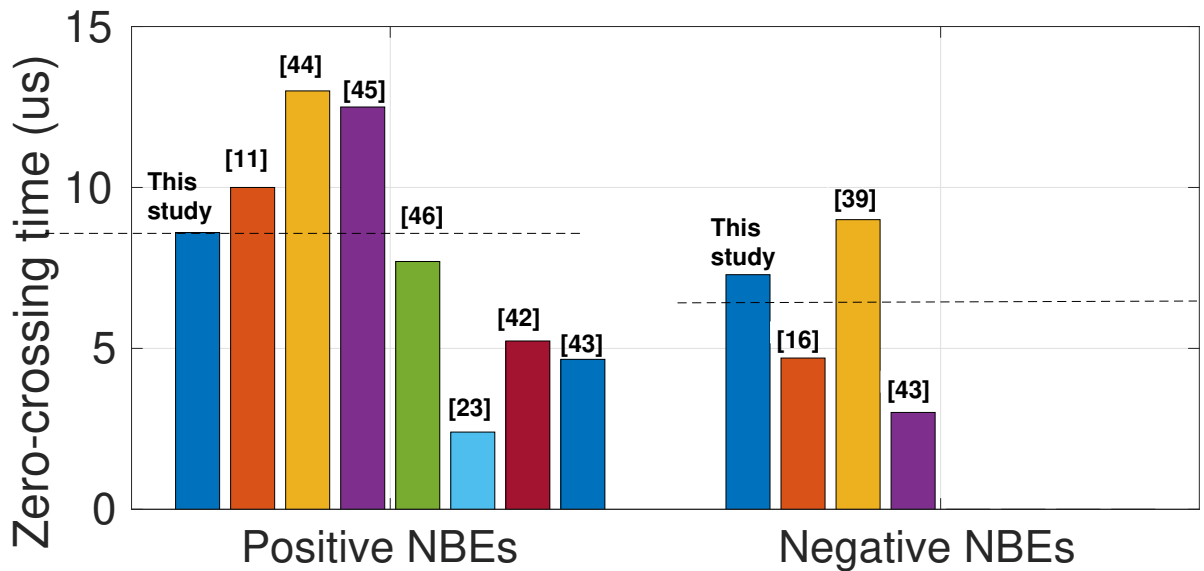
Figure 4-16.: The figure shows a comparison of proportions of NBEs according to their polarity in different studies.

Fig. **4-17** summarizes results obtained related to the Full Width Half Maximum of NBEs,

focusing on comparison with previous studies. Both positive and negative NBEs are similar to the mean value.
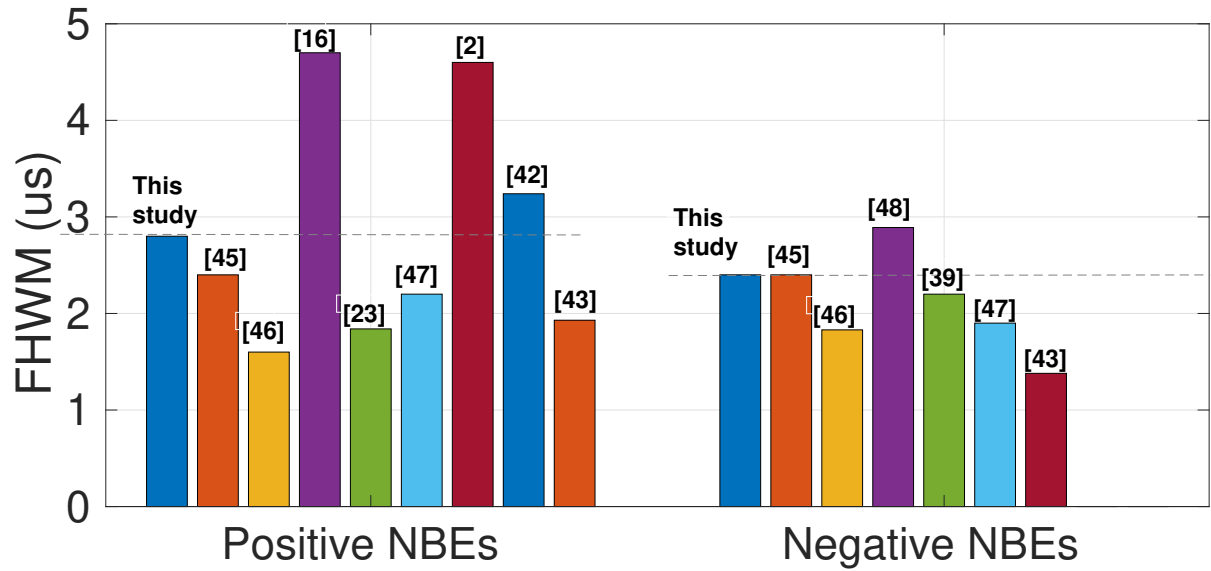
Figure 4-17.: The figure shows a comparison of proportions of NBEs according to their polarity in different studies.

Fig. **4-18** summarizes results obtained related to the total pulse duration of NBEs, focusing on comparison with previous studies. Both positive and negative NBEs are under the mean value.
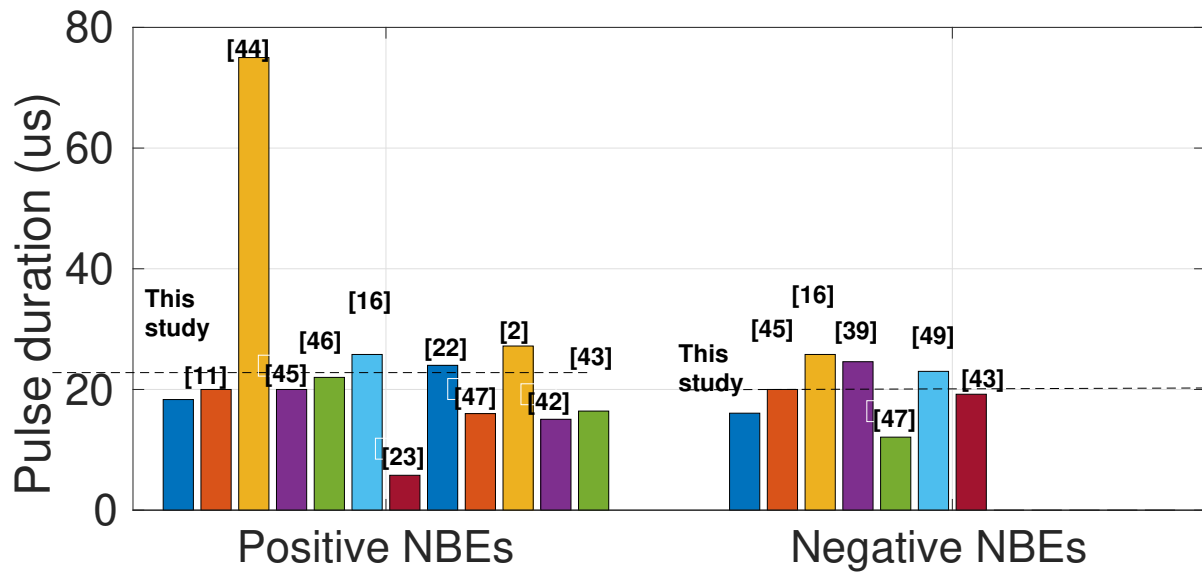
Figure 4-18.: The figure shows a comparison of proportions of NBEs according to their polarity in different studies.

4.3.5. Geographic location of NBEs

A comparison of data sets gives a wider view of the acquired data and its distribution across Colombian territory. As shown in Figure **4-19**, NBEs occurred in regions with a high density of lightning activity, as determined by matching the acquired data with entries in Vaisala's database.
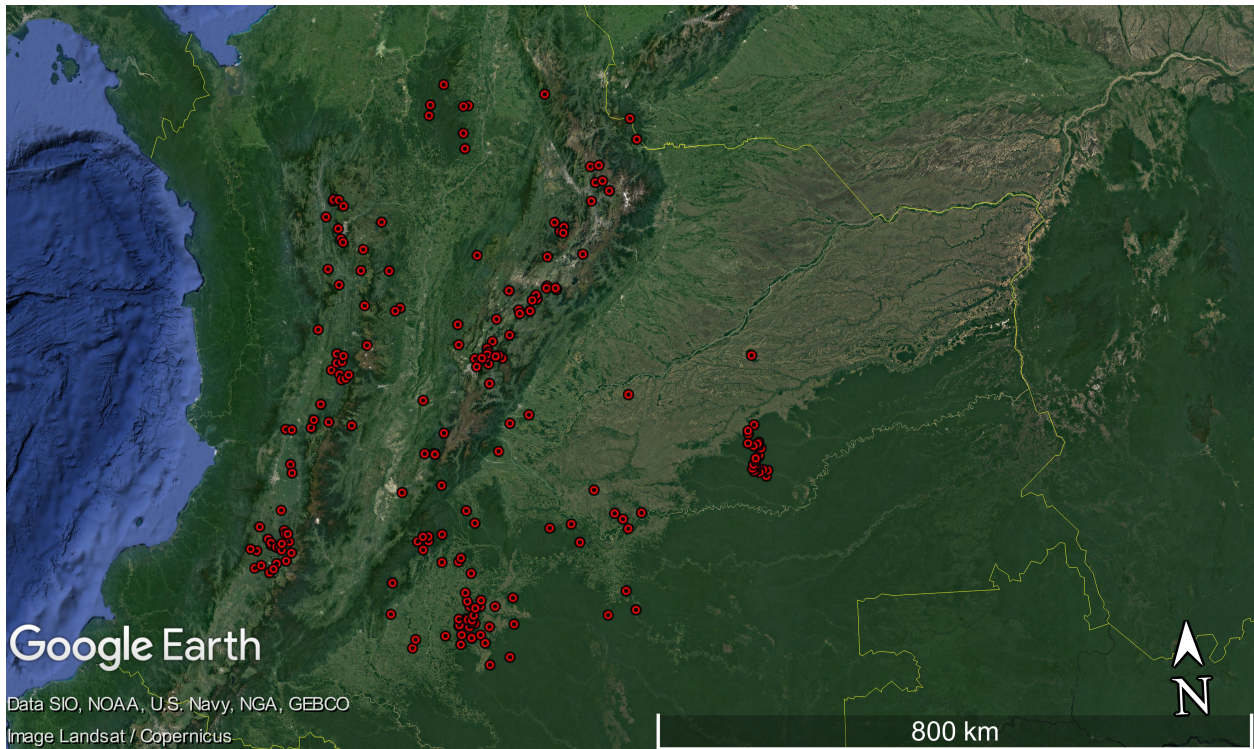
Figure 4-19.: The figure displays the location of 193 NBEs detected during the campaign. Source: Google earth V 7.3.4.8248. (November 19, 2021). Colombia. 4° 42′ 40″ N, 74° 4′ 20 W, Eye alt 1400 km. http://www.earth.google.com.

Figure **4-19** shows NBEs occurred around the Andes foothills and valleys, similar to previous lightning distribution studies in Colombia [122], [26]. NBEs detected are within 200 km of the instrument location, consistent with studies where they were detected up to 500 km away ([105]).

4.3.6. Groups of NBEs

A group of NBEs is defined as a collection of two or more NBEs that are closely related. This study uses a similar approach as Bandara et al. [123] which involves temporal and spatial proximity. A group can consist of NBEs with the same polarity, or it can include both polarities.

In this study, 22 groups of NBEs were identified. These groups consist of 45 NBEs, which is roughly 23 % of all detected NBEs. 31 NBEs were positive (69 %), and 14 were negative (31 %). Table **4-16** shows details about the groups' composition found in this study.

Table 4-16.: Summary of groups of NBEs identified in this study.

NBE Group Type	Number of groups	Isolated	Not-isolated
Three Positive NBEs	1	0	1
Two Positive NBEs	7	0	7
Two Positive NBEs and One Negative NBE	1	1	0
One Negative NBE and One Positive NBE	4	1	3
One Positive NBE and One Negative NBE	7	0	7
One Positive NBE and Two Negative NBE	1	0	1

Data collected suggests that one group of NBEs is isolated in relation to other lightning activities, while the rest appear to be related to the subsequent activity. However, this claim is not entirely reliable because the temporal observation window is not long enough to guarantee the isolation of the group due to its extent.

4.3.7. Spatio-temporal relationship with other lightning events

Isolation is relevant in the NBE context because the first studies consistently reported this behavior as a typical trait of these events. Thus, apart from its enormous power emission in the VHF band, the other principal characteristic of NBEs was their apparent lack of relation with other lightning activity. However, recent studies have demonstrated that the situation is the opposite, probably because of better and more accurate instrumentation. Then NBEs seem to be present in most lightning discharges, especially at the inception stage. Therefore at this point, a definition of isolation is a challenging question.

Most legacy studies used time as the variable to establish isolation in this type of event. Then, an NBE was identified as isolated when there was no other electrical activity before or after a time interval. The amount of time to declare isolation was variable and ranged from tens to hundreds of milliseconds based on researchers' criteria.

Isolation in time is a tricky issue due to inherent uncertainty related to firmly accepting no existence of other lightning activity. Still, this study performed an analysis assuming a period of inactivity of at least 130 ms around the pulse. Employing this metric, the results obtained were that 30 % of all NBEs detected were time-isolated. That means there is no detectable activity 130 ms after or before the occurrence of the NBE. The rest of the NBEs (70 %) seem closely related to intracloud discharges or were the preliminary activity of cloud-to-ground discharges. Figure **4-20** depicts an example of that type of time-isolated NBEs.
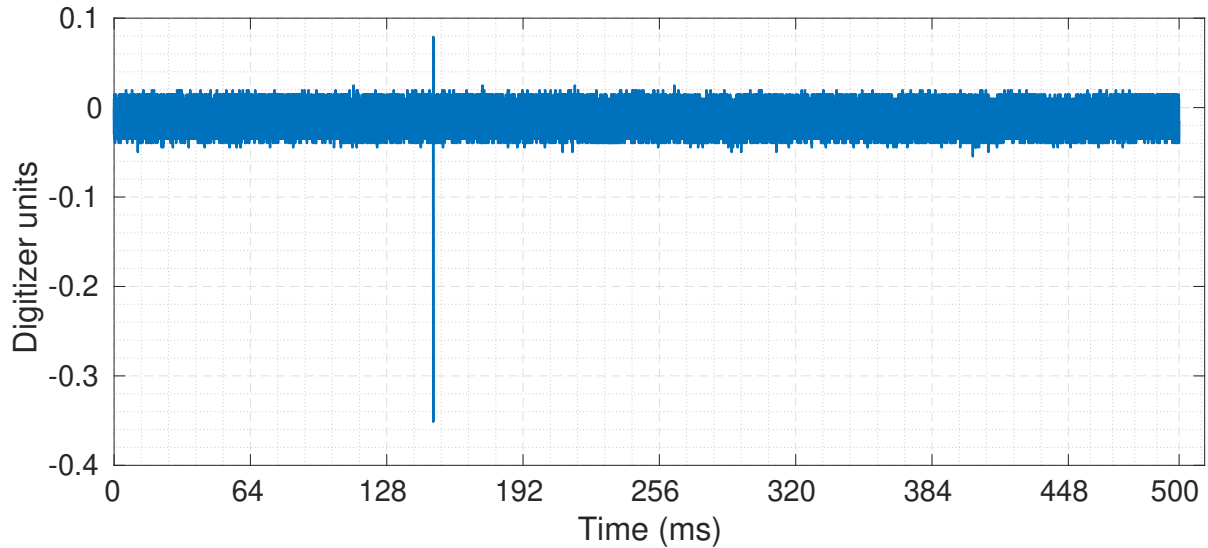
Figure 4-20.: An example of a temporal isolated NBE. The pulse was recorded on November 14, 2019, at 17:35:55 UTC. The source of emission was 90 km from the lightning station (Latitude 5° 14′ 38,76″ N, Longitude 73° 34′ 33,599 W, Villapinzón, Cundinamarca).

Isolation in space is not a common practice in legacy studies. Only a few previous references of this type of analysis are in Karunarathne et al., and Bandara et al. [51], [119]. The idea behind this spatial isolation is to determine another lightning activity near the NBE location. For this purpose, it is essential to have lightning location data to corroborate the vicinity of lightning discharges. In this study, LLS data was kindly provided by Vaisala, and the definition of spatial isolation was set to a 10 km radius around the NBE. As a result, only 38 % of NBE detected can be considered isolated in space under this assumption. Figure **4-21** shows an example of an NBE classified as isolated in space.

Figure 4-21.: An example of a spatial isolated NBE. The pulses were recorded on November 20, 2019, at 19:32:55 UTC. Lightning events in the figure took place for 8 seconds. The source of the emissions is approximately 350 km from the lightning station (Latitude 3° 38′ 13,2″ N, Longitude 71° 0′ 33,479 W, Puerto Gaitán, Meta). Source: Google earth V 7.3.4.8248. (November 19, 2021). Puerto Gaitán, Meta, Colombia. 3° 38′ 13,2″ N, 71° 0′ 33,479 W, Eye alt 50 km. http://www.earth.google.com.

Combining both conditions, temporal and spatial isolation, less than 13 % of all NBEs detected in this study could be considered truly isolated events. Then, the remaining 87 % is related to other electrical activity in the cloud. Figure **4-22** shows a graphical summary of these findings.
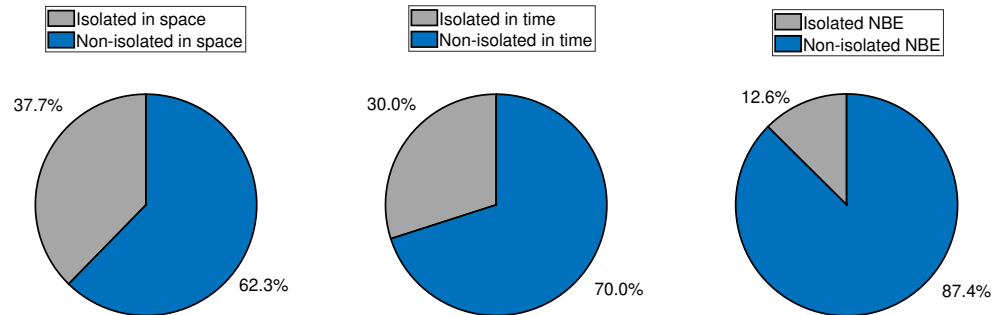
Figure 4-22.: Proportion of NBEs isolated in space, NBEs isolated in time, and NBEs that could be considered completely isolated NBEs.

4.4.   Findings of broadband lightning interferometer

The lightning measuring station used two different triggering systems, one for FA, SA, and dE/dt antennas and the other for BINTF. This decision was made to have a sort of practical validation of the correct operation of the interferometer.

This decision implied that sometimes there are no coincident data from both subsystems, e.g., there are records of FA, SA, and dE/dt without BINTF data and vice versa. The possible reason behind this situation was triggering threshold for BINTF was set up expressly for intracloud activity with strong VHF emissions.
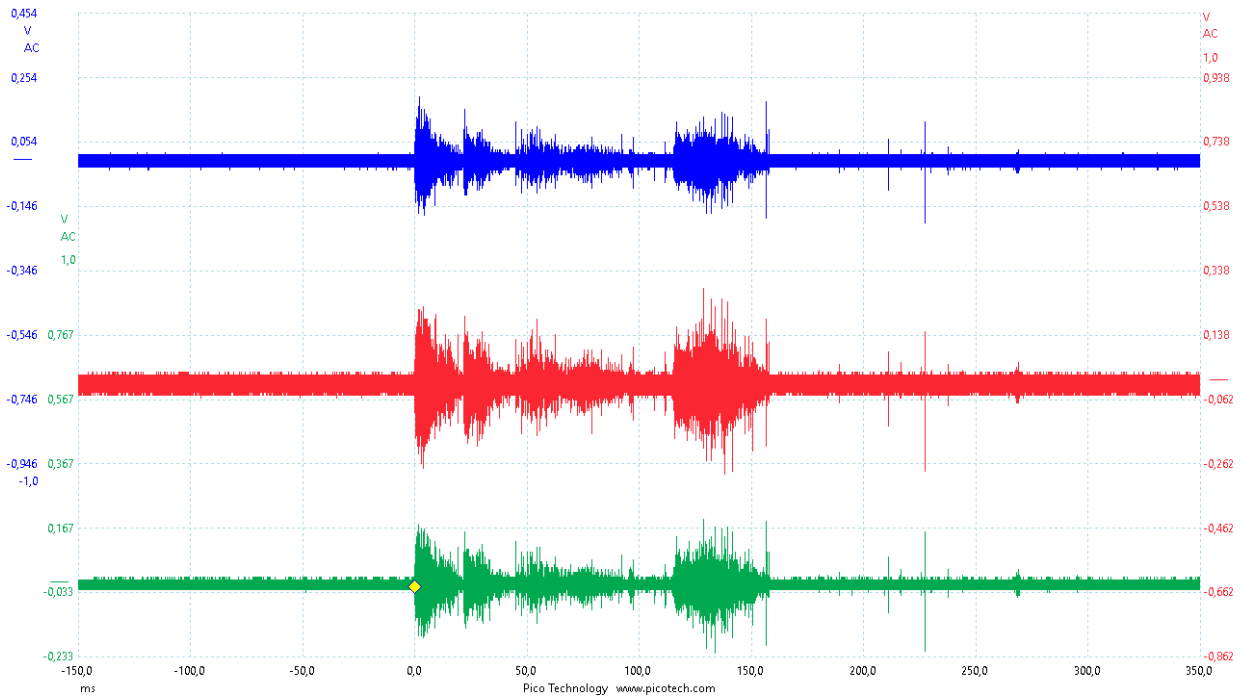
Figure 4-23.: Screenshot of a single record from the broadband lightning interferometer. The capture corresponds to a lightning event on March 22, 2019, at 17:24:45 UTC.

Table 4-17.: Summary of BINTF records during measuring campaign.

Number	Storm date	BINTF records
1	Nov-20 2019	11
2	Nov-22 2019	20
3	Dec-07 2019	42
4	Dec-08 2019	80
5	Dec-11 2019	118
6	Dec-29 2019	9
7	Dec-30 2019	78
8	Jan-01 2020	82
9	Feb-08 2020	2
10	Feb-25 2020	95

Continued on next page

Table 4-17 – continued from previous page

Number	Storm date	BINTF records
11	Feb-26 2020	11
12	Feb-29 2020	2
13	Mar-03 2020	18
14	Mar-08 2020	2
15	Mar-10 2020	217
16	Mar-11 2020	3
17	Mar-13 2020	51
18	Mar-16 2020	53

Table **4-17** summarizes 894 records over 18 days, but this number is lower after considering coincidences with FA, SA, and dE/dt records. Table **4-18** displays the adjusted results, with 599 records over 11 days.

Table 4-18.: Summary of BINTF records during measuring campaign with coincident records from FA, SA, and dE/dt antennas.

Number	Storm date	BINTF records
1	Nov-20 2019	11
2	Nov-22 2019	20
3	Dec-11 2019	118
4	Feb-25 2020	95
5	Feb-26 2020	11
6	Feb-29 2020	2
7	Mar-03 2020	18
8	Mar-10 2020	217
9	Mar-11 2020	3

Table 4-18 – continued from previous page

Number	Storm date	BINTF records
10	Mar-13 2020	51
11	Mar-16 2020	53

As mentioned before, the main feature of a BINTF is the ability to show lightning development inside the cloud. Then it is possible to focus and follow evolving of specific intracloud events as NBEs.

4.5.   Discussion of results

Classifying NBE waveforms is challenging due to varying instrumentation and sorting criteria. Comparing studies is difficult because of differences in instruments, observation times, triggering criteria, and sampling rates. However, a general trend is evident, allowing for good results and insights into findings and disagreements with prior studies.

The proportion of positive NBE and negative NBE is according to previous studies. Actual explanations for this suggests that positive are more prevalent because they tend to occur at lower altitudes being easier to detect. Also, it seems that negative NBEs are produced in presence of stronger convection inside thunderclouds, a hard condition to fulfill.

The relatively small percentage of Type A, less than 9 %, could be explained due to the high sampling rate used to digitize FA signals (i.e., sample period of 3.2 ns) allowing detection of rapid changes of the ambient electric field. Thus, in a minority of cases only possible to detect a pulse without ringing.

For sorting criteria, there are several modes of classification and even tagging a single pulse to a category depends on expert decisions applied directly or through rules executed by an algorithm. As a result, some actual NBE pulses can be discarded based on power emission or the number of antennas that recorded the event. Therefore, the classification system is not perfect but it is undoubtedly useful to determine the characteristics and behavior of NBEs.

In this study, findings about NBEs occurrence frequency agreed with prior studies confirming NBEs as a rare type of IC. This change is probably caused by the actual use of more accurate instrumentation with longer records and higher sampling rates, which provides a wider perspective

of these apparently elusive discharges. Thus, it is possible to recognize their presence more often than previously thought.

Differences among NBEs waveforms are generally related to the presence of additional ringing in some parts of the "basic NBE shape". That ringing can be before or after the main pulse or the overshoot. Thus, additional ringing justifies the existence of many types of NBE. The nature of that ringing is a matter of debate, some authors attribute its existence to the dispersion of negative charge reaching the origin of concurrent positive streamers.

NBE waveforms are susceptible to the effects of terrain because propagation over finite conductive planes generates attenuation, especially of high frequencies, then, waveform features such as pulse amplitudes and pulse duration are distorted. This aspect is relevant because the location and measurements performed in this study were entirely over mountainous terrain. The author of this study was aware of this condition but determining a single factor that encompasses conductive of varied mountainous terrain would be the main question for a dissertation. Then for analysis and comparison purposes, some degree of uncertainty on values of amplitude and time needs to be considered.

More studies are needed because NBEs are more common than previously believed, but not always present at the start of every lightning. Some lightning activity appears to start from an NBE occurrence. However, in this study, many records seem to start with a type of sub-microsecond pulse with a VHF signature, indicating a potential streamer origin. Given the time gap between the sub-microsecond pulse and the start of a leader, it is likely that the pulse marks the start of slow changes in the ambient electric field, setting the stage for a leader to emerge.

4.6.   Summary of findings

A summary of findings obtained from this extensive study on NBEs are:

- NBEs are only present in (15 %) of all lightning activity detected.

- Positive NBEs were 69 % and negative NBEs were 31 %.

- Type A waveforms were roughly 9 % of NBEs total.

- Type B waveforms were roughly 41 % of NBEs total.

- Type C waveforms were roughly 6 % of NBEs total.

- Type D waveforms were roughly 44 % of NBEs total.

- Type A NBEs: 76 % positive polarity, and 24 % negative polarity.

- Type B NBEs: 62 % of positive polarity, and 38 % negative polarity.

- Type C NBEs: 77 % of positive polarity, and 23 % negative polarity.

- Type D NBEs: 73 % of positive polarity, and 27 % negative polarity.

- The mean of the rise time is around 2.5 μs, where type B has the higher standard deviation.

- The mean of zero-crossing time is around 9 μs with a standard deviation of 3 μs.

- The mean of total pulse duration is under 20 μs, where type A has the lower standard deviation meanwhile type D has the higher standard deviation.

- Time isolated NBEs, according to 250 ms absent activity criterion, counts 30 % of the total.

- Spatial isolated NBEs, according to the absent activity criterion in a radius of 10 km, count 38 % of the total.

- Combining time and spatial isolation criteria, 13 % of the total can be considered truly isolated NBEs.

- Most of the records acquired during this study (approximately 80 %) have sub-microsecond pulses at any moment of their process.

5. Conclusions and recommendations

5.1. Conclusions

- NBEs are present in about 15 % of all lightning activity in the area of study (193 NBEs out of 1,316 events), a number similar to previous findings reported from Sri Lanka [23], Malaysia [118] and Indonesia [124] but higher than studies conducted in Sweden [125], Japan [126] and Northern China [38].

- There is a higher proportion of positive polarity NBEs, roughly in a ratio of 3 to 1 (133 positive NBEs vs 60 negative NBEs). This result is also similar to previous studies, even in higher latitudes. It appears that the right conditions for producing negative NBEs are more difficult to meet.

- Although Type C is the least frequent type found in this study with 6 %, Types B, C, and D account for 94 % of all NBEs recorded in this study, suggesting that additional ringing is a regular feature in NBEs [119], [28], [11].

- Negative polarity NBEs have a shorter waveform than positive polarity NBEs for Rise Time and FWHM, but longer for Zero Crossing and Total Duration due to the presence of ringing at the start and before the end of the main pulse.

- This study found a proportion of 30 % of negative polarity NBEs, suggesting the existence of stronger convection inside some of the recorded storms, a situation similar to studies in lower latitudes.

- NBEs seem to be a rare event (15 %) but once they occur, they appear to be related to other lightning activity. Considering temporal and spatial conditions, only 13 % can be considered truly isolated.

- Groups of NBEs are collections of two or more NBEs that are temporally close and located close together. In this study, they are not a rare event because about 23 % of all NBEs recorded were part of a group. According to the records, only a small proportion of groups can be considered isolated.

- As a whole, the occurrence rates, polarity ratios, and waveform parameters found in this study are reasonably similar to previous studies, and the similarity increases with studies conducted in lower latitudes.

5.2. Implications

- The occurrence rate suggests NBEs are a by-product of lightning inception instead of its cause, meaning that other phenomena initiate lightning. In fact, during this project, researchers identified a new type of fast breakdown discharge, seemingly compounded by positive streamers moving faster than ordinary electrical discharges [7], [96]. From interferometric measurements, they hypothesize that both lightning inception and some NBEs are produced by fast breakdowns [78], [108]. However, it is not clear if those fast breakdowns are at the start of any electrical discharge or why only sometimes they produce NBEs.

- The rate of occurrence of NBEs implies the existence of storms with a larger vertical extent, while the rate of occurrence of negative polarity NBEs suggests stronger convection inside some of those storms. These conditions are more common in tropical regions because of the high tropopause. Despite these findings, the exact circumstances that give rise to NBEs and their role in the overall picture of electrical activity inside clouds are still unclear.

- The production of additional ringing in types B, C, and D should be related to the discontinuous motion of negative charge. A fast positive breakdown could explain this condition because fast breakdowns are associated with the development of thousands of positive streamers in virgin air [76]. In this scenario, the discontinuity of charge could be explained by the physics behind the development and evolution of streamers [78] or by the simultaneous overlap of fast positive and fast negative breakdowns [127].

- In this study, hundreds of records started with one or more sub-microsecond pulses, which is consistent with recent studies relating these pulses to electrical charges starting to move inside clouds. This motion seems to be related to a re-accommodation of electrical charge, which leads to intensifying the electric field and the production of other pulses. The possible proof of this process is the record of slow but increasing changes in the ambient electric field after sub-microsecond pulses take place [128], [129], [130].

- The occurrence rate of NBEs, especially negative polarity NBEs, suggests that similar rates should be present for TLEs due to the relationship suggested between them in previous studies. A similar situation occurs with Terrestrial Gamma-Ray Flashes (TGFs). In fact, Lopez et al. [22] reported simultaneous observations of NBEs and blue light emissions from the top of thunderclouds observed in Barracabermeja, Colombia.

5.3. Recommendations for further study

- Findings suggest that NBEs are not the cause of lightning inception. For further studies, the author recommends including extended observation periods with a focus on the output of slow

antennas to deepen the understanding of the relationship between sub-microsecond pulses and changes in the slow ambient electric field. The latter condition appears to be related to the redistribution of electrical charge inside the cloud prior to the initial breakdown pulses [130], [129], [131].

- The preliminary results from the broadband lightning interferometer show that it is a valuable instrument that deserves further improvement. To provide reliable data, additional instrumentation and calibration are needed, including the validation of source location through a pulse generator attached to an unmanned aerial vehicle [96]. It is also important to choose a method for determining the three-dimensional source location, either through signal processing or complementary instrumentation [132], [133], [134].

- The author believes there is potential for improvement in lightning instrumentation through the application of digital signal processing techniques in embedded systems. These techniques could be used for tasks such as filtering and signal conditioning [135]. These improvements would increase the flexibility of lightning instrumentation, making it easier to adapt to different contexts and goals [11]. These approaches would also reduce costs and make it easier to deploy instrumentation in varying and challenging conditions [136].

- Taking advantage of the favorable conditions for lightning activity in Colombia, the author strongly recommends deploying lightning instrumentation in areas with more persistent lightning activity in future studies. Lightning activity in Bogota is high, but it is only significant for four months a year. In contrast, the activity in northern areas of Colombia and around the Magdalena River valley is higher and consistent for almost nine months, providing easier access to lightning data [137], [122].

A. Appendix: Method for NBEs source height estimation

Discharge height estimation is essential because the location of the event gives useful information to understand the electrical phenomenon, the structure of the thundercloud, its correlation with both other intracloud discharges and the meteorological conditions present at the moment of occurrence of the NBE. At present, there are two methodologies to estimate the height of an NBE. The first methodology uses the basic geometry of the model sketched in Figure **A-1**.
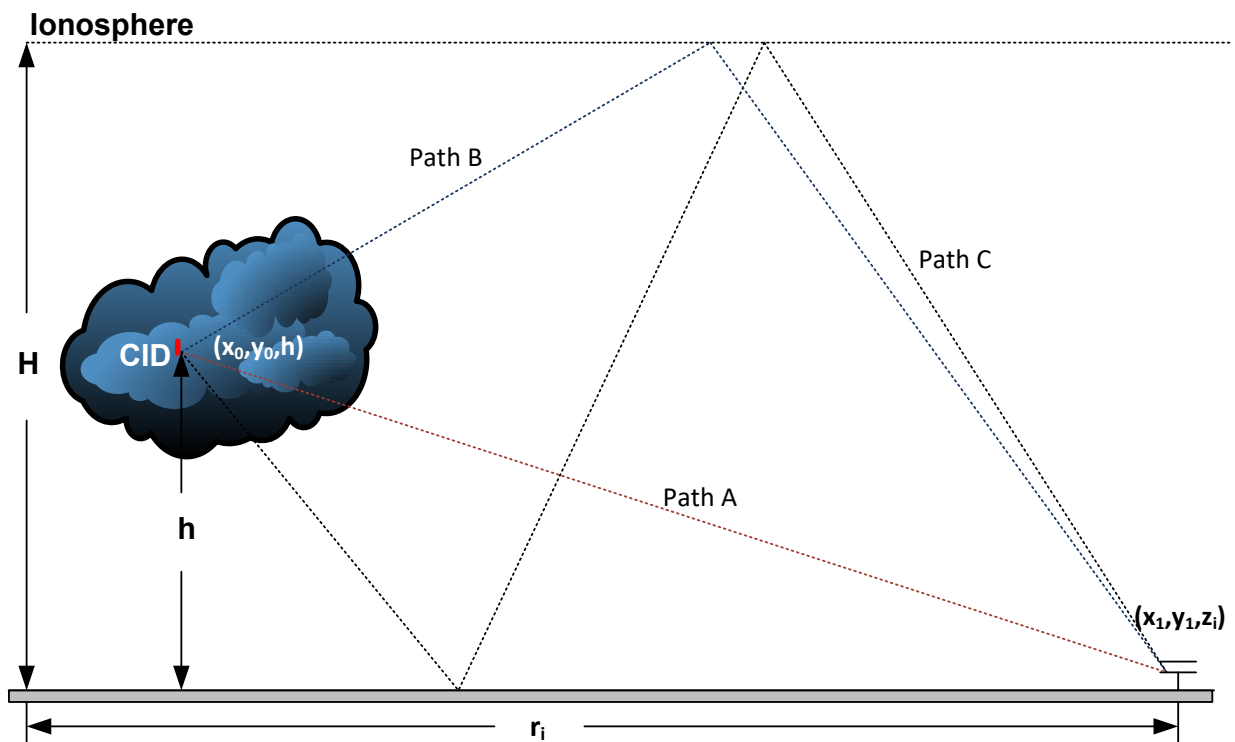
Figure A-1.: The reference model is showing the defined geometric parameters to estimate the height of the NBE source pointing out the multiple paths of the signal to arrive at the observation site.

Mostly, in this approach, it is assumed a flat ground model (no obstacles) with a series of signals coming from reflection paths. This methodology needs to have accurate information about the horizontal distance between the measuring station and the NBE, and both the electric field and

magnetic field related to the NBE. The latter because these two magnitudes are related as follows

$$\frac{\mathbf{E}_z}{\mathbf{B}_\phi} = c \cos \alpha \tag{A-1}$$

where c is the speed of light and α is the elevation angle that can be found as

$$\alpha = \operatorname{arc\,cos} \left(\frac{\mathbf{E}_z}{c\mathbf{B}_\alpha} \right) \tag{A-2}$$

Finally, the height of the NBE can be estimated as

$$h = r \tan \alpha \tag{A-3}$$

where r is the horizontal distance from the NBE source to the observation site.

The second methodology only uses the information of the vertical electric field ($\mathbf{E}_z$) but introduces the concept of the virtual height of the ionosphere (H). The virtual height is a convenient simplification to calculate reflections on the higher atmosphere depicted in Fig. **A-2**. The idea was originally proposed by Smith [14]. In this way, the process of estimation involves measuring the NBE pulse and its subsequent reflection pulses. Therefore, the time difference between the main pulse and its reflections have information about the location of the NBE pulse. Fig. **A-1** shows the geometry used to estimated the NBE location. According to Fig. **A-1**, there are the following relations:
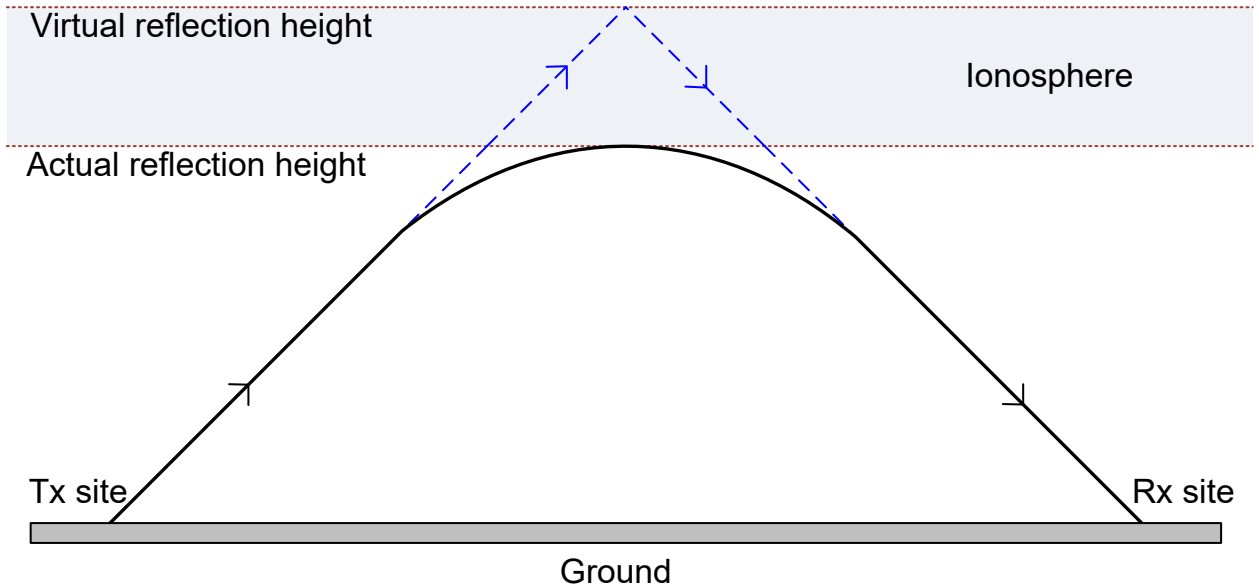
Figure A-2.: Depiction of the definition of virtual height of the ionosphere (H) used to estimate the NBE height location.

$$ct_{ia} = \sqrt{(2H - h - z_i)^2 + r_i^2} - \sqrt{(h - z_i)^2 + r_i^2} \tag{A-4}$$

$$ct_{ib} = \sqrt{(2H + h - z_i)^2 + r_i^2} - \sqrt{(h - z_i)^2 + r_i^2} \tag{A-5}$$

where t_{ia} is the time difference between the NBE pulse and its first reflection. t_{ib} is the time difference between the NBE pulse and its second reflection. r_i is given by

$$r_i = R \arccos(\sin(x_0)\sin(x_i) + \cos(x_0)\cos(x_i)\cos(y_0 - y_i)) \tag{A-6}$$

where R is the radius of the Earth, x_0 and y_0 are the latitude and longitude of the source NBE, and x_i and y_i are the latitude and longitude of the observation site.

Substituting equation A-6 in the equations A-4 and using a minimum mean square error approach to solving the unknown variables, it constructs the following function:

$$f(H, h, x_0, y_0) = \left(ct_{ia} - \sqrt{(2H - h - z_i)^2 + r_i^2} - \sqrt{(h - z_i)^2 + r_i^2} \right)^2$$
$$+ \left(ct_{ib} - \sqrt{(2H + h - z_i)^2 + r_i^2} - \sqrt{(h - z_i)^2 + r_i^2} \right)^2 \tag{A-7}$$

Equation A-7 has four unknown variables, but as it was proposed by [16] it is possible to assume a value for the virtual ionospheric height H and as a consequence reduce one unknown variable improving the accuracy of the solution given by the equation.

B. Appendix: Summary of the data collected for this study

A detailed compendium of data collected during the measuring campaign is now presented. Hereby is a set of tables with information of NBEs detected in each stormy day recorded. This data was the source of information for all the findings and analysis discussed in previous chapters.

Thursday, November 14 2019

Type of waveform	Positive polarity	Percentage	Negative polarity	Percentage	Total number of pulses	Percentage
A	0	0.0 %	0	0.0 %	0	0.0 %
B	0	0.0 %	7	26.9 %	7	26.9 %
C	14	53.8 %	2	7.7 %	16	61.5 %
D	1	3.8 %	2	7.7 %	3	11.5 %

Monday, November 18 2019

Type of waveform	Positive polarity	Percentage	Negative polarity	Percentage	Total number of pulses	Percentage
A	5	13.1 %	3	7.8 %	8	21.0 %
B	2	5.2 %	5	13.1 %	7	18.4 %
C	16	42.1 %	2	5.2 %	18	47.3 %
D	5	13.1 %	0	13.1 %	5	13.1 %

Tuesday, November 19 2019

Type of waveform	Positive polarity	Percentage	Negative polarity	Percentage	Total number of pulses	Percentage
A	4	7.8 %	3	5.8 %	7	13.7 %
B	11	21.5 %	8	15.6 %	19	37.2 %
C	13	25.4 %	1	1.9 %	14	27.4 %
D	11	21.5 %	0	0.0 %	11	21.5 %

Wednesday, November 20 2019

Type of waveform	Positive polarity	Percentage	Negative polarity	Percentage	Total number of pulses	Percentage
A	2	3.8 %	6	11.5 %	8	15.3 %
B	2	3.8 %	7	13.4 %	9	17.3 %
C	12	23.0 %	6	11.5 %	18	34.6 %
D	12	23.0 %	5	9.6 %	17	32.6 %

Thursday, November 21 2019

Type of waveform	Positive polarity	Percentage	Negative polarity	Percentage	Total number of pulses	Percentage
A	1	12.5 %	0	0.0 %	1	12.5 %
B	0	0.0 %	1	12.5 %	1	12.5 %
C	3	37.5 %	1	12.5 %	4	50.0 %
D	2	25.0 %	0	0.0 %	2	25.0 %

Friday, November 22 2019

Type of waveform	Positive polarity	Percentage	Negative polarity	Percentage	Total number of pulses	Percentage
A	1	4.7 %	1	4.7 %	2	9.5 %
B	8	38.0 %	2	9.5 %	10	47.6 %
C	0	0.0 %	1	4.7 %	2	9.5 %
D	6	28.5 %	1	4.7 %	7	33.3 %

Thursday, November 23 2019

Type of waveform	Positive polarity	Percentage	Negative polarity	Percentage	Total number of pulses	Percentage
A	0	0.0 %	0	0.0 %	0	0.0 %
B	0	0.0 %	1	50.0 %	1	50.0 %
C	1	50.0 %	0	0.0 %	1	50.0 %
D	0	0.0 %	0	0.0 %	0	0.0 %

Friday, November 29 2019

Type of waveform	Positive polarity	Percentage	Negative polarity	Percentage	Total number of pulses	Percentage
A	9	39.1 %	1	4.3 %	10	43.4 %
B	7	30.4 %	2	8.6 %	9	39.1 %
C	2	8.6 %	0	0.0 %	2	8.6 %
D	8	34.7 %	1	4.3 %	9	39.1 %

Wednesday, December 11 2019

Type of waveform	Positive polarity	Percentage	Negative polarity	Percentage	Total number of pulses	Percentage
A	2	50.0 %	0	0.0 %	2	50.0 %
B	0	0.0 %	2	50.0 %	2	50.0 %
C	0	0.0 %	0	0.0 %	0	0.0 %
D	0	0.0 %	0	0.0 %	0	0.0 %

Thursday, February 25 2020

Type of waveform	Positive polarity	Percentage	Negative polarity	Percentage	Total number of pulses	Percentage
A	1	50.0 %	0	0.0 %	1	50.0 %
B	1	50.0 %	0	0.0 %	1	50.0 %
C	0	0.0 %	0	0.0 %	0	0.0 %
D	0	0.0 %	0	0.0 %	0	0.0 %

Thursday, February 26 2020

Type of waveform	Positive polarity	Percentage	Negative polarity	Percentage	Total number of pulses	Percentage
A	0	0.0 %	0	0.0 %	0	x %
B	0	0.0 %	0	0.0 %	0	x %
C	0	0.0 %	0	0.0 %	0	x %
D	1	100.0 %	0	0.0 %	1	100.0 %

Thursday, March 3 2020

Type of waveform	Positive polarity	Percentage	Negative polarity	Percentage	Total number of pulses	Percentage
A	0	0.0 %	0	0.0 %	0	0.0 %
B	0	0.0 %	0	0.0 %	0	0.0 %
C	0	0.0 %	0	0.0 %	0	0.0 %
D	1	100.0 %	0	0.0 %	1	100.0 %

Thursday, March 10 2020

Type of waveform	Positive polarity	Percentage	Negative polarity	Percentage	Total number of pulses	Percentage
A	4	8.1 %	1	2.0 %	5	10.2 %
B	13	26.5 %	4	8.1 %	17	34.6 %
C	7	14.2 %	2	4.0 %	9	18.3 %
D	13	26.5 %	5	10.2 %	18	36.7 %

Thursday, March 11 2020

Type of waveform	Positive polarity	Percentage	Negative polarity	Percentage	Total number of pulses	Percentage
A	0	0.0 %	0	0.0 %	0	0.0 %
B	2	66.7 %	1	33.3 %	3	100 %
C	0	0.0 %	0	0.0 %	0	0.0 %
D	0	0.0 %	0	0.0 %	0	0.0 %

Thursday, March 13 2020

Type of waveform	Positive polarity	Percentage	Negative polarity	Percentage	Total number of pulses	Percentage
A	0	0.0 %	0	0.0 %	0	0.0 %
B	0	0.0 %	0	0.0 %	0	0.0 %
C	0	0.0 %	0	0.0 %	0	0.0 %
D	1	100.0 %	0	0.0 %	1	100.0 %

Thursday, March 16 2020

Type of waveform	Positive polarity	Percentage	Negative polarity	Percentage	Total number of pulses	Percentage
A	1	50.0 %	0	0.0 %	1	50.0 %
B	0	0.0 %	0	0.0 %	0	0.0 %
C	0	0.0 %	0	0.0 %	0	0.0 %
D	1	50.0 %	0	0.0 %	1	50.0 %

Thursday, March 26 2020

Type of waveform	Positive polarity	Percentage	Negative polarity	Percentage	Total number of pulses	Percentage
A	4	8.5 %	0	0.0 %	4	8.5 %
B	25	53.1 %	8	17.0 %	33	70.2 %
C	1	2.1 %	0	0.0 %	1	2.1 %
D	7	14.8 %	2	4.2 %	9	19.1 %

Thursday, March 27 2020

Type of waveform	Positive polarity	Percentage	Negative polarity	Percentage	Total number of pulses	Percentage
A	0	0.0 %	0	0.0 %	0	0.0 %
B	1	100.0 %	0	0.0 %	1	100.0 %
C	0	0.0 %	0	0.0 %	0	0.0 %
D	0	0.0 %	0	0.0 %	0	0.0 %

Thursday, March 29 2020

Type of waveform	Positive polarity	Percentage	Negative polarity	Percentage	Total number of pulses	Percentage
A	0	0.0 %	0	0.0 %	0	0.0 %
B	0	0.0 %	1	100.0 %	1	100.0 %
C	0	0.0 %	0	0.0 %	0	0.0 %
D	0	0.0 %	0	0.0 %	0	0.0 %

C. Appendix: Measurements of NBE pulses classified by type

Type A, positive polarity

No	Rise time (μs)	FWHM (μs)	Zero crossing time (μs)	Pulse duration (μs)	Ratio O_s/P_a
1	0.7	1.4	3.3	4.6	0.2
2	1.2	2.3	5.4	8.8	0.4
3	3.9	4.1	10.8	27	0.4
4	1.9	3.2	6.4	11.9	0.3
5	1.9	2.7	6.2	12.8	0.3
6	3.0	3.8	13	26.9	0.3
7	1.5	3.2	8.4	13	0.3
8	0.8	1.5	2.9	4.7	0.6
9	0.8	1.6	2.8	4.6	0.5
10	1.3	1.9	3.7	6.4	0.6
11	2.0	2.1	5.0	8.7	0.4
12	1.2	2.0	4.4	9.2	0.6
13	2.1	1.9	6.2	10.1	0.3

Table C-1.: A compendium of results obtained for Type A, positive polarity, NBE pulses.

Type A, negative polarity

The mean value for negative polarity, type A NBEs were:

No	Rise time (μs)	FWHM (μs)	Zero crossing time (μs)	Pulse duration (μs)	Ratio O_s/P_a
1	1.2	1.5	3.5	6.6	0.3
2	1.6	2.0	4.5	6.9	0.2
3	1.9	1.5	3.9	5.3	0.1
4	2.0	1.6	4.6	7.4	0.1

Table C-2.: A compendium of results obtained for Type A, negative polarity, NBE pulses.

Type B, positive polarity

No	Rise time (μs)	FWHM (μs)	Zero crossing time (μs)	Pulse duration (μs)	Ratio O_s/P_a
1	1.2	1.6	4.2	9.0	0.5
2	1.1	1.4	3.9	12	0.6
3	1.5	1.7	3.2	18.6	0.6
4	1.4	1.6	3.9	7.8	0.3
5	1.3	1.6	4.9	8.3	0.2
6	0.9	1.1	3.0	5.7	0.2
7	0.9	1.2	4.7	11	0.6
8	1.7	2.8	7.9	15	0.3
9	1.3	1.7	3.3	12	0.3
10	1.7	1.7	5.4	20	0.5
11	2.0	1.9	5.1	23	0.2
12	1.1	1.9	6.3	29	0.5
13	1.8	1.5	6.7	14	0.2
14	2.4	1.9	9.5	17	0.2
15	2.0	2.3	6.1	14	0.1
16	1.6	1.9	4.2	18	0.2
17	2.2	1.7	6.1	21	0.3
18	2.2	1.5	6.1	14	0.2
19	2.1	2.4	6.7	17	0.3

Table C-3 – continued from previous page

No	Rise time (μs)	FWHM (μs)	Zero crossing time (μs)	Pulse duration (μs)	Ratio O_s/P_a
20	2.2	3.8	10.0	20.0	0.2
21	5.2	2.9	9.7	18	0.2
22	1.6	2.2	4.5	14	0.4
23	2.2	3.1	6.8	14	0.3
24	3.8	2.6	7.6	22	0.4
25	3.3	5.9	11	28	0.3
26	4.6	2.7	11	21	0.2
27	1.6	3.2	8.6	17	0.3
28	2.6	2.9	9.1	20	0.4
29	2.7	2.6	6.3	18	0.4
30	1.4	2.2	4.5	17	0.3
31	1.5	2.9	7.6	37	0.7
32	2.2	2.4	7.6	20	0.3
33	1.6	3.7	7.3	20	0.4
34	3.2	2.8	7.6	19	0.3
35	4.5	3.4	8.7	25	0.5
36	1.4	1.7	3.4	11	0.4
37	1.9	2.4	6.7	28	0.3
38	1.1	1.2	3.6	14	0.4
39	1.8	1.5	4.1	14	0.4
40	4.1	5.0	11	19	0.2
41	4.0	3.3	8.8	20	0.4
42	6.8	4.2	12	24	0.4
43	1.7	4.0	10	18	0.3
44	1.9	2.9	5.8	13	0.3
45	4.5	3.0	10	25	0.2
46	2.3	3.6	6.3	20	0.3
47	3.9	5.1	9.7	21	0.4

Table C-3 – continued from previous page

No	Rise time (μs)	FWHM (μs)	Zero crossing time (μs)	Pulse duration (μs)	Ratio O_s/P_a
48	5.4	4.4	10	22	0.4
49	7.6	5.6	13	29	0.4

Table C-3.: A compendium of results obtained for Type B, positive polarity, NBE pulses.

Type B, negative polarity

No	Rise time (μs)	FWHM (μs)	Zero crossing time (μs)	Pulse duration (μs)	Ratio O_s/P_a
1	1.6	1.7	6.5	28	0.1
2	0.9	1.7	6.3	18	0.3
3	2.9	1.9	6.0	9.8	0.2
4	1.5	1.7	5.6	8.0	0.3
5	2.5	3.0	8.4	25	0.3
6	3.2	3.0	14	23	0.2
7	1.3	1.5	4.1	8.1	0.2
8	0.9	2.2	3.6	7.2	0.4
9	0.9	2.2	5.4	23	0.3
10	1.3	1.3	3.5	12	0.4
11	0.8	1.3	3.6	11	0.3
12	1.3	1.4	4.0	7.9	0.3
13	1.4	2.0	4.6	16	0.7
14	2.4	2.5	6.5	11	0.2
15	3.3	3.5	9.5	25	0.3
16	1.1	1.7	3.8	12	0.3
17	1.3	1.7	4.9	13	0.2
18	2.4	2.2	4.7	9.6	0.5
19	3.7	1.8	7.1	14	0.4

Table C-4 – continued from previous page

No	Rise time (μs)	FWHM (μs)	Zero crossing time (μs)	Pulse duration (μs)	Ratio O_s/P_a
20	1.7	2.9	6.0	16	0.3
21	1.4	2.4	5.2	14	0.3
22	1.6	3.1	5.6	15	0.6
23	1.4	2.6	6.3	12	0.2
24	3.6	2.7	6.2	12	0.4
25	3.0	3.2	9.2	25	0.4
26	1.9	2.2	4.9	18	0.5
27	1.2	1.9	3.4	8.4	0.4
28	3.0	2.2	6.7	13	0.2
29	1.2	1.9	3.7	11	0.4
30	1.3	1.9	4.5	12	0.5
31	3.6	2.2	6.8	19	0.3

Table C-4.: A compendium of results obtained for Type B, negative polarity, NBE pulses.

Type C, positive polarity

No	Rise time (μs)	FWHM (μs)	Zero crossing time (μs)	Pulse duration (μs)	Ratio O_s/P_a
1	0.5	1.0	3.5	5.8	0.4
2	2.5	2.0	11	21	0.1
3	1.4	2.0	5.1	12	0.2
4	2.2	2.1	8.9	23	0.4
5	1.8	1.9	6.5	7.4	0.1
6	1.3	2.6	7.0	15	0.5
7	3.0	2.4	12	26	0.6
8	3.0	4.5	12	28	0.6
9	1.9	6.3	11	25	0.3

Table C-5 – continued from previous page

No	Rise time (μs)	FWHM (μs)	Zero crossing time (μs)	Pulse duration (μs)	Ratio O_s/P_a

Table C-5.: A compendium of results obtained for Type C, positive polarity, NBE pulses.

Type C, negative polarity

No	Rise time (μs)	FWHM (μs)	Zero crossing time (μs)	Pulse duration (μs)	Ratio O_s/P_a
1	0.5	1.0	3.1	5.5	0.1
2	0.8	1.7	5.5	14	0.6
3	1.4	4.4	10	16	0.1

Table C-6.: A compendium of results obtained for Type C, negative polarity, NBE pulses.

Type D, positive polarity

No	Rise time (μs)	FWHM (μs)	Zero crossing time (μs)	Pulse duration (μs)	Ratio O_s/P_a
1	3.3	3.3	6.1	11	0.2
2	9.2	3.3	14	18	0.2
3	5.4	4.3	13	25	0.3
4	6.6	2.5	12	25	0.4
5	6.3	4.0	9.5	14	0.3
6	3.3	1.5	5.8	15	0.5
7	2.9	3.5	4.9	13	0.6
8	2.2	1.7	4.8	8.3	0.3
9	6.3	4.8	9.3	14	0.2
10	17	4.7	24	36	0.3
11	3.3	1.7	6.4	22	0.3
12	4.2	4.0	12	20	0.3

Table C-7 – continued from previous page

No	Rise time (μs)	FWHM (μs)	Zero crossing time (μs)	Pulse duration (μs)	Ratio O_s/P_a
13	5.8	2.3	9.3	12	0.2
14	4.1	1.5	7.1	13	0.4
15	5.7	1.8	10	18	0.2
16	13	1.5	19	22	0.2
17	3.6	1.5	7.9	13	0.3
18	4.2	3.4	8.7	29	0.3
19	1.3	1.7	4.9	15	0.4
20	7.6	1.5	10	28	0.3
21	3.1	1.8	7.0	19	0.2
22	6.5	1.7	10	30	0.4
23	6.7	1.9	12	20	0.2
24	5.8	3.4	11	25	0.4
25	8.2	5.5	19	31	0.3
26	14	2.0	21	32	0.3
27	3.0	1.6	5.2	9.3	0.2
28	3.6	1.6	5.2	7.2	0.5
29	5.7	2.9	8.0	11	0.4
30	4.7	4.0	7.9	11	0.4
31	5.4	4.7	8.4	14	0.2
32	4.4	2.4	9.0	24	0.4
33	3.6	2.0	8.1	29	0.6
34	15	5.2	21	43	0.3
35	8.9	1.8	12	39	0.4
36	5.1	1.9	8.5	10	0.2
37	3.2	1.5	5.8	11	0.4
38	6.5	5.2	12	24	0.3
39	9.6	4.1	23	38	0.2
40	6.8	3.2	16	30	0.2

Table C-7 – continued from previous page

No	Rise time (μs)	FWHM (μs)	Zero crossing time (μs)	Pulse duration (μs)	Ratio O_s/P_a
41	6.1	3.2	10	16	0.6
42	9.5	3.0	17	24	0.3
43	6.7	2.8	10	18	0.3
44	6.3	1.1	7.8	11	0.3
45	19	14	24	32	0.3
46	12	12	15	21	0.7
47	3.2	2.1	7.1	10	0.3
48	9.1	7.4	13	22	0.4
49	4.4	5.8	14	30	0.2
50	7.4	2.4	13	28	0.5
51	8.0	2.8	15	27	0.2
52	5.6	3.7	8.9	22	0.4
53	1.5	3.6	12	21	0.2
54	1.1	1.3	10	16	0.7
55	6.1	1.2	8.1	20	0.7
56	5.2	1.1	7.4	14	0.3
57	4.5	1.9	6.8	8.4	0.4
58	4.6	1.5	7.4	12	0.4
59	6.6	1.7	8.8	13	0.6
60	4.6	1.6	10	12	0.3
61	3.0	1.3	6.1	13	0.2
62	3.5	2.1	6.1	13	0.2

Table C-7.: A compendium of results obtained for Type D, positive polarity, NBE pulses.

Type D, negative polarity

No	Rise time (μs)	FWHM (μs)	Zero crossing time (μs)	Pulse duration (μs)	Ratio O_s/P_a
1	7.9	1.9	17	31	0.2
2	3.4	1.6	6.0	9.4	0.2
3	4.9	2.5	7.6	9.3	0.2
4	2.9	1.5	6.2	9.6	0.2
5	2.9	1.5	5.5	8.5	0.3
6	4.0	1.3	6.8	16	0.5
7	3.5	2.4	6.4	8.7	0.2
8	6.4	6.3	10	17	0.2
9	4.4	2.5	8.4	19	0.4
10	2.4	1.8	6.7	8.7	0.3
11	1.2	1.3	5.6	9.9	0.5
12	3.5	1.7	8.1	16	0.3
13	7.2	2.8	11	20	0.4
14	1.8	5.0	16	26	0.3
15	3.9	5.4	9.0	16	0.4
16	4.9	3.6	14	31	0.4
17	8.6	4.9	14	22	0.3
18	8.3	4.0	13	19	1.0
19	4.5	2.1	7.0	13	0.3
20	3.7	1.9	6.1	7.7	0.3
21	8.4	2.6	15	25	1.0
22	4.2	2.1	9.2	17	0.4

Table C-8.: A compendium of results obtained for Type D, negative polarity, NBE pulses.

Bibliografía

[1] T. J. Lang, S. Pédeboy, W. Rison, R. S. Cerveny, J. Montanyà, S. Chauzy, D. R. MacGorman, R. L. Holle, E. E. Ávila, Y. Zhang, G. Carbin, E. R. Mansell, Y. Kuleshov, T. C. Petersrson, M. Brunet, F. Driouech, and D. S. Krahenbuhl, "Wmo world record lightning extremes: Longest reported flash distance and longest reported flash duration," *Bulletin of the American Meteorological Society*, vol. 98, pp. 1153–1168, 2017.

[2] J. R. Dwyer and M. a. Uman, "The physics of lightning," *Physics Reports*, vol. 534, pp. 147–241, 10 2013. [Online]. Available: http://linkinghub.elsevier.com/retrieve/pii/S037015731300375X

[3] T. Warner, M. Saba, C. Schumann, J. H. Jr, and R. Orville, "Observations of bidirectional lightning leader initiation and development near positive leader channels," *Journal of Geophysical Research: Atmospheres*, vol. 121, pp. 9251–9260, 2016.

[4] J. Montanyà, O. van der Velde, and E. R. Williams, "The start of lightning: Evidence of bidirectional lightning initiation," *Scientific Reports*, vol. 5, p. 15180, 2015. [Online]. Available: http://www.nature.com/articles/srep15180

[5] M. D. Tran and V. A. Rakov, "Initiation and propagation of cloud-to-ground lightning observed with a high-speed video camera," *Scientific Reports*, vol. 6, pp. 1–11, 2016. [Online]. Available: http://dx.doi.org/10.1038/srep39521

[6] W. Rison, P. R. Krehbiel, M. G. Stock, H. E. Edens, X.-M. Shao, R. J. Thomas, M. A. Stanley, and Y. Zhang, "Observations of narrow bipolar events reveal how lightning is initiated in thunderstorms," *Nature Communications*, vol. 7, p. 10721, 2016. [Online]. Available: http://www.nature.com/doifinder/10.1038/ncomms10721

[7] J. N. Tilles, N. Liu, M. A. Stanley, P. R. Krehbiel, W. Rison, G. Michael, J. R. Dwyer, R. Brown, and J. Wilson, "Fast negative breakdown in thunderstorms," *Nature Communications*, pp. 1–12, 2018. [Online]. Available: http://dx.doi.org/10.1038/s41467-019-09621-z

[8] F. Shi, N. Liu, J. R. Dwyer, and K. M. Ihaddadene, "Vhf and uhf electromagnetic radiation produced by streamers in lightning," *Geophysical Research Letters*, vol. 46, pp. 443–451, 2019.

[9] D. M. L. Vine, "Sources of the strongest rf radiation from lightning," *Journal of Geophysical Research*, vol. 85, p. 4091, 1980. [Online]. Available: http://doi.wiley.com/10.1029/JC085iC07p04091 http://hdl.handle.net/2060/19790015388

[10] D. L. Vine, "The spectrum of radiation from lightning," 1980.

[11] A. F. Leal, V. A. Rakov, and B. R. P. Rocha, "Upgrading a low-cost system for measuring lightning electric field waveforms," *IEEE Transactions on Electromagnetic Compatibility*, vol. 61, pp. 595–598, 2019.

[12] S. Karunarathne, T. C. Marshall, M. Stolzenburg, and N. Karunarathna, "Electrostatic field changes and durations of narrow bipolar events," *Journal of Geophysical Research: Atmospheres*, pp. 1–14, 2016.

[13] R. J. Thomas, P. R. Krehbiel, T. Hamlin, J. Harlin, and D. Shown, "Observations of vhf source powers radiated by lightning," *Geophysical Research Letters*, vol. 28, pp. 143–146, 2001.

[14] D. A. Smith, X. M. Shao, D. N. Holden, C. T. Rhodes, M. Brook, P. R. Krehbiel, M. Stanley, W. Rison, and R. J. Thomas, "A distinct class of isolated intracloud lightning discharges and their associated radio emissions," *Journal of Geophysical Research Atmospheres*, vol. 104, pp. 4189–4212, 1999. [Online]. Available: http://www.scopus.com/inward/record.url?eid=2-s2.0-0033608497partnerID=tZOtx3y1

[15] A. R. Jacobson and T. E. L. Light, "Revisiting "narrow bipolar event"intracloud lightning using the forte satellite," *Annales Geophysicae*, vol. 30, pp. 389–404, 2012.

[16] T. Wu, W. Dong, Y. Zhang, T. Funaki, S. Yoshida, T. Morimoto, T. Ushio, and Z. Kawasaki, "Discharge height of lightning narrow bipolar events," *Journal of Geophysical Research*, vol. 117, p. D05119, 3 2012. [Online]. Available: http://www.scopus.com/inward/record.url?eid=2-s2.0-84863375330partnerID=tZOtx3y1

[17] A. Nag, "Characterization and modeling of lightning processes with emphasis on compact intracloud discharges," p. 508, 2010.

[18] M. Ahmad, M. Esa, V. Cooray, Z. Baharudin, and P. Hettiarachchi, "Latitude dependence of narrow bipolar pulse emissions," *Journal of Atmospheric and Solar-Terrestrial Physics*, vol. 128, pp. 40–45, 6 2015. [Online]. Available: http://www.scopus.com/inward/record.url?eid=2-s2.0-84925435106partnerID=tZOtx3y1

[19] K. C. Wiens, T. Hamlin, J. D. Harlin, and D. M. Suszcynsky, "Relationships among narrow bipolar events, total lightning and radar inferred convective strength in great plains thunderstorms," *Journal of Geophysical Research*, vol. 113, pp. 1–31, 2008. [Online]. Available: http://www.scopus.com/inward/record.url?eid=2-s2.0-77949294233partnerID=tZOtx3y1

[20] S. Karunarathne, T. C. Marshall, M. Stolzenburg, and N. Karunarathna, "Modeling initial breakdown pulses of cg lightning flashes," *Journal of Geophysical Research Atmospheres*, vol. 119, 2014.

[21] A. Nag, V. A. Rakov, D. Tsalikis, and J. A. Cramer, "On phenomenology of compact intracloud lightning discharges," *Journal of Geophysical Research*, vol. 115, p. D14115, 7 2010. [Online]. Available: http://www.scopus.com/inward/record.url?eid=2-s2.0-77955396523partnerID=tZOtx3y1

[22] J. A. López, J. Montanyà, O. van der Velde, D. Romero, F. J. Gordillo-Vázquez, F. J. Pérez-Invernón, A. Luque, C. A. M. Rodriguez, T. Neubert, W. Rison, P. Krehbiel, J. N. González, N. Østgaard, and V. Reglero, "Initiation of lightning flashes simultaneously observed from space and the ground: Narrow bipolar events," *Atmospheric Research*, vol. 268, 4 2022.

[23] S. Sharma, M. Fernando, and V. Cooray, "Narrow positive bipolar radiation from lightning observed in sri lanka," *Journal of Atmospheric and Solar-Terrestrial Physics*, vol. 70, pp. 1251–1260, 7 2008. [Online]. Available: http://www.scopus.com/inward/record.url?eid=2-s2.0-45449093166partnerID=tZOtx3y1

[24] M. Ahmad, M. Esa, E. R. Williams, D. Periannan, M. Aziz, G. Lu, H. Zhang, and V. Cooray, "Emission height of narrow bipolar events of a tropical storm over malacca strait," 2016.

[25] R. Albrecht, S. Goodman, D. Buechler, R. Blakeslee, and H. Christian, "Where are the lightning hotspots on earth?" *Builletin America Meteorological Society*, vol. 97, pp. 2051–2068, 2016.

[26] J. Herrera, C. Younes, and L. Porras, "Cloud-to-ground lightning activity in colombia: A 14-year study using lightning location system data," *Atmospheric Research*, vol. 203, pp. 164–174, 2018. [Online]. Available: https://doi.org/10.1016/j.atmosres.2017.12.009

[27] D. J. Cecil, D. E. Buechler, and R. J. Blakeslee, "Trmm lis climatology of thunderstorm occurrence and conditional lightning flash rates," *Journal of Climate*, vol. 28, pp. 6536–6547, 2015.

[28] N. Karunarathna, T. C. Marshall, M. Stolzenburg, and S. Karunarathne, "Narrow bipolar pulse locations compared to thunderstorm radar echo structure," *Journal of Geophysical Research: Atmospheres*, vol. 120, pp. 11,690–11,706, 11 2015. [Online]. Available: http://www.scopus.com/inward/record.url?eid=2-s2.0-84954441993partnerID=tZOtx3y1

[29] F. Lü, B. Zhu, H. Zhou, V. A. Rakov, W. Xu, and Z. Qin, "Observations of compact intracloud lightning discharges in the northernmost region of china," *Journal of Geophysical Research: Atmospheres*, vol. 118, pp. 4458–4465, 5 2013. [Online]. Available: http://www.scopus.com/inward/record.url?eid=2-s2.0-84881170346partnerID=tZOtx3y1

[30] A. V. Gurevich, G. M. Milikh, and R. Roussel-Dupre, "Runaway electron mechanism of air breakdown and preconditioning during a thunderstorm," *Physics Letters A*, vol. 165, pp. 463–468, 1992.

[31] L. P. Babich, E. I. Bochkov, and T. Neubert, "The role of charged ice hydrometeors in lightning initiation," *Journal of Atmospheric and Solar-Terrestrial Physics*, vol. 154, pp. 43–46, 2017. [Online]. Available: http://dx.doi.org/10.1016/j.jastp.2016.12.010

[32] D. Li, F. Liu, F. J. Pérez-Invernón, G. Lu, Z. Qin, B. Zhu, and A. Luque, "On the accuracy of ray-theory methods to determine the altitudes of intracloud electric discharges and ionospheric reflections: Application to narrow bipolar events," *Journal of Geophysical Research: Atmospheres*, vol. 125, pp. 1–10, 2020.

[33] F. Liu, D. Ma, B. Zhu, M. Ma, and P. Liu, "Characteristics of narrow bipolar events," 2016.

[34] T. Wu, Y. Takayanagi, S. Yoshida, T. Funaki, T. Ushio, and Z. Kawasaki, "Spatial relationship between lightning narrow bipolar events and parent thunderstorms as revealed by phased array radar," *Geophysical Research Letters*, vol. 40, pp. 618–623, 2 2013. [Online]. Available: http://www.scopus.com/inward/record.url?eid=2-s2.0-84878180257partnerID=tZOtx3y1

[35] H. Zhang, G. Lu, X. Qie, R. Jiang, Y. Fan, Y. Tian, Z. Sun, M. Liu, Z. Wang, D. Liu, and G. Feng, "Locating narrow bipolar events with single-station measurement of low-frequency magnetic fields," *Journal of Atmospheric and Solar-Terrestrial Physics*, vol. 143-144, pp. 88–101, 2016. [Online]. Available: http://dx.doi.org/10.1016/j.jastp.2016.03.009

[36] D. A. Smith, M. J. Heavner, A. R. Jacobson, X. M. Shao, R. S. Massey, R. J. Sheldon, and K. C. Wiens, "A method for determining intracloud lightning and ionospheric heights from vlf/lf electric field records," *Radio Science*, vol. 39, pp. 124–134, 2004. [Online]. Available: http://www.scopus.com/inward/record.url?eid=2-s2.0-1942474628partnerID=tZOtx3y1

[37] A. Nag and V. A. Rakov, "Compact intracloud lightning discharges: 2. estimation of electrical parameters," *Journal of Geophysical Research*, vol. 115, p. D20103, 10 2010. [Online]. Available: http://www.scopus.com/inward/record.url?eid=2-s2.0-78049406039partnerID=tZOtx3y1

[38] F. C. Lü, B. Y. Zhu, M. Ma, L. X. Wei, and D. Ma, "Observations of narrow bipolar events during two thunderstorms in northeast china," *Science China Earth Sciences*, vol. 56, pp. 1459–1470, 2013.

[39] T. Wu, S. Yoshida, and T. Ushio, "Observations of narrow bipolar events initiating regular lightning flashes." IEEE, 8 2014, pp. 1–4. [Online]. Available: http://www.scopus.com/inward/record.url?eid=2-s2.0-84919776651partnerID=tZOtx3y1

[40] V. Cooray and S. Lundquist, "Characteristics of the radiation fields from lightning in sri lanka in the tropics," *Journal of Geophysical Research*, vol. 90, pp. 6099–6109, 1985.

[41] J. C. Willett, J. C. Bailey, and E. P. Krider, "A class of unusual lightning electric field waveforms with very strong high-frequency radiation," *Journal of Geophysical Research*, vol. 94, p. 16255, 1989.

[42] P. J. Medelius, E. M. Thomson, and J. S. Pierce, "E and de/dt waveshapes for narrow bipolar pulses in intracloud lightning." NASA. Kennedy Space Center, The 1991 International Aerospace and Ground Conference on Lightning and Static Electricity, Volume 1; 10 p, 1991, pp. 12–1 – 12–10, available in eBooks Doctorado.

[43] J. Zhang, "Development and test of the langmuir electric field array," p. 101, 2010.

[44] A. Hazmi, P. Emeraldi, M. I. Hamid, and N. Takagi, "Research on positive narrow bipolar events in padang," *Proceedings - 2016 3rd International Conference on Information Technology, Computer, and Electrical Engineering, ICITACEE 2016*, pp. 156–159, 2017.

[45] T. Gunasekara, M. Fernando, U. Sonnadara, and V. Cooray, "Characteristics of narrow bipolar pulses observed from lightning in sri lanka," *Journal of Atmospheric and Solar-Terrestrial Physics*, vol. 138-139, pp. 66–73, 2 2016. [Online]. Available: http://www.scopus.com/inward/record.url?eid=2-s2.0-84951286333partnerID=tZOtx3y1

[46] D. Wansheng, W. Ting, and L. Hengyi, "Comparison of electrical waveforms of positive and negative polarity narrow bipolar events," vol. 2010, 2010, pp. 2–4.

[47] N. A. Ahmad, M. Fernando, and V. Coora, "On the derivatives of narrow bipolar pulses," 2010, pp. 1–4.

[48] Y. Wang, G. Zhang, X. Qie, D. Wang, T. Zhang, Y. Zhao, Y. Li, and T. Zhang, "Characteristics of compact intracloud discharges observed in a severe thunderstorm in northern part of china," *Journal of Atmospheric and Solar-Terrestrial Physics*, vol. 84-85, pp. 7–14, 2012. [Online]. Available: http://dx.doi.org/10.1016/j.jastp.2012.05.003

[49] K. B. Eack, "Electrical characteristics of narrow bipolar events," *Geophysical Research Letters*, vol. 31, p. L20102, 2004. [Online]. Available: http://www.scopus.com/inward/record.url?eid=2-s2.0-11844302162partnerID=tZOtx3y1

[50] A. R. Jacobson, "How do the strongest radio pulses from thunderstorms relate to lightning flashes?" *Journal of Geophysical Research*, vol. 108, pp. 1–17, 2003. [Online]. Available: http://dx.doi.org/10.1029/2003JD003936

[51] S. Karunarathne, T. Marshall, M. Stolzenburg, and N. Karunarathna, "Observations of positive narrow bipolar pulses," *Journal of Geophysical Research: Atmospheres*, vol. 120, pp. 7128–7143, 2015.

[52] S. Bandara, T. Marshall, S. Karunarathne, N. Karunarathne, R. Siedlecki, and M. Stolzenburg, "Characterizing three types of negative narrow bipolar events in thunderstorms," *Atmospheric Research*, vol. 227, pp. 263–279, 2019. [Online]. Available: https://doi.org/10.1016/j.atmosres.2019.05.013 https://linkinghub.elsevier.com/retrieve/pii/S0169809519301383

[53] E. M. Smith, T. C. Marshall, S. Karunarathne, R. Siedlecki, and M. Stolzenburg, "Initial breakdown pulse parameters in intracloud and cloud-to-ground lightning flashes," *Journal of Geophysical Research: Atmospheres*, vol. 123, pp. 2129–2140, 2018.

[54] F. Liu, B. Zhu, G. Lu, Z. Qin, J. Lei, K.-M. Peng, A. B. Chen, A. Huang, S. A. Cummer, M. Chen, M. Ma, F. Lyu, and H. Zhou, "Observations of blue discharges associated with negative narrow bipolar events in active deep convection," *Geophysical Research Letters*, 2018. [Online]. Available: http://doi.wiley.com/10.1002/2017GL076207

[55] R. A. Marshall, C. L. da Silva, and V. P. Pasko, "Elve doublets and compact intracloud discharges," *Geophysical Research Letters*, vol. 42, pp. 6112–6119, 7 2015. [Online]. Available: http://www.scopus.com/inward/record.url?eid=2-s2.0-84938962666partnerID=tZOtx3y1

[56] Y. Wada, T. Enoto, Y. Nakamura, Y. Furuta, T. Yuasa, K. Nakazawa, T. Morimoto, M. Sato, T. Matsumoto, D. Yonetoku, T. Sawano, H. Sakai, M. Kamogawa, T. Ushio, K. Makishima, and H. Tsuchiya, "Gamma-ray glow preceding downward terrestrial gamma-ray flash," *Communications Physics*, vol. 2, p. 67, 2019. [Online]. Available: http://www.nature.com/articles/s42005-019-0168-y

[57] N. Liu, J. R. Dwyer, and S. A. Cummer, "Elves accompanying terrestrial gamma ray flashes," *Journal of Geophysical Research: Space Physics*, vol. 122, pp. 10,563–10,576, 2017.

[58] M. A. Stanley, X. M. Shao, D. M. Smith, L. I. Lopez, M. B. Pongratz, J. D. Harlin, M. Stock, and A. Regan, "A link between terrestrial gamma-ray flashes and intracloud lightning discharges," *Geophysical Research Letters*, vol. 33, pp. 1–5, 2006.

[59] G. Lu, R. J. Blakeslee, J. Li, D. M. Smith, X. M. Shao, E. W. McCaul, D. E. Buechler, H. J. Christian, J. M. Hall, and S. A. Cummer, "Lightning mapping observation of a terrestrial gamma-ray flash," *Geophysical Research Letters*, vol. 37, pp. 1–5, 2010.

[60] T. E. L. Light and A. R. Jacobson, "Characteristics of impulsive vhf lightning signals observed by the forte satellite," *Journal of Geophysical Research Atmospheres*, vol. 107, pp. 1–8, 2002.

[61] A. R. Jacobson, R. H. Holzworth, and X.-M. Shao, "Observations of multi-microsecond vhf pulsetrains in energetic intracloud lightning discharges," *Annales Geophysicae*, vol. 29, pp. 1587–1604, 9 2011. [Online]. Available: http://www.scopus.com/inward/record.url?eid=2-s2.0-84855274315partnerID=tZOtx3y1

[62] R. S. Zuelsdorf, R. C. Franz, R. J. Strangeway, and C. T. Russell, "Determining the source of strong lf/vlf tipp events: Implications for association with npbps and nnbps," *Journal of Geophysical Research*, vol. 105, p. 20725, 2000. [Online]. Available: http://doi.wiley.com/10.1029/2000JD900214

[63] M. S. Dolgonosov, V. M. Gotlib, D. I. Vavilov, L. M. Zelenyi, and S. I. Klimov, ""solitary" trans-ionospheric pulse pairs onboard of the microsatellite "chibis-m"," *Advances in Space Research*, vol. 56, pp. 1177–1184, 2015. [Online]. Available: http://www.sciencedirect.com/science/article/pii/S0273117715004275

[64] A. R. Jacobson, W. Boeck, and C. Jeffery, "Comparison of narrow bipolar events with ordinary lightning as proxies for the microwave-radiometry ice-scattering signature," *Monthly Weather Review*, vol. 135, pp. 1354–1363, 4 2006. [Online]. Available: http://www.scopus.com/inward/record.url?eid=2-s2.0-34248343450partnerID=tZOtx3y1

[65] S. Soler, F. J. Pérez-Invernón, F. J. Gordillo-Vázquez, A. Luque, D. Li, A. Malagón-Romero, T. Neubert, O. Chanrion, V. Reglero, J. Navarro-Gonzalez, G. Lu, H. Zhang, A. Huang, and N. Østgaard, "Blue optical observations of narrow bipolar events by asim suggest corona streamer activity in thunderstorms," *Journal of Geophysical Research: Atmospheres*, vol. 125, 8 2020.

[66] F. Liu, G. Lu, T. Neubert, J. Lei, O. Chanrion, N. Østgaard, D. Li, A. Luque, F. J. Gordillo-Vázquez, V. Reglero, W. Lyu, and B. Zhu, "Optical emissions associated with narrow bipolar events from thunderstorm clouds penetrating into the stratosphere," *Nature Communications*, vol. 12, 2021.

[67] L. S. Husbjerg, T. Neubert, O. Chanrion, K. Dimitriadou, D. Li, M. Stendel, E. Kaas, N. Østgaard, and V. Reglero, "Observations of blue corona discharges in thunderclouds," *Geophysical Research Letters*, vol. 49, 6 2022.

[68] I. Kolmašová, O. Santolík, E. Defer, W. Rison, S. Coquillat, S. Pedeboy, R. Lán, L. Uhlíř, D. Lambert, J. P. Pinty, S. Prieur, and V. Pont, "Lightning initiation: Strong pulses of vhf radiation accompany preliminary breakdown," *Scientific Reports*, vol. 8, pp. 4–13, 2018.

[69] D. M. Suszcynsky and M. J. Heavner, "Narrow bipolar events as indicators of thunderstorm convective strength," *Geophysical Research Letters*, vol. 30, 2003. [Online]. Available: http://www.scopus.com/inward/record.url?eid=2-s2.0-0346216932partnerID=tZOtx3y1

[70] B. Zhu, F. Lv, D. Ma, and H. Zhou, "A pocket discharge model for narrow bipolar events and possible applications," *2010 Asia-Pacific Symposium on Electromagnetic Compatibility, APEMC 2010*, pp. 1558–1561, 2010.

[71] T. Wu, W. Dong, Y. Zhang, and T. Wang, "Comparison of positive and negative compact intracloud discharges," *Journal of Geophysical Research*, vol. 116, p. D03111, 2 2011. [Online]. Available: http://www.scopus.com/inward/record.url?eid=2-s2.0-79951843629partnerID=tZOtx3y1

[72] H. Liu, W. Dong, T. Wu, D. Zheng, and Y. Zhang, "Observation of compact intracloud discharges using vhf broadband interferometers," *Journal of Geophysical Research*, vol. 117, p. D01203, 1 2012. [Online]. Available: http://www.scopus.com/inward/record.url?eid=2-s2.0-84862973185partnerID=tZOtx3y1

[73] A. Nag, V. A. Rakov, and J. A. Cramer, "Remote measurements of currents in cloud lightning discharges," *IEEE Transactions on Electromagnetic Compatibility*, vol. 53, pp. 407–413, 5 2011. [Online]. Available: http://www.scopus.com/inward/record.url?eid=2-s2.0-79957840753partnerID=tZOtx3y1

[74] D. A. Smith, K. B. Eack, J. Harlin, M. J. Heavner, A. R. Jacobson, R. S. Massey, X. M. Shao, and K. C. Wiens, "The los alamos sferic array: A research tool for lightning investigations," *Journal of Geophysical Research Atmospheres*, vol. 107, pp. 1–15, 2002.

[75] B. Zhu, H. Zhou, M. Ma, and S. Tao, "Observations of narrow bipolar events in east china," *Journal of Atmospheric and Solar-Terrestrial Physics*, vol. 72, pp. 271–278, 2010. [Online]. Available: http://dx.doi.org/10.1016/j.jastp.2009.12.002

[76] V. Cooray, G. Cooray, M. Rubinstein, and F. Rachidi, "Modeling compact intracloud discharge (cid) as a streamer burst," *Atmosphere*, vol. 11, 2020.

[77] P. R. Krehbiel, "Studies of lightning initiation," vol. 9169, 2017, p. 90070.

[78] M. G. Stock, P. R. Krehbiel, J. Lapierre, T. Wu, M. A. Stanley, and H. E. Edens, "Fast positive breakdown in lightning," *Journal of Geophysical Research*, vol. 122, pp. 8135–8152, 2017.

[79] C. E. Baum, "Sensor for measurements of intense electromagnetic pulses," p. 28, 1981.

[80] V. A. Rakov, S. Mallick, A. Nag, and V. B. Somu, "Lightning observatory in gainesville (log), florida: A review of recent results," *Electric Power Systems Research*, vol. 113, 2014.

[81] H. E. Rojas, C. A. Rivera, J. Chaves, C. A. Cortés, F. J. Román, and M. Fernando, "New circuit for the measurement of lightning generated electric fields," *2017 International Symposium on Lightning Protection, XIV SIPDA 2017*, pp. 188–194, 2017.

[82] R. A. Watson and M. A. Appleton, "On the nature of atmospherics," *Proceedings of the Royal Society of London. Series A, Containing papers of a mathematical and physical character*, vol. 103, pp. 563–579, 1923.

[83] G. Karnas, K. Filik, P. Szczupak, and G. Maslowski, "Calibration of electric field antennae operating in the elf-mf frequency range at the lightning research station in rzeszow," *2016 Selected Issues of Electrical Engineering and Electronics, WZEE 2016*, 2016.

[84] J. W. Warwick, C. O. Hayenga, and J. W. Brosnahan, "Interferometric directions of lightning sources at 34 mhz," pp. 2457–2468, 1979. [Online]. Available: http://dx.doi.org/10.1029/JC084iC05p02457

[85] D. E. Proctor, "A hyperbolic system for obtaining vhf radio pictures of lightning," *Journal of Geophysical Research*, vol. 76, p. 1478, 1971, this paper has the description of how to estimate the location of VHF sources inside a thundercloud. [Online]. Available: http://dx.doi.org/10.1029/JC076i006p01478

[86] O. Hayenga, "Characteristics of lightning vhf radiation near the time of return strokes," *Journal of Geophysical Research*, vol. 89, pp. 1403–1410, 1984.

[87] C. T. Rhodes and P. R. Krehbiel, "Interferometric observations of a single stroke cloud-to-ground flash," *Geophysical Research Letters*, vol. 16, pp. 1169–1172, 1989.

[88] X. M. Shao, P. R. Krehbiel, R. J. Thomas, and W. Rison, "Radio interferometric observations of cloud-to-ground lightning phenomena in florida," *Journal of Geophysical Research*, vol. 100, p. 2749, 1995.

[89] Z. Kawasaki, R. Mardiana, and T. Ushio, "Broadband and narrowband rf interferometers for lightning observations," *Geophysical Research Letters*, vol. 27, pp. 3189–3192, 2000.

[90] M. Stock, "Broadband interferometry of lightning," p. 255, 2014.

[91] C. T. Rhodes, X. M. Shao, P. R. Krehbiel, R. J. Thomas, and C. O. Hayenga, "Observations of lightning phenomena using radio interferometry," *J. Geophys. Res.*, vol. 99, pp. 13 059–13 082, 1994. [Online]. Available: http://dx.doi.org/10.1029/94JD00318

[92] M. Akita, M. Stock, Z. Kawasaki, P. Krehbiel, W. Rison, and M. Stanley, "Data processing procedure using distribution of slopes of phase differences for broadband vhf interferometer," *Journal of Geophysical Research Atmospheres*, vol. 119, pp. 6085–6104, 2014.

[93] M. G. Stock, M. Akita, P. R. Krehbiel, W. Rison, H. E. Edens, Z. Kawasaki, and M. A. Stanley, "Continuous broadband digital interferometry of lightning using a generalized cross-correlation algorithm," *Journal of Geophysical Research Atmospheres*, vol. 119, pp. 3134–3165, 2014.

[94] M. Nishihashi, K. I. Shimose, K. Kusunoki, S. Hayashi, K. I. Arai, H. Y. Inoue, W. Mashiko, M. Kusume, and H. Morishima, "Three-dimensional vhf lightning mapping system for winter thunderstorms," *Journal of Atmospheric and Oceanic Technology*, vol. 30, pp. 325–335, 2013.

[95] X. M. Shao, C. Ho, M. Caffrey, P. Graham, B. Haynes, G. Bowers, W. Blaine, B. Dingus, D. Smith, and H. Rassoul, "Broadband rf interferometric mapping and polarization (bimap) observations of lightning discharges: Revealing new physics insights into breakdown processes," *Journal of Geophysical Research: Atmospheres*, vol. 123, pp. 10,326–10,340, 2018.

[96] X. M. Shao, C. Ho, G. Bowers, W. Blaine, and B. Dingus, "Lightning interferometry uncertainty, beam steering interferometry, and evidence of lightning being ignited by a cosmic ray shower," *Journal of Geophysical Research: Atmospheres*, vol. 125, 2020. [Online]. Available: https://doi.org/10.1029/2019JD032273

[97] X. Fan, P. Krehbiel, J. Tilles, M. Stanley, S. Senay, H. Edens, W. Rison, and Y. Zhang, "Radio interferometer observations and analysis of an radio interferometer observations and analysis of an energetic in-cloud pulse based on ensemble empirical mode decomposition," *IEEE Transactions on Geoscience and Remote Sensing*, pp. 1–17, 2021.

[98] S. Yoshida, C. J. Biagi, V. A. Rakov, J. D. Hill, M. V. Stapleton, D. M. Jordan, M. A. Uman, T. Morimoto, T. Ushio, and Z. I. Kawasaki, "Three-dimensional imaging of upward positive leaders in triggered lightning using vhf broadband digital interferometers," *Geophysical Research Letters*, vol. 37, pp. 1–5, 2010.

[99] L. Elbaghdady, M. Akita, A. Allam, Z. Kawasaki, and M. E. Ragab, "One site three dimensions lightning location system using vhf broadband interferometers," *Journal of atmospheric electricity*, vol. 33, pp. 91–105, 2013.

[100] L. Samy, Y. Nakamura, A. Allam, T. Ushio, and Z. Kawasaki, "Ten minutes continuous recording lightning using broadband vhf interferometer," *Advances in Space Research*, vol. 56, pp. 2218–2234, 2015. [Online]. Available: http://dx.doi.org/10.1016/j.asr.2015.07.038

[101] V. Cooray, *The lightning flash*, V. Cooray, Ed. IET, 2003, 2003.

[102] K. L. Cummins and M. J. Murphy, "An overview of lightning locating systems: History, techniques, and data uses, with an in-depth look at the u.s. nldn," *IEEE Transactions on Electromagnetic Compatibility*, vol. 51, pp. 499–518, 2009.

[103] C. E. Baum, "The circular parallel-plate dipole," p. 36, 1969.

[104] H. Enrique and R. Cubides, "Técnicas avanzadas para el tratamiento y procesamiento de señales de campos electromagnéticos generados por rayos," 2018.

[105] A. F. R. Leal, V. A. Rakov, and B. Rocha, "Classification of cids observed in florida using the lightning detection and waveform storage system," 2017, pp. 1–8.

[106] V. Cooray, "Effects of propagation of narrow bipolar pulses , generated by compact cloud discharges , over finitely conducting ground," *Atmosphere*, vol. 9, 2018.

[107] A. F. Leal, V. A. Rakov, J. P. Filho, B. R. P. Rocha, and M. D. Tran, "A low-cost system for measuring lightning electric field waveforms, its calibration and application to remote measurements of currents," *IEEE Transactions on Electromagnetic Compatibility*, vol. 60, pp. 1–9, 2017.

[108] N. Liu, J. R. Dwyer, J. N. Tilles, M. A. Stanley, P. R. Krehbiel, W. Rison, R. G. Brown, and J. G. Wilson, "Understanding the radio spectrum of thunderstorm narrow bipolar events," *Journal of Geophysical Research: Atmospheres*, vol. 124, pp. 10 134–10 153, 2019.

[109] Y. Huang, J. Benesty, and J. Chen, "Time delay estimation and source localization," pp. 1043–1063, 2008.

[110] Z. Koochak and A. Fraser-Smith, "Single-station lightning location using azimuth and time of arrival of sferics," *Radio Science*, vol. 55, 2020.

[111] A. Chilingarian, M. Dolgonosov, A. Kiselyov, Y. Khanikyants, and S. Soghomonyan, "Lightning observations using broadband vhf interferometer and electric field measurements," *Journal of Instrumentation*, vol. 15, 2020.

[112] C. Knapp and G. C. Carter, "The generalized correlation method for estimation of time delay," *IEEE Transactions on Acoustic, Speech, and Signal Processing*, vol. 2, pp. 320–327, 1976.

[113] R. Marinescu and A. Buzo, "Applying the accumulation of cross-power spectrum technique for traditional generalized cross-correlation time delay estimation," *International Journal On ...*, vol. 6, pp. 98–108, 2013. [Online]. Available: http://www.thinkmind.org/index.php?view=articlearticleid=tele$_v$6$_n$34$_2$013$_3$

[114] A. O. Hero and S. C. Schwartz, "A new generalized cross correlator," *IEEE Transactions on Acoustics, Speech, and Signal Processing*, vol. 33, pp. 38–45, 1985.

[115] S. Sugasawa, "Time difference measurement of ultrasonic pulses using cross-correlation function between analytic signals," *Japanese Journal of Applied Physics, Part 1: Regular Papers and Short Notes and Review Papers*, vol. 41, pp. 3299–3307, 2002.

[116] M. T. Taner, F. Koehler, and R. E. Sheriff, "Complex seismic trace analysis," *Geophysics*, vol. 44, pp. 1041–1063, 1979. [Online]. Available: http://library.seg.org/doi/10.1190/1.1440994

[117] J. Ville, "Theorie et applications de la notion de signal analytique," *Cables et transmissions*, vol. 1, pp. 61–74, 1948. [Online]. Available: http://www.albayan.ae

[118] N. A. Ahmad, M. Fernando, Z. Baharudin, V. Cooray, H. Ahmad, and Z. A. Malek, "Characteristics of narrow bipolar pulses observed in malaysia," *Journal of Atmospheric and Solar-Terrestrial Physics*, vol. 72, pp. 534–540, 4 2010. [Online]. Available: http://www.scopus.com/inward/record.url?eid=2-s2.0-77950518238partnerID=tZOtx3y1

[119] S. Bandara, T. Marshall, S. Karunarathne, and M. Stolzenburg, "Electric field change and vhf waveforms of positive narrow bipolar events in mississippi thunderstorms," *Atmospheric Research*, vol. 243, p. 105000, 2020. [Online]. Available: https://doi.org/10.1016/j.atmosres.2020.105000

[120] V. Cooray, M. Fernando, L. Gunasekara, and S. Nanayakkara, "Propagation effects on radiation fields known as narrow bipolar pulses generated by compact cloud discharges discharges," 2014, pp. 22–25.

[121] A. F. R. Leal, V. A. Rakov, and B. R. P. da Rocha, "Compact intracloud discharges: New classification of field waveforms and identification by lightning locating systems," *Electric Power Systems Research*, vol. 173, pp. 251–262, 2019.

[122] D. Aranguren, J. López, J. Inampués, H. Torres, and H. D. Betz, "Cloud-to-ground ligthning activity in colombia and the influence of topography," *Journal of Atmospheric and Solar-Terrestrial Physics*, vol. 154, pp. 1850–1855, 2014. [Online]. Available: http://dx.doi.org/10.1016/j.jastp.2016.08.010

[123] S. Bandara, T. Marshall, S. Karunarathne, and M. Stolzenburg, "Groups of narrow bipolar events within thunderstorms," *Atmospheric Research*, vol. 252, p. 105450, 2021. [Online]. Available: https://doi.org/10.1016/j.atmosres.2021.105450

[124] A. Hazmi, P. Emeraldi, E. P. Waldi, and N. Takagi, "Characteristics of discharge initiation processes of tropical lightning flashes," *International Journal on Electrical Engineering and Informatics*, vol. 14, pp. 379–391, 6 2022.

[125] S. R. Sharma, V. Cooray, and M. Fernando, "Isolated breakdown activity in swedish lightning," *Journal of Atmospheric and Solar-Terrestrial Physics*, vol. 70, pp. 1213–1221, 2008.

[126] T. Wu, S. Yoshida, T. Ushio, Z. Kawasaki, Y. Takayanagi, and D. Wang, "Large bipolar lightning discharge events in winter thunderstorms in japan," *Journal of Geophysical Research: Atmospheres*, vol. 119, pp. 555–566, 1 2014. [Online]. Available: http://www.scopus.com/inward/record.url?eid=2-s2.0-84900606778partnerID=tZOtx3y1

[127] D. Li, A. Luque, F. J. Gordillo-Vázquez, C. da Silva, P. R. Krehbiel, F. Rachidi, and M. Rubinstein, "Secondary fast breakdown in narrow bipolar events," 4 2022.

[128] A. Y. Kostinskiy, T. C. Marshall, and M. Stolzenburg, "The mechanism of the origin and development of lightning from initiating event to initial breakdown pulses," *arXiv*, pp. 0–2, 2019.

[129] M. H. Sabri, M. R. Ahmad, M. R. Esa, D. Periannan, G. Lu, H. Zhang, V. Cooray, E. Williams, M. Z. Aziz, Z. Abdul-Malek, A. A. Alkahtani, and M. Z. Kadir, "Initial electric field changes of lightning flashes in tropical thunderstorms and their relationship to the lightning initiation mechanism," *Atmospheric Research*, vol. 226, pp. 138–151, 2019.

[130] M. Haziq, M. Sabri, M. R. Ahmad, M. Riza, and M. Esa, "Environmental analysis of quasi-static electric field changes of tropical environmental analysis of quasi-static electric field changes of tropical lightning flashes," *Ekoloji*, vol. 28, pp. 373–378, 2019.

[131] T. Marshall, S. Bandara, N. Karunarathne, S. Karunarathne, I. Kolmasova, R. Siedlecki, and M. Stolzenburg, "A study of lightning flash initiation prior to the first initial breakdown pulse," *Atmospheric Research*, vol. 217, pp. 10–23, 2019. [Online]. Available: https://doi.org/10.1016/j.atmosres.2018.10.013

[132] R. Mardiana, Z. I. Kawasaki, and T. Morimoto, "Three-dimensional lightning observations of cloud-to-ground flashes using broadband interferometers," *Journal of Atmospheric and Solar-Terrestrial Physics*, vol. 64, pp. 91–103, 2002.

[133] H. Liu, S. Qiu, and W. Dong, "The three-dimensional locating of vhf broadband lightning interferometers," *Atmosphere*, vol. 9, pp. 1–14, 2018.

[134] Y. Li, S. Qiu, L. Shi, Z. Huang, T. Wang, and Y. Duan, "Three-dimensional reconstruction of cloud-to-ground lightning using high-speed video and vhf broadband interferometer," *Journal of Geophysical Research: Atmospheres*, vol. 122, pp. 13,420–13,435, 2017.

[135] H. E. Rojas and C. A. Cortés, "Denoising of measured lightning electric field signals using adaptive filters in the fractional fourier domain," *Measurement*, vol. 55, pp. 616–626, 2014. [Online]. Available: http://dx.doi.org/10.1016/j.measurement.2014.05.026

[136] S. A. S. Baharin, M. R. Ahmad, D. Periannan, M. H. M. Sabri, B. Y. Seah, M. Z. A. A. Aziz, M. M. Ismail, M. R. M. Esa, S. A. Mohammad, J. Bahru, N. Yusop, V. Cooray, G. Lu, and G. Lu, "Wavelet analysis of the onset of vhf and microwave radiation emitted by lightning," vol. 17, 2018, pp. 297–300.

[137] F. Diaz, D. Ortiz, and F. Roman, "Lightning climatology in colombia," *Theoretical and Applied Climatology*, 2022. [Online]. Available: https://doi.org/10.1007/s00704-022-04012-9